Suppression of Peptide Ions Dissociation under Electron Capture Condition

WONG, Pui Shuen

A Thesis Submitted for Partial Fulfillment
of the Requirements for the Degree of
Master of Philosophy
in
Chemistry

The Chinese University of Hong Kong
September 2011

Thesis/ Assessment Committee

Professor Chai Mei Jimmy Yu (Chair)
Professor Tak Wah Dominic Chan (Thesis Supervisor)
Professor Bo Zheng (Committee Member)
Professor Robert Z. Qi (External Examiner)

ABSTRACT

This project investigates the origin(s) of the suppression of fragmentation under electron capture conditions in tandem mass spectrometry of peptide/protein ions. Following the discovery of the suppression of fragmentation in the electron capture dissociation (ECD) of glutamic acid-rich (E ≥ 4) peptide ions, several structural parameters, including the number and nature of the proton carrier and peptide chain length, were investigated. Increasing the number of arginine residues (from 2 to 3) had no significant impact on the observed suppression effect in ECD experiments of peptide ions with different number of glutamic acid residues. Switching the proton carrier from arginine (R) to lysine (K) or histidine (H) showed a lesser extent of suppression effect. A more pronounced impact was obtained in ECD analysis of peptide ions with different chain lengths. For diarginated peptides with six glutamic acid residues, series of c-/z˙- fragment ions and $[M+2H-H^{\cdot}]^{+}$ were found in ECD spectrum of peptide ions with 8 amino acid residues. Substantial reduction of the number and intensities of these fragment ions were observed in the corresponding spectrum of 15-mer peptides. An almost complete suppression of the fragment ions formation was observed for longer peptide ions (n = 23). Conformational analysis showed that there was hydrogen bonding "ladder" formed between backbone amide hydrogen and carbonyl oxygen in 23-mer polypeptide, in which no significant occurrence in 15-mer peptide conformer. A model based on the resonant stabilization of the H˙ along the hydrogen bond "ladder" and thus preventing the N-C_{α} cleavages of peptide, was proposed. The validity of the proposed model was further evaluated by performing ECD experiments on E-riched 15-mer peptides with (a) no hydrogen bonding "ladder" (replacing the amide hydrogen atoms with methyl groups); (b) reduced backbone flexibility (replacing the glycine spacers with proline residues); and (c) different charge carriers (using divalent metal ions, such as Mn^{2+}, Co^{2+}, Ni^{2+}, Cu^{2+}, Zn^{2+}, Cd^{2+} and Hg^{2+}, rather than protons).

摘要

本課題研究了多肽/蛋白質離子在電子捕獲裂解 (ECD) 反應中的碎片離子抑制化現象，考慮了若干的結構參數，包括質子載體的數目、性質以及肽主鏈長度對於碎片化抑制現象的影響。研究發現對於含不同穀氨酸殘基 (E) 數目的多肽，增加精氨酸殘基 (R) 的數目由二到三的 ECD 碎片離子抑制沒有影響；改變質子載體由精氨酸殘基 (R) 爲賴氨酸殘基 (K) 或組氨酸殘基 (H)，碎片離子抑制化程度降低；增加肽主鏈長度，碎片離子抑制化增強：對於含有六個穀氨酸殘基 (E)和兩個精氨酸殘基 (R) 的八個氨基酸殘基組成的肽，ECD 會生成系列的 *c/z*˙-型碎片離子以及脫氫自由基母離子 ($[M+2H-H^{\bullet}]^{+}$)；至於相對應的十五個氨基酸殘基肽，碎片離子的數目和強度有明顯的下降；相對應的二十三個氨基酸殘基肽，幾乎所有的碎片離子都有被抑制。構象分析發現在二十三個氨基酸殘基肽中存在由氨基氫 (N-H) 和碳基氧 (C=O)形成的「梯形」氫鍵鏈。基於構象分析結果，提出了共振穩定化模型，即：氫自由基 (H˙) 通過「梯形」氫鍵鏈被囚禁，從而阻止 N-C_{α} 鏈斷裂，並通過以下試驗：(a) 除去氫鍵鏈 (用甲基取代氨基氫)、 (b) 降低主鏈的柔性 (用脯氨酸殘基 (P) 取代甘氨酸殘基 (G)) 和 (c) 改變電荷載體 (利用二價金屬離子，例如錳(II)、鈷(II)、鎳(II)、銅(II)、鋅(II)、鎘(II) 和汞(II)取代質子驗證該模型的合理性。

ACKNOWLEDGMENTS

I would like to express my deepest gratitude to the following people for supporting me throughout this two-year study.

- ✧ I would like to express my sincere thanks to my supervisor, Prof. Dominic T. W. Chan, for his invaluable guidance, patience, advice and encouragements. He has enriched my knowledge in the area of analytical chemistry and mass spectrometry. More importantly, I have learnt how to think critically and logically in order to solve a problem.
- ✧ I am grateful to Mr. Chi Chiu Chan and Mr. Ka Fai Woo for their assistance in rendering instrumental devices and resolving computer-related problems.
- ✧ I would like to thank my group members, including Dr. Kelly Wai Yi Chan, Dr. Xiangfeng Chen, Ms. Fan Chen, Ms. Hoi Sze Yeung and Mr. Guoqiang Liu and my colleagues, including Ms. Mei Yang, Ms. Ping Wei, Mr. Zhenwu Liao, Dr. Lei Yan and Mr. Feng Wang, for their help and friendship during these two years.
- ✧ I would like to thank my best friends, including Ms. Angel Man Yee Li, Ms. Karen Kar Yan Leung, Ms. Amy Wing Lam Lee, Ms. Kate Wing Yan Tsoi, Ms. Anna Sheung Chuen Lam, Ms. Diora Kong, Ms. Saffi Hoi Yi Lam and Mr. Benny Ka Hou Wong, for their continuous support and encouragements.
- ✧ I would like to thank my family and Mr. Siu Kit Chan for their unfailing support, especially to my parents, my sister, Ms. Pui Shan Wong and my brother, Mr. Shu Yan Wong, for their endless love and care.
- ✧ I am grateful to Graduate School for providing the University Postgraduate Studentship.

TABLE OF CONTENTS

LIST OF TABLES

LIST OF FIGURES

LIST OF SCHEMES

SYMBOLS and ABBREVIATIONS

AI	Activated ion
B	Magnetic field strength
BIRD	Blackbody infrared radiative dissociation
CAD	Collision activated dissociation
Cat	Cation
CI	Chemical ionization
CID	Collision induced dissociation
EA	Electron affinity
ECD	Electron capture dissociation
EI	Electron impact ionization
ESI	Electrospray ionization
ETD	Electron transfer dissociation
eV	Eletron volt
FAB	Fast atom bombardment
FD	Field desorption
FFT	Fast Fourier transform
FID	Free induction decay
FTICR	Fourier transform ion cyclotron resonance
FTMS	Fourier transform mass spectrometry
%$H^{\bullet}$ loss	Percentage of $H^{\bullet}$ loss from $[M+nH]^{(n-1)+\bullet}$
HECD	Hot electron capture dissociation
HPLC	High performance liquid chromatography
IRMPD	Infrared multi-photon dissociation
LMCS	Low Mode Conformational Search
$\dot{M}^{+\bullet}$	Peptide radical cations
$_{m}A$	N-methylalanine
MALDI	Matrix-assisted laser desorption/ ionization
MCMM	Monte Carlo Multiple Minimum
$_{m}E$	N-methylglutamic acid
MECA	Multiple excitation collisional activation
MMFFs	Merck molecular force fields
MS	Mass spectrometry
MS/MS or MS^{n}	Tandem mass spectrometry
m/q or m/z	Mass-to-charge ratio
$[M+nH]^{(n-1)+\bullet}$	Charge reduced precursor ions
PD	Plasma desorption

P(D)	Probability for dissociation
PTMs	Post-translational modifications
rf	radiofrequency
SORI	Sustained off-resonance irradiation
TNCG	Truncated Newton Conjugate Gradient
TOF	Time of flight
UW	Utah-Washington
VLE	Very low energy
XA	External accumulation
Ø	Diameter

Dedication

to

My Parents

Chapter 1

Introduction

1.1 Mass spectrometry of peptides/ proteins

Proteins constitute a major component in organisms. They play a vital role in virtually all biological processes, such as enzymatic catalysis, transport of molecules and ions, etc [1]. Amino acids are the basic unit of proteins. There are 20 common amino acids in organisms, in which they are different in the side chains of the C_α atom. Condensation of two amino acids forms a peptide bond to give a dipeptide. A polypeptide refers to the linear chain of many amino acid residues. The amino acid residues might be chemically modified by post-translational modifications (PTMs) after the translation process of polypeptide from mRNA template. They may then fold into different structures to form proteins.

Each protein has its own amino acid sequence and structure motif, which are important for it to carry out its specific functions. By knowing the amino acid sequences, additional insight on the catalytic reaction of enzymes and folding of polypeptide chains into their three-dimensional structures may be obtained. The abnormal behaviour of chemically-modified proteins can also be studied. It is thus important to develop analytical methods for peptides/ proteins sequencing. With the development of proper peptides/ proteins sequencing methods, the identification of known or unknown proteins in organisms becomes achievable.

Edman degradation and mass spectrometry (MS) are two common sequencing methods for peptides/ protein. Edman degradation involves the sequential cleavage of an amino acid residue from the N-terminal of a peptide [2, 3]. It is done by the reaction of phenyl isothiocyanate with the uncharged terminal amino group to give a

phenylthiocarbamoyl (PTC) derivative. The cyclic derivative of the terminal amino acid can be liberated out under mild acidic condition without hydrolyzing the remaining peptides. The derivative can then be identified using chromatographic procedures. However, if the N-terminal is chemically modified or trapped in the protein, then this method cannot be used. Furthermore, the presence of disulfide linkage has to be reduced before performing Edman degradation. Alkylation of cysteine residues prevents the re-oxidation of the thiol group to form the disulfide bond. Disulfide linkage present in protein, if there is any, has to be determined by other methods.

Mass spectrometry (MS) is another analytical technique that commonly used in protein identification. MS measures the mass-to-charge ratio (m/z) of the analyte ions. With high sensitivity and accuracy of mass measurement, the application of MS to biomolecules has been widely used in past few decades. The concept of MS was first introduced by J. J. Thomson in 1899 [4]. The most challenging part for successful MS analysis is to produce representative sample ions in gas phase. Different ionization methods were developed to facilitate the ion production for different types of molecules. Electron impact ionization (EI) [5] and chemical ionization (CI) [6] are commonly used for ionizing small and volatile organic molecules. To generate the intact ions from nonvolatile and thermally unstable substances, a number of so-called "soft" ionization techniques were developed. Field desorption (FD) [7], plasma desorption (PD) [8] and fast atom bombardment (FAB) [9] are "soft" ionization methods that can transfer small to medium size nonvolatile molecules into gas phase. With the development of two Nobel winning ionization methods in late 1980s, electrospray ionization (ESI) [10] and matrix-assisted laser desorption/ ionization (MALDI) [11] have become the techniques of choices for analysis of large biomolecules in mass spectrometry. ESI and MALDI are gentle

desorption/ ionization methods that intact molecular ions could be produced. The upper mass limit that can be attained by these methods is much higher than that of FD, PD and FAB. They are widely used for the ionization of peptides/ proteins intact with PTMs, protein-ligand complexes or protein-metal ion complexes. Their development has been a milestone of the applications of MS in studying peptides/ proteins.

1.1.1 Electrospray ionization of peptides/ proteins

Electrospray ionization mass spectrometry was introduced by J. B. Fenn and co-workers in 1984 [12, 13]. ESI is operated under ambient conditions. The sample solution prepared in polar and volatile solvent was delivered to a hypodermic needle at a flow rate of 1-5 μL/min. The hypodermic needle is floated at a high electrical potential (a few kilovolts) relative to the nozzle. The surface of the liquid at the needle tip is charged by the high potential. The liquid is then dispersed to a fine spray of the charged droplets by the columbic repulsion forces. Under the applied electric field, the droplets migrate towards the entrance of the mass spectrometer. Evaporation of the solvent is aided by a gentle flow of warm inert gas (e.g. nitrogen gas). With the removal of solvent molecules, the diameters of the charged droplets would decrease progressively. The charge density on the droplet surface would gradually increase to the Rayleigh limit of instability. The unstable droplets then undergo columbic explosions to give droplets with even smaller diameters. After repeated droplet explosions, the radius of the curvature of the droplets might be small enough so that the self-generated electric field on the surface of the droplets could become high enough to desorb the ions from the droplets into the ambient gas. The ions formed are subsequently directed to the high vacuum system for mass analysis.

ESI has several distinctive features for being a useful tool for ionization of large proteins. Sample preparation step is much simpler when compared to MALDI or other ionization methods. The analytes only need to be dissolved in water with suitable organic solvent, such as methanol and acetonitrile. More importantly, ESI is capable of generating multiply charged ions, with the charge number depending on the number of basic residues in the molecule. This property allows the analysis of large proteins in mass analyzers with limited mass range. It is also possible to study non-covalently bonded complexes using ESI-MS. Furthermore, ESI can easily be coupled to separation instrument, such as high performance liquid chromatography (HPLC). This enhances the capability of ESI-MS to analyze complex mixtures by preventing the undesirable suppression of analyte signals due to the charge competition with other substances in the sample solution.

1.2 Tandem mass spectrometry of peptides/ proteins

To obtain structural information of proteins, tandem mass spectrometry method (MS/MS or MS^n) can be used in conjunction with ESI. Tandem mass spectrometry is a technique that multiple stages of mass selection and separation are used in the mass analyzers to facilitate the structural analysis of molecules. The ions of interests, (i.e. precursor ions) are first isolated by removing other unwanted ions produced in the ion source. By using a suitable ion activation method, the precursor ions can be dissociated to give fragment ions. The structure of the precursor ions can then be obtained through analyzing the fragment ions that generated. Further MS can also be done by isolating a primary fragment ion for subsequent dissociation.

In general, there are two approaches for peptides/ proteins sequencing: (a) bottom up and (b) top down strategies. Bottom up strategy involves the enzymatic

digestion or chemical digestion of the proteins into smaller peptides prior to MS analysis. The masses of the peptides can then be measured by mass spectrometry. Selected peptide ions can further be isolated to perform MS/MS experiments to obtain partial sequence information. The identity of the protein can be found by comparing the peptide masses and sequence tags information with the theoretical one predicted from the database [14]. Bottom up strategy is commonly performed using on-line HPLC-MS or CE-MS after the proteolytic digestion of the proteins. There are several drawbacks in using bottom up strategy for protein identification. To facilitate enzymatic digestion, some of the PTMs have to be removed chemically prior to digestion. This leads to the permanent loss of these structural information [15]. Top down strategy involves the accurate mass measurement of the intact protein ions that directly generated by ESI or MALDI [16]. The protein ions are subjected to different ion activation methods to generate their fingerprint fragmentation patterns [17]. The complete sequence coverage at both the intact molecular ions and fragment ions level and the ability of PTM detection are the hallmarks of top down strategy in peptide/ protein sequencing [18]. No loss of information is resulted from the analytical procedure of top down experiments. Identification of substitutions and modifications of amino acid residues have been reported using top down strategy [19].

1.2.1 Nomenclature of peptide fragment ions

There are many different covalent bonds present in peptide molecules that can be broken during ion activation. The bond cleavage may include backbone linkages and/ or side chain groups of the amino acid residues. To facilitate analysis and report of the peptide fragment ions, special nomenclature of the peptide fragment ions has

been developed.

The nomenclature of peptide fragments along the backbone was first suggested by Roepstorff and Fohlmann in 1984 [20]. Backbone fragment ions with the charge localized on the N-terminus of the original peptide are assigned as *a*, *b* and *c* ions, while their complementary ions are *x*, *y* and *z* ions respectively if the charge is retained on the C-terminus (Scheme 1.1). The subscript next to the letter represents the number of amino acid residues from N-terminus (*a*, *b* and *c* ions) or C-terminus (*x*, *y* and *z* ions). Johnson and coworkers further modified the nomenclature in 1987 with the introduction of additional notation for fragment ions with the cleavage of C_β-C_γ bond of *z* ions to give *w* ions [21].

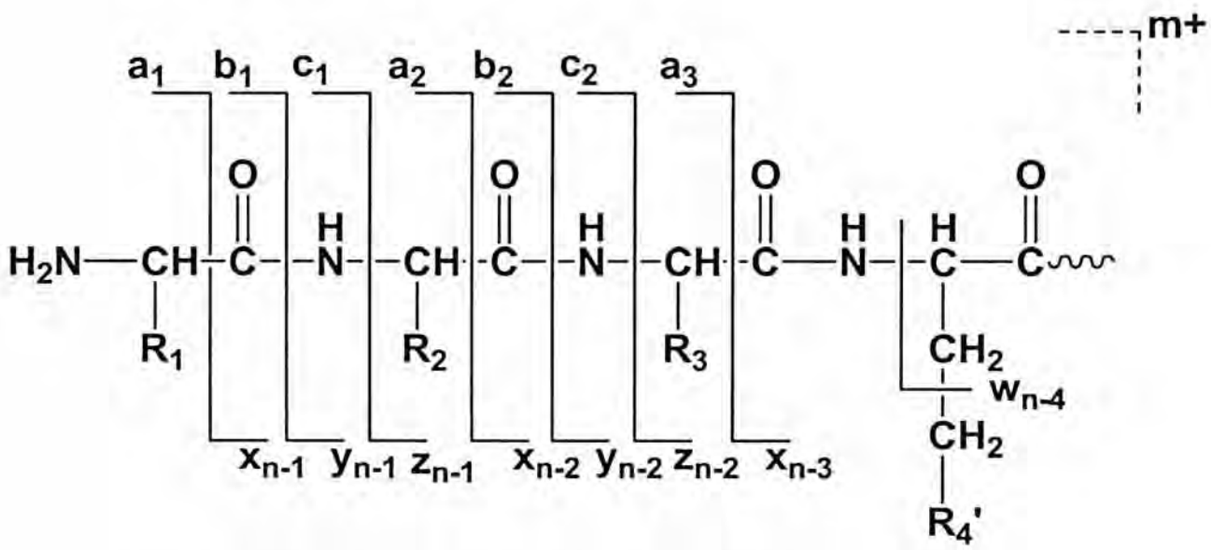

Scheme 1.1 Nomenclature of peptide fragment ions

1.2.2 Slow heating methods for MS^n

To successfully perform tandem mass spectrometry, appropriate ion activation method has to be applied in order to obtain the desired structural information. Various ion activation methods have been developed throughout the history of MS^n in order to extract maximum structural information from the analytes. There are a few dissociation methods that are commonly used for peptide fragmentation.

Collision induced dissociation (CID) or collision activated dissociation (CAD) is one of the most common dissociation methods being used [22]. Together with infrared multi-photon dissociation (IRMPD) [23, 24] and blackbody infrared radiative dissociation (BIRD) [25], they are regarded as conventional slow heating methods [26].

The basic principle of slow heating methods is the stepwise deposition of energy to the analyte ions through collisions or photon absorption. The vibrational degrees of freedom of the molecular ions are usually excited. Through redistribution of energy, the weakest bond of the ions is preferentially cleaved. For peptide ions, -C=O(N)- linkages are preferentially cleaved under the slow heating ion activation methods, forming series of *b/y*-ions in the mass spectrum. However, the bond cleavage site is sequence dependent. Preferential cleavage of the amide bond next to N-terminal of proline (P) residues and C-terminal of acidic amino acid residues (aspartic acid (D) and glutamic acid (E)) has been reported [27, 28]. Small neutral molecules, such as water, carbon dioxide and PTMs group can also be lost from the precursor/ fragment ions through the ion activation process.

1.2.2.1 Collision induced dissociation

Collision induced dissociation (CID) is one of the most widely used tandem mass spectrometry techniques for structural determination of the analyte ions. This technique was first demonstrated by Haddon and McLafferty in the dissociation of $C_3H_7^+$ using a time-of-flight (TOF) mass spectrometer [22]. It involves collisions of the analyte ions with inert gas molecules. Study of the applications of CID in different mass analyzers has been performed. Freiser and co-workers performed CID experiments in a Fourier-transform ion cyclotron resonance mass spectrometer (FTICR-MS/ FTMS) [29, 30].

For FTMS, the precursor ions can be isolated in the cell by over-excitation of the unwanted ions. By applying a short *rf*-waveform at the cyclotron frequency of the precursor ions, resonant excitation of their cyclotron motion will be resulted. Activation occurs through collisions of the translationally excited ions and the inert gas molecules under an elevated background pressure of 10^{-6} – 10^{-7} Torr. With multiple collisions, part of the translation energy of the precursor ions can be converted to internal energy of the ions. The internal energy would be redistributed among different degrees of freedom of the ions. Temporary accumulation of enough internal energy at the weakest linkage within the ion would ultimately lead to dissociation. By varying the duration, frequency and the number of waveforms, CID were further divided into different classes, including multiple excitation collisional activation (MECA) [31], sustained off-resonance irradiation CID (SORI-CID) [32, 33] and very-low-energy CID (VLE-CID) [34, 35]. SORI-CID is the most widely used method for the fragmentation of large biomolecule ions due to its ease of implementation [36].

1.2.3 Electron based ion activation for MS^n

Comparatively, electron based ion activation methods, including ion/ electron (electron capture dissociation (ECD) [37]) and ion/ ion reactions (electron transfer dissociation (ETD) [38]), are relatively new dissociation methods. Because of the difference in the way of energy deposition to the ions and the intermediates formed, the ion/electron or ion/ion reactions resulted in different fragmentation pattern as compared to that of slow heating methods.

Cleavage of N-C_α bond is the major dissociation for protonated peptide ions when they undergo ECD/ ETD leading to the formation of series of *c*/ $z^{\bullet}$ fragment ions. A minor dissociation pathway leading to the formation of *a*-/*y*-ions has also

been identified. The fragmentation of ECD/ ETD depends less on the identity of amino acid residues. No preferential cleavage has been observed, except for proline residues. At the N-terminal side of proline residues, single N-C_α bond cleavage would not result in any *c/ z*˙-fragment ions. Interestingly, many common PTM groups were found to be unaffected during the dissociation process [39-42]. The localization of PTMs on peptides/ proteins has become practically possible. However, the dissociation efficiency of ECD/ ETD is relatively low when compared to that of slow heating methods. Based on the characteristic fragment ions and dissociation efficiency properties, ECD/ ETD are regarded as the complementary method to slow heating ion activation methods. The use of two or more different dissociation methods can help to retrieve more structural information and get better understanding of the analyte molecules.

1.3 Electron capture dissociation

Electron capture dissociation has become an important ion activation method for peptide sequencing since its first introduction by Zubarev and co-workers in 1998 [37]. ECD is a radical driven dissociation method which is commonly operated in a FTMS instrument. Low energy electrons can be generated by a hot filament, a hollow dispenser cathode or a cold cathode electron emitter [43]. When a precursor ion captures a low energy electron, neutralization of one of the charges of the ion would lead to the formation a radical intermediate and cause predominantly cleavage of backbone N-C_α bond to give *c-/z*˙- ions.

$$[\mathrm{M} + \mathrm{nH}]^{n+} \xrightarrow{e^-} [\mathrm{M} + (\mathrm{n}-1)\mathrm{H}]^{(n-1)+\bullet} \rightarrow c/z^{\bullet}$$

Besides of non-selective nature of backbone cleavages and preservation of PTMs, ECD would preferentially cleave the disulfide bond in proteins [44], which is

stable to slow heating methods.

$$R_1S - SR_2(H^+) + e^- \rightarrow R_1SH + \bullet SR_2$$

1.3.1 ECD mechanisms for protonated peptides ions

There are two major mechanistic models for the dissociation of peptide/ proteins ions in ECD. They are known as the "hot hydrogen atom" model (Cornell Mechanism) [44] and the "amide-superbase" model (Utah-Washington/ UW Mechanism) [45]. Scheme 1.2 shows a schematic diagram for the "hot hydrogen model". In this model, the electron is captured to the high Rydberg state of the precursor ion, which is followed by the auto-emission of the captured electron to the continuum or landing on the protonated site of the peptide/ protein. Charge neutralization occurs with the formation of a hypervalent radical intermediate. The unstable hypervalent species will then emit a hydrogen atom with parties of the recombination energy. Capture of the hot hydrogen atom by a backbone carbonyl will give an aminoketyl radical intermediate. The radical will then initiate cleavage of the adjacent N-C_α bond.

Scheme 1.3 illustrates a schematic diagram of the "amide-superbase" model. For the "amide-superbase" model, it suggests the presence of remote charge is believed to increase the electron affinity (EA) of the amide group of peptide/ protein ions. The high EA amide π^* orbital of amide bond will then capture an electron exothermically. The anionic amide carbonyl group resulted will then abstract a proton from the protonation site in the vicinity and form a labile aminoketyl radical. The peptide ions will then dissociate through the N-C_α bond cleavage. This mechanism provides an alternate to explain the non-selective backbone cleavage in ECD. Furthermore, it explains the existence of ECD fragments even when mobile proton does not exist for electron capture, such as in the case of fixed charge

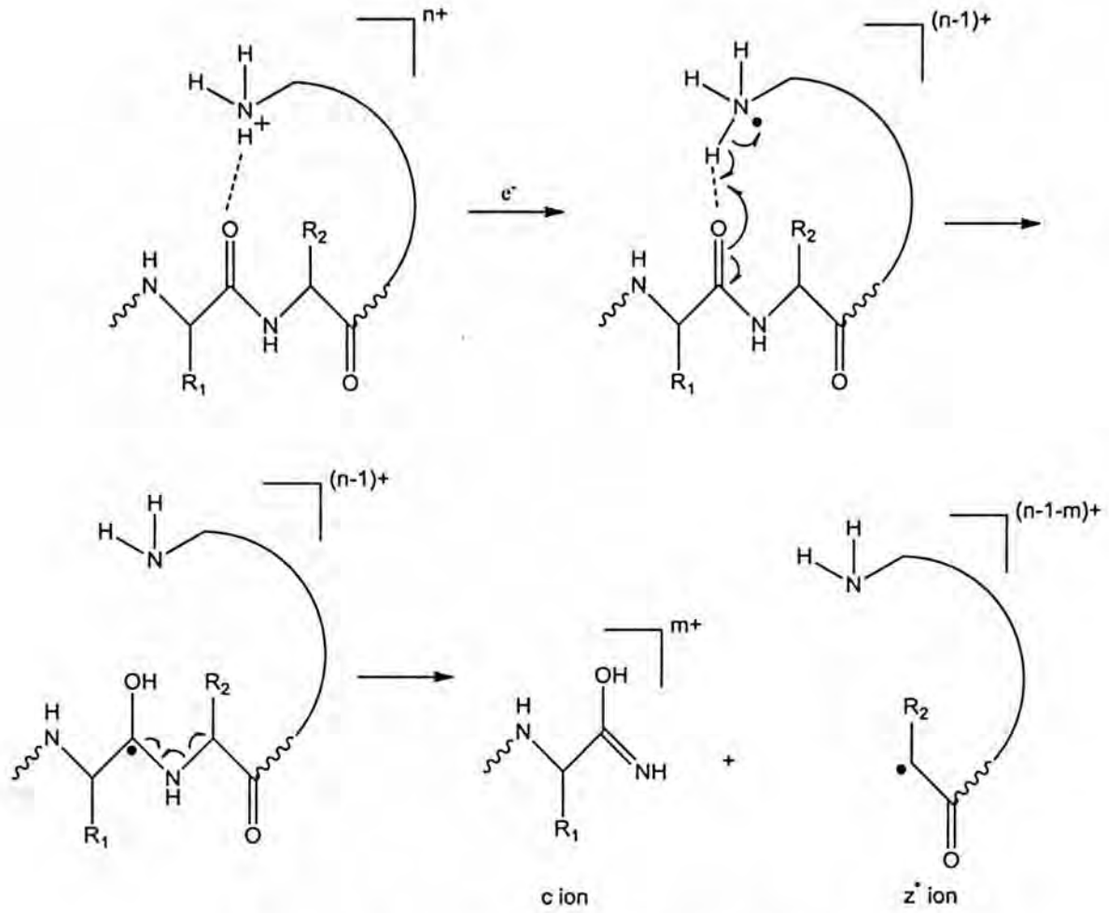

Scheme 1.2 "Hot hydrogen atom" model

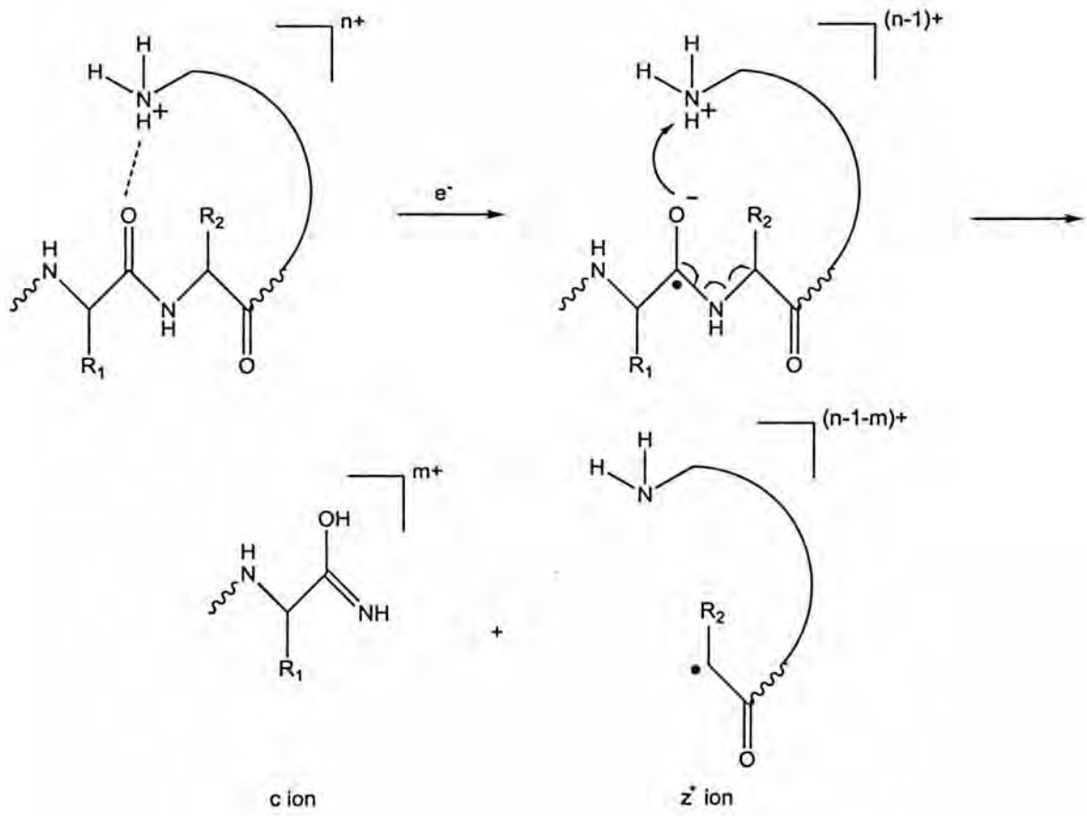

Scheme 1.3 "Amide-superbase" model

derivatives (quaternary ammonium groups).

1.3.2 ECD efficiency

Even though ECD has many advantages for peptide sequencing, one of the major limitations that reduce its propensity for wide usage is the low dissociation efficiency. Some modified ECD methods are developed to improve the situation. These methods include the use of dispenser cathode as electron emitter instead of hot filament [47], activated ion electron capture dissociation (AI-ECD) [48], external accumulation before electron capture dissociation (XA-ECD) [49], hot electron capture dissociation (HECD) [50] and sustained off-resonance irradiation electron capture dissociation (SORI-ECD) [51].

Efficient electron capture by the precursor ions is one of the important aspects to increase the dissociation efficiency. The hollow dispenser cathode can produce higher electron flux and result in better overlap of electron beam and ions. Besides of the low overlapping of the electron beam and the precursor ions, another reason for the low dissociation efficiency of ECD is the holding of the fragment ions together by the intra-molecular non-covalent interactions (mainly hydrogen bonding). In AI-ECD, a slow heating ion activation technique is used in conjunction with ECD. This is developed to increase the population of ions with less intra-molecular non-covalent interactions. Examples of AI method include IR laser and thermal heating of precursor ions [52, 53]. They are usually used prior ECD. In-beam ECD [44, 54, 55] and plasma ECD [56] are modified AI-ECD methods. For in-beam ECD, precursor ions and electrons are introduced to the trapped cell along with the collision gas (argon or nitrogen gas) at a pressure of $\sim 10^{-6}$ Torr. For plasma ECD, the electrons are first introduced into the cell with a gas pulse, followed by the ion beam to form a "plasma". This method helps to increase the number of backbone cleavages,

reduces the probability of secondary dissociation of large fragment ions and is able to locate the PTM groups when compared to conventional AI-ECD. XA-ECD not only provides a higher abundance of precursor ions, but also results a more centered ion beam, which can maximize overlapping of precursor with the electron beam. In HECD, the energy of the electrons are 3-13 eV, which is higher than those used in normal ECD (< 0.2 eV). With excess energy, abundant secondary fragmentation of amino acid side chain from $z^{\bullet}$- ions is induced. This is useful to distinguish the isomeric amino acid residues, such as leucine and isoleucine. SORI-ECD is presented to solve the problem of misalignment of ion cloud and electron beams that leading to the low fragmentation efficiency of ECD. By applying the SORI conditions to the ions trapped in the cell, the ion cloud can move into or cross the electron beam during irradiation. The probability of electron capture is then increased and thus the fragmentation efficiency is improved.

1.3.3 ECD of metal-adducted peptide ions

Instead of using proton as the charge carrier, other types of charge carriers have been adducted onto the peptides/ proteins to study their dissociation behavior under electron capture conditions. It aims to provide more complementary sequencing information of the peptides/ proteins compared to protonated peptides. ECD of peptides adducted with different types of metal ions, including the alkali metal ions [57], alkaline earth metal ions [58, 59] and transition metal ions [59-61], have been studied. Since the amount of internal energy that deposit onto the peptide ions after electron capture depends on ion-electron recombination energy, which is deduced from the ionization potential, the use of metal ions as charge carriers can be a tunable parameter for internal energy deposition. Since the binding properties of metal ions to peptides are generally different from that of protons, other sequence specific

fragment ions might be formed.

1.4 Overview of present work

This project aims to investigate the origin(s) of the suppression of fragmentation under electron capture conditions in tandem mass spectrometry of peptide/ protein ions. Chapter One of this thesis introduces the importance of tandem mass spectrometry in protein sequencing. Different ion activation methods used currently and the details of underlying mechanism of ECD are also provided. Chapter Two describes the details of the instrument used in this study. Experimental conditions and the method for performing conformational search are also included. Chapter Three summarizes the experimental results of model peptides with various structural parameters, including the number and type of proton carriers and also the length of the peptide. Their effect on the suppression of N-C_α bond cleavages and also $H^\bullet$ loss from the charge reduced precursor ions under typical ECD conditions were studied. A model is proposed for explaining the suppression observed for peptides with 23 amino acid residues. The validity of the model suggested was tested and discussed in Chapter Four. ECD experiments were performed on peptide ions with N-methylated amino acid residues, proline residues instead of glycine spacers and the use of metal ions as charge carriers. Finally, Chapter Five gives the concluding remarks of the project.

Chapter 2

Instrumentation, Experimental and Calculation

2.1 Fourier-transform ion cyclotron resonance mass spectrometer

The theory of cyclotron resonance was first introduced by Lawrence in the 1930s [62]. Sommer and his colleagues then incorporated the principle of ion cyclotron resonance into a mass spectrometer in the 1940s [63]. The first experiment using FTICR-MS was performed by Comisarow and Marshall in the 1970s [64, 65]. Fourier-transform ion cyclotron resonance mass spectrometer (FTICR-MS) is an instrument with the advantages of high mass resolution and accuracy among different types of mass analyzers. Moreover, it can be coupled to many different sample ionization techniques, such as EI, CI, FAB, MALDI and ESI, etc. It is an ion trapping instrument, which tandem mass spectrometry (including the slow heating ion activation methods and electron capture dissociation) can be performed inside the analyzer cell. Thus, it has been one of the analytical tools that widely used in the research of biological studies.

2.1.1 Basic principle of FTICR-MS

A trapped ion cell is placed under a static magnetic field in a typical FTICR-MS. Two trapping plates, which located at the two end of the trapped ion cell, are orientated perpendicular to the magnetic field. Figure 2.1 shows a typical ICR trapped ion cell. The motion of ions inside the trapped ion cell is governed by the static magnetic and electric field, which are perpendicular to each other. The ions inside the cell are under three independent motions, including cyclotron motion, trapping harmonic oscillation and magnetron motion [66, 67].

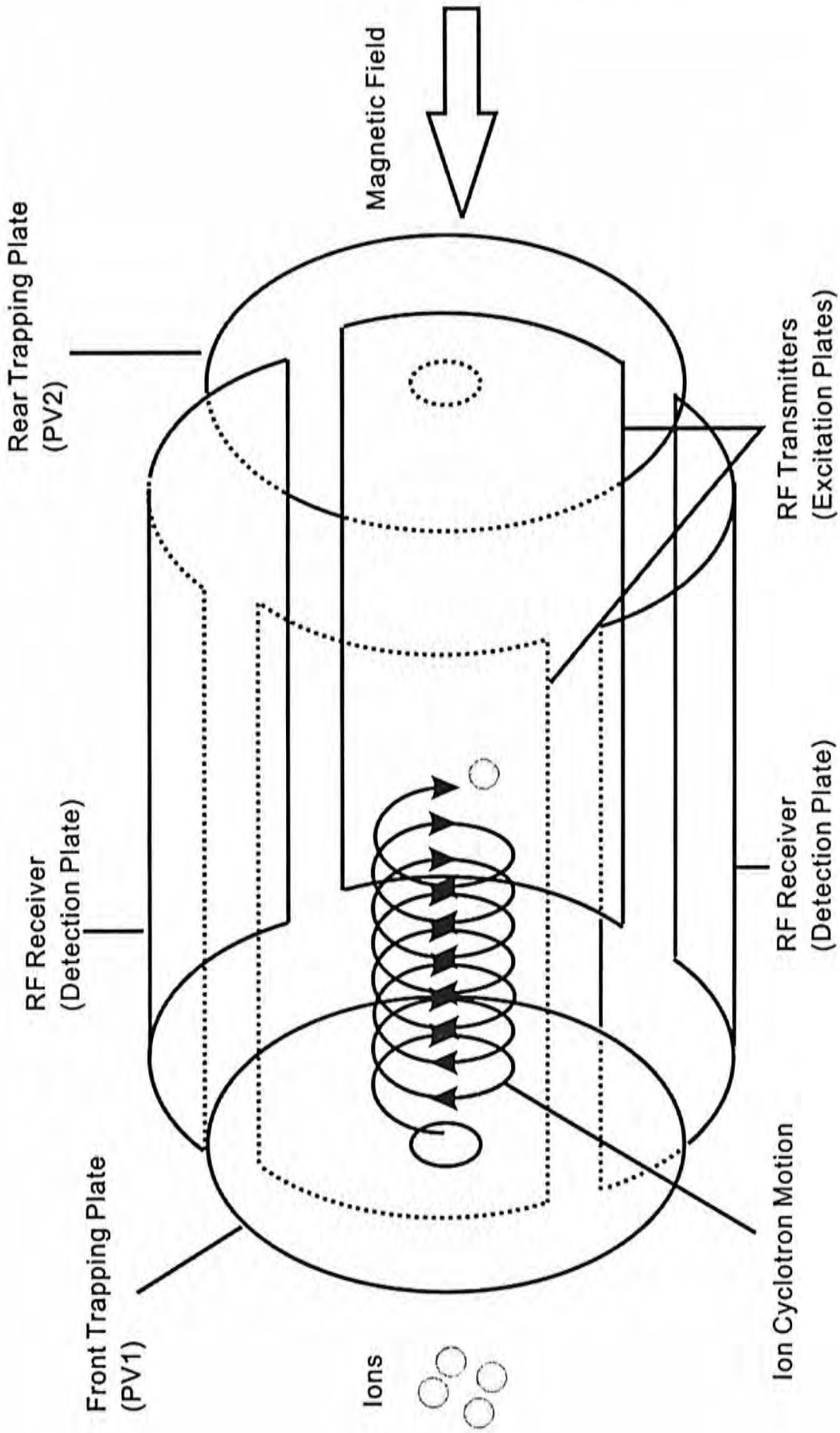

Figure 2.1 A schematic diagram of a typical ICR trapped ion cell

In a strong magnetic field, the motion of ions is constrained to circular cyclotron orbits, which results cyclotron motion of ions in the xy plane (the plane perpendicular to the magnetic field). The ions experience the Lorentz force, which is perpendicular to the magnetic field and also the direction of ions. The expression of the force is shown in equation 2.1,

$$\vec{F} = \vec{B}qv_{xy} \qquad [2.1]$$

where $\vec{B}$, q and v_{xy} are the magnetic field strength, the ionic charge and ion velocity in xy plane respectively. With angular acceleration, equation 2.1 becomes equation 2.2 as follows:

$$\frac{mv_{xy}^2}{r} = \vec{B}qv_{xy} \qquad [2.2]$$

where m is the mass of the ion and r is the cyclotron radius. The angular cyclotron frequency (ω_c) is defined by equation 2.3,

$$\omega_c = \frac{v_{xy}}{r} = \frac{q\vec{B}}{m} \qquad [2.3]$$

From the equation, the ion cyclotron frequency is thus directly proportional to the magnetic field strength (B) and inversely proportional to the mass-to-charge ratio (m/q or m/z), while it is independent of the ion velocity and thus kinetic energy. The magnetic field B can be treated as constant if it is stable, unidirectional and homogenous. Thus, the cyclotron frequency can be accurately determined and accurate mass measurement can be achieved.

Trapping harmonic oscillation of the ions along the z-axis of the trapped ion cell is caused by the electric field generated by the two trapping plates. The trapping frequency (ω_T) of an ion depends on the applied trapping potential (V_T), the mass-to charge ratio of the ions, the dimension of the analyzer cell (a) and the geometry factor of the cell (α). The trapping frequency can be expressed in equation 2.4:

$$\omega_T = \sqrt{\frac{2qV_T\alpha}{ma^2}} \quad [2.4]$$

The electric field (E_0) generated from the trapping electrodes produces a radial force with magnitude $\frac{qV_T\alpha}{a^2}r$ that acted onto the orbiting ions. This force opposes the direction of the Lorentz force generated from the magnetic field. The magnetron motion of ions is thus resulted [68-71]. The ion cyclotron motion is perturbed and the analytical solution for the ion motion is modified from equation 2.2 to equation 2.5 as follows:

$$m\omega^2 r = qB\omega r - qE_0 r \quad [2.5a]$$

or

$$\omega^2 - \frac{qB}{m}\omega + \frac{qV_T\alpha}{ma^2} = 0 \quad [2.5b]$$

By solving equation 2.5b, the reduced cyclotron frequency (ω_R) and the magnetron frequency (ω_M) can be obtained in equations 2.6 and 2.7 respectively:

$$\omega_R = \omega_+ = \frac{\omega_c}{2} + \sqrt{\left(\frac{\omega_c}{2}\right)^2 - \frac{{\omega_T}^2}{2}} \quad [2.6]$$

$$\omega_M = \omega_- = \frac{\omega_c}{2} - \sqrt{\left(\frac{\omega_c}{2}\right)^2 - \frac{{\omega_T}^2}{2}} \quad [2.7]$$

where ω_c is the "unperturbed" cyclotron frequency. Since the magnetron motion of the ions moves in the same plane as the cyclotron motion, the observed cyclotron frequency (ω_{Obs}) is slightly lower than its original cyclotron frequency. ω_{Obs} is obtained by equation 2.8:

$$\omega_{Obs} = \omega_c - \omega_M \quad [2.8]$$

The cyclotron motions of the ions induce an "image current" on the two detection plates. The incoherent motion of the ions in a small cyclotron radius will result in the cancelation of the detected image current induced by the ions and no current will be detected. In order to detect ions inside the analyzer cell, a radio frequency (*rf*) waveform provided by the two excitation plates is used to excite the trapped ions as shown in Figure 2.2. The *rf* electric field excites the ions of the same

ion cyclotron frequency to a larger radius and makes them move in a coherent motion as shown in Figure 2.2. Since the ions with different m/z have different ion cyclotron frequency, an image current that is at the characteristic frequency for ions with the same m/z is then generated by the detection plates. Different from other mass analyzers, FTICR-MS is not relied on the spatial separation of ions with different m/z [72]. The cyclotron frequency of all the ions in the cell will be detected in a transient signal. The time domain signal of the ions can be converted to the frequency domain signal by Fourier transformation. The frequency domain plot is then mass calibrated to give the mass spectrum.

2.1.2 The instrument

All experiments were performed in a 4.7 Tesla FTICR-MS (APEX III, Bruker Daltonics Inc., Boston, MA). A schematic diagram of the instrument is shown in Figure 2.3. The instrument composed of several parts, including a vacuum assembly, an external electrospray ion source (Analytica, Branfrod, CT), an electrostatic ion transfer system, an ICR trapped ion cell, a 65 mm wide-bore 4.7 Tesla horizontal superconducting magnet and a standard electrically heated filament electron source. The ion source has been modified to a homemade nanospray ion source. The details and functions of each part are described below.

2.1.2.1 Vacuum system

The vacuum system can be divided into three regions: the ion source region, the ion focusing region and the analyzer cell region. In order to achieve accurate mass measurement, ion-molecule collisions that would perturb ion cyclotron motion have to be minimized. Thus, ultra high vacuum conditions in the analyzer region need to be maintained. Differential pumping system is applied to separate the analyzer region

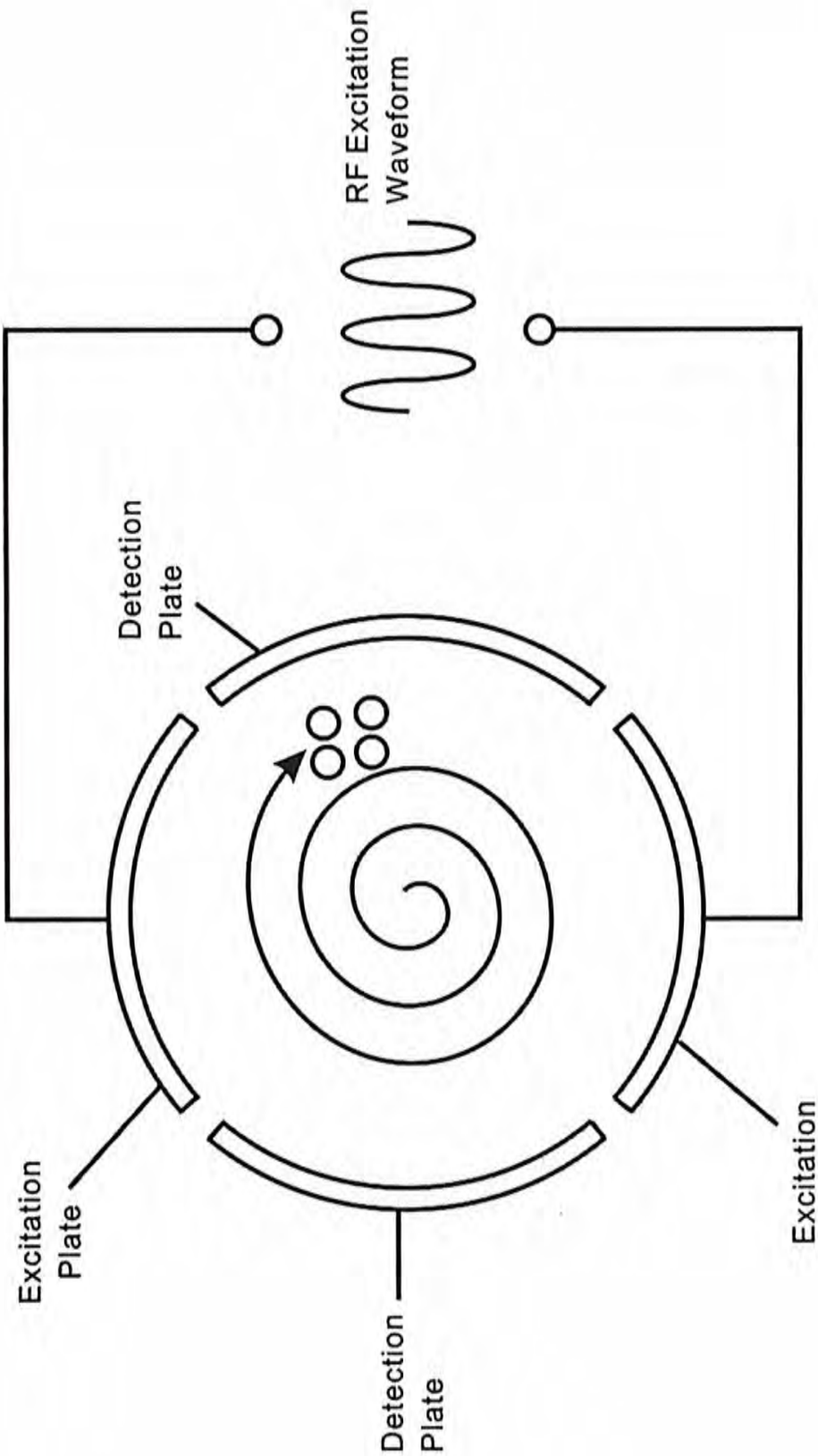

Figure 2.2 A schematic diagram of an ion excited by a radiofrequency (*rf*) excitation waveform inside an ICR cell.

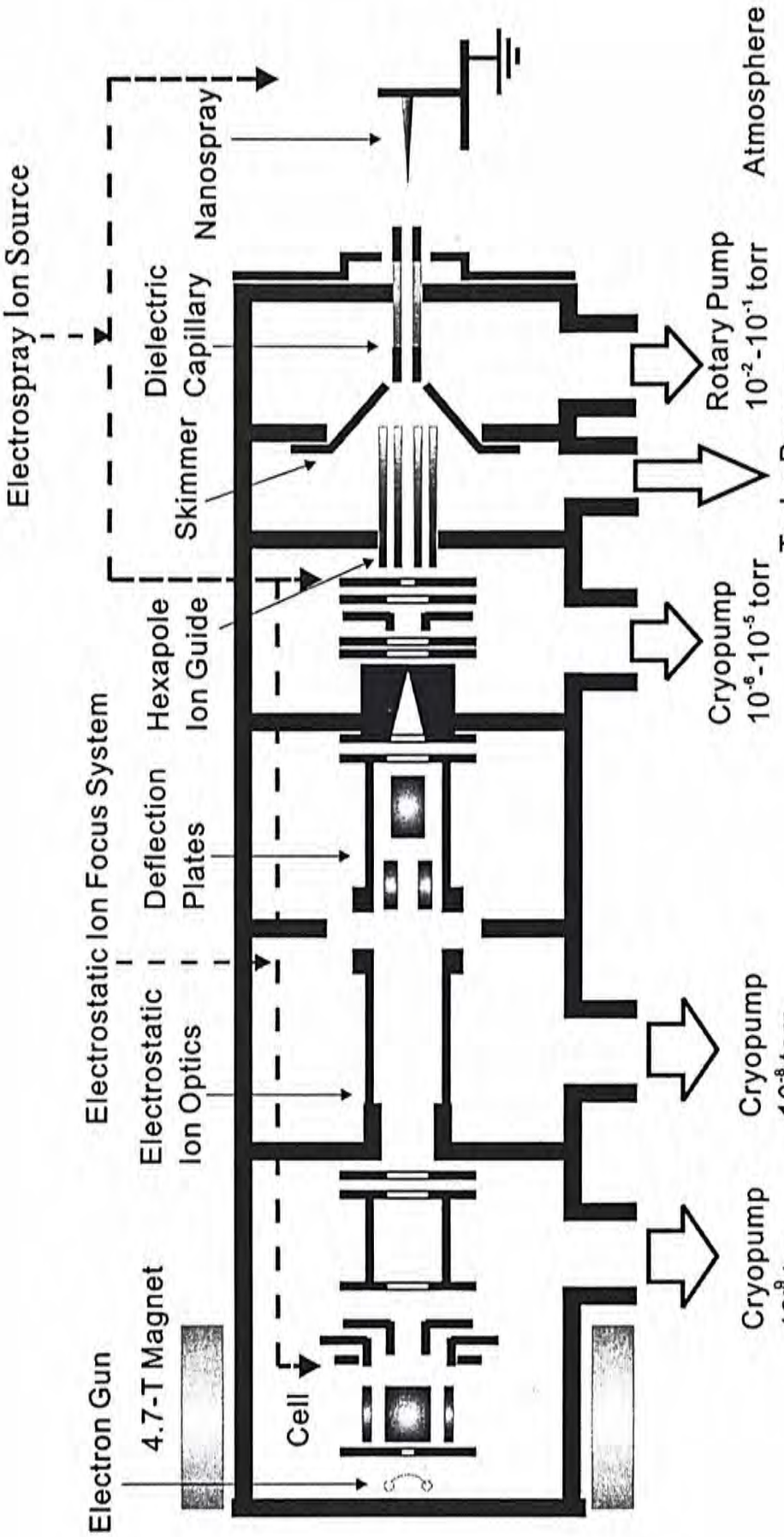

Figure 2.3 A schematic diagram of the Bruker FTICR-MS equipped with a homemade nanospray ion source.

from the ion source region, which there is a small opening for the entrance of the ions generated in the ambient conditions.

An auxiliary rotary pump (E2M18, Edwards Corporation, UK) and a 250 L/min turbomolecular pump (EXT250HI, Edwards Corporation, UK) were installed in the ion source region. The turbomolecular pump was interconnected with the auxiliary rotary pump. There was a roughing rotary pump (E2M18, Edwards Corporation, UK) at the front of the ion transfer region for the source roughing. To achieve higher vacuum, there were three cryopumps installed in the vacuum system, including a Coolstar cryopump 800 L/min (Edwards Corporation, UK) in the ion source region, a Coolstar cryopump 400 L/min (Edwards Corporation, UK) in the ion transfer region and a Coolstar cryopump 800 L/min (Edwards Corporation, UK) in the analyzer cell. All three pumps were controlled by a Cryodrive 3.0 (Ricor Limited, Israel), which could be computer-controlled through a program called Ricor PLC Communications.

Under typical pumping process, compressed liquid helium was circulated to the three cryopumps from the cryodrive. The cryodrive was then cooled by a refrigerated recirculator (CFT-150, Neslab, US). There was a hydrogen gas thermometer associated with each cryopump, which was used to monitor the temperature of cold head and thus the performance of the cryopump.

To pump down the whole system from the atmospheric pressure, the opening of the dielectric capillary in the ion source region was covered with paraffin film. The vacuum system was first pumped by two rotary pumps until the pressure below 10^{-2} Torr. The turbomolecular pump was then turned on to pump the system until the pressure reached 5×10^{-3} Torr. The cryodrive was then switched on and thus the three cryopumps were then turned on. A valve located between the roughing rotary pump and the vacuum assembly was closed automatically when the pressure of the system was lower than 8.0×10^{-4} Torr. The system was continued to pump down

until the pressure was around 10^{-9} Torr. Under normal working conditions, the pressure at the dielectric capillary and the hexapole ion guide were $10^{-2} - 10^{-1}$ Torr and $10^{-4} - 10^{-3}$ Torr respectively; the pressure at the front and rear of the ion transfer region were $10^{-6} - 10^{-5}$ Torr and 10^{-8} Torr respectively; and the pressure at the analyzer cell region was about 10^{-9} Torr. The vacuum conditions of the ion focusing region and analyzer cell region were monitored by two cold cathode gauges (IKR 020, Balzers, Liechtensteion), which were located above the two Coolstar cryopump 800. Since the cold cathode gauge has to be operated under the pressure of 1×10^{-4} Torr, a pirani gauge (TPR 010 Balzers, Liechtensteion) was used instead when the pressure of the ion focusing region reached 1×10^{-4} Torr.

To preserve the ultrahigh vacuum conditions of the analyzer cell region and the pumping status of the front Coolstar cryopump 800 in the ion source region when venting the ion source for exchange of ion sources and cleaning the dielectric capillary, a mini UHV-Schieber gate valve (DN50, VAT Vakuumventile AG, Haag) and a Vatterfly valve (DN160 Vatterfly Valve Series 20, Vat Vakuumventile AG, Haag) were installed. The gate valve was installed to isolate the ion source region from the analyzer cell region, while the Vatterfly valve was installed to separate the front Coolstar cryopump 800 from the ion source region.

Besides the above two valves, there were a leak valve and an electromagnetic pulse valve installed near the analyzer region. The leak valve was controlled manually by adjusting the knob of the leak valve. It was used for the introduction of the volatile samples into the analyzer ion cell. The electromagnetic pulse valve was controlled by a TTL pulse generated by the console. It was used when introducing buffer or collision gases into the analyzer cell. A small gas cylinder was connected to the pulse valve system. The buffer or collision gas was first introduced to the gas cylinder, so as to control the pressure of gas loaded into the analyzer cell.

2.1.2.2 Nanospray source

The commercial available electrospray ionization source composed of two major parts, a spray chamber and ion transfer optics. The spray chamber was modified to adapt a homemade nanospray assembly as shown in Figure 2.4 [73]. The homemade nanospray ion source consisted of a platform, which could be adjusted in x, y and z directions. A thin gold-plated tungsten wire (Ø = 10 μm) was spot-welded onto a platinum wire (Ø = 0.3 mm), which was screwed on the platform. Sample solution was loaded into a homemade glass capillary tip. The gold-plated tungsten wire was placed inside the glass capillary tip for electrical contact. The glass capillary tip was placed a few centimeters away from the opening of the dielectric capillary. The dielectric capillary was made in glass with two stainless steel caps at both ends (18.0 cm long). The platinum wire was grounded and a negative potential (V_{cap} ~1000 V) was applied to the entrance of the metal cap of dielectric capillary to produce a stable spray of sample solution. Negative potential was for positive ion mode, while positive potential was for negative ion mode. A flow of heated dry nitrogen gas (~ 275 ℃) was used to facilitate solvent evaporation from the sprayed droplets.

The entrance and exit of the dielectric capillary acted as two electrodes (V_{cap} and L1 respectively). The ion transfer optics was located in the low vacuum region of the nanospray assembly. It consisted of a skimmer (L2), an Iris^{TM} hexapole ion guide (L3) and a gated electrode (L6). The hexapole ion guide was used for external ion accumulation for a pre-defined time. The ion transfer optics helps to focus the ions across the relatively high pressure region.

The dielectric capillary and the skimmer were of small orifice, so as to limit gas flow from the atmosphere into the vacuum region during ion spraying process. The region between the capillary and the skimmer was pumped to a low vacuum of

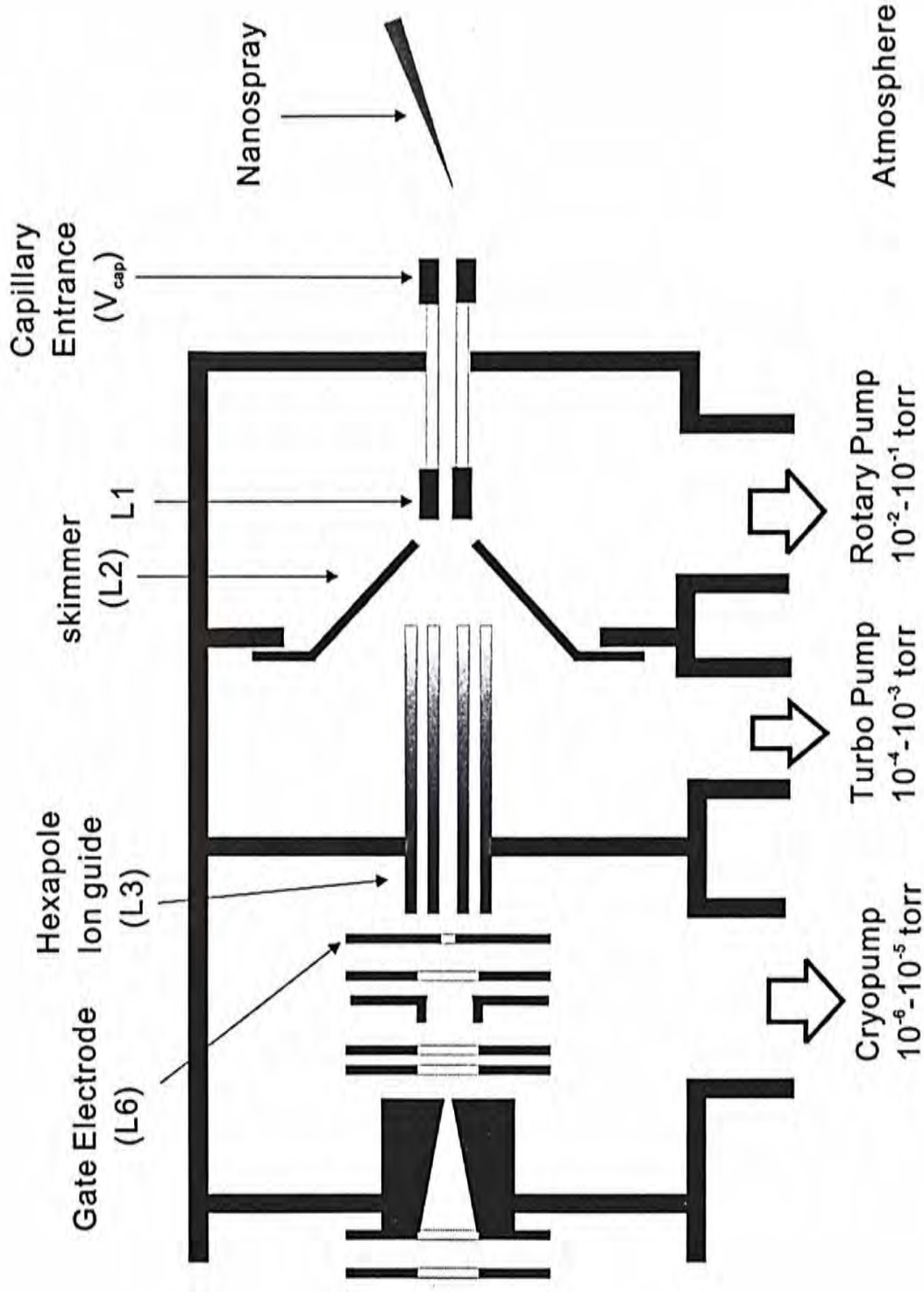

Figure 2.4 A schematic diagram of homemade nanospray source.

around 10^{-1} – 10^{-2} Torr by the rotary pump. The pressure between the region of the skimmer and the hexapole ion guide was pumped down to 10^{-3} – 10^{-4} Torr by the turbomolecular pump.

The typical potential applied to L1 was about 100 V (positive potential for positive ion mode and vice versa), which was the potential barrier for the transfer of analyte ions. The gas flow due to the pressure difference between the atmospheric region and the capillary skimmer region (~10^{-2} – 10^{-3} Torr) was believed to help the ions to overcome the barrier. The *rf*-only hexapole ion guide focused the analyte ions and the ions would be accumulated and oscillated along the central line of the ion guide under the influence of the *rf*-potential for a predefined time. In positive ion mode, ions were trapped inside the ion guide when L6 was held at positive potential. When a negative potential was applied to L6, the ions were extracted and directed to the analyzer cell through the ion transfer region.

2.1.2.3 Electrostatic ion focusing system

The electrostatic ion focusing system was composed of a series of electrostatic lens, which installed in between the ion source region and the analyzer cell region. It was used to guide and focus the ions that transferred from the ion source to the analyzer cell. Figure 2.5 shows a schematic diagram of all the ion optics and their corresponding potential gradient curve.

The system consisted of two different kinds of ion optics, including the ion focusing lens and the ion beam steering electrodes. PL1, PL9, FOCL1 and FOCL2 were the ion focusing lens, while PL2/ DPL2 and PL4/DPL4 were ion beam steering electrodes in y- and x-axis respectively. The potentials of the ion beam steering electrodes were set at some preset values, so as to guide the ions into the analyzer cell.

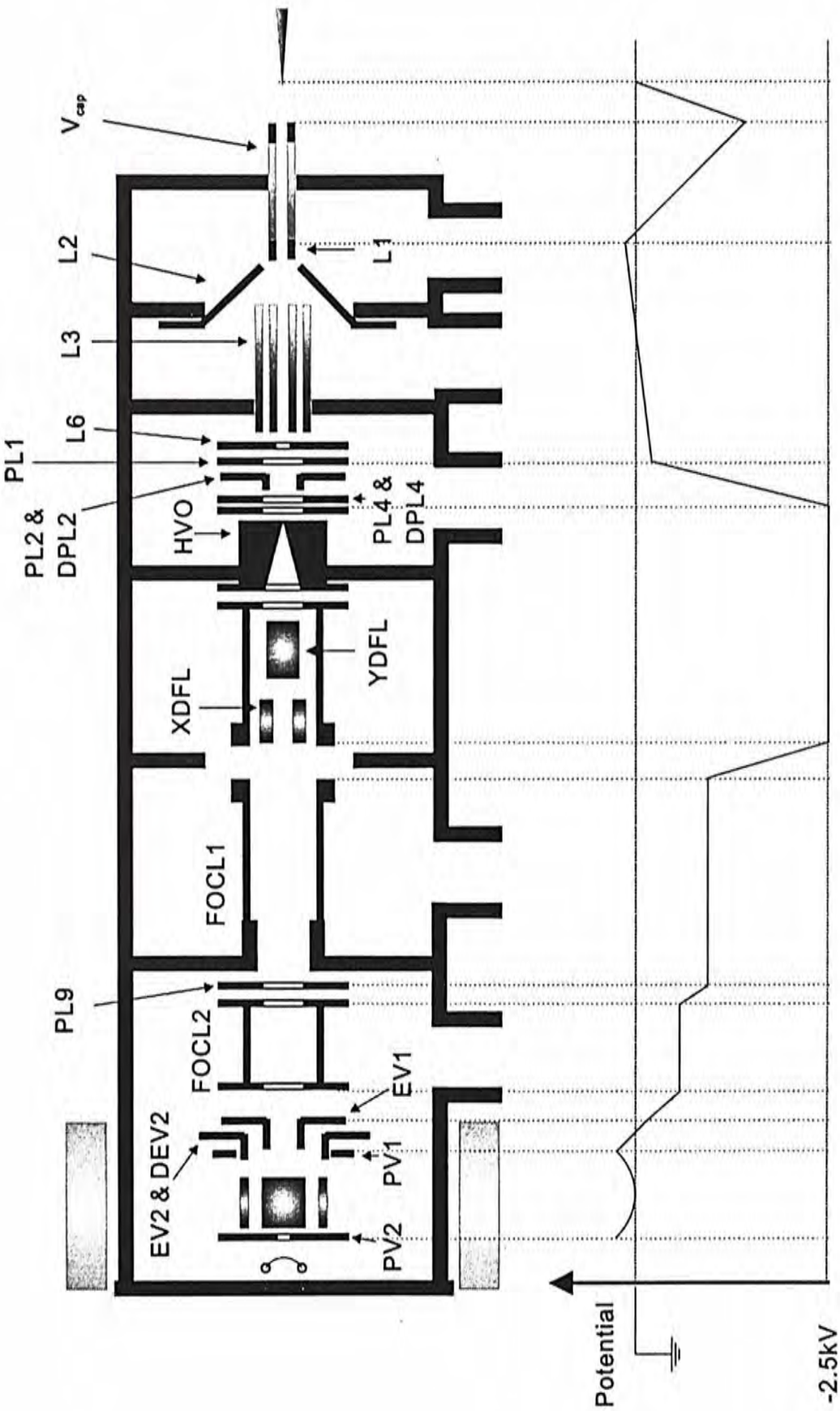

Figure 2.5 A scheme diagram of potential gradient along the ion source, the electrostatic focusing system and the Infinity™ Cell .

HPO, as shown in the figure, was a high potential electrode with a typical potential of -2.5 kV for positive ion mode and 2.5 kV for negative ion mode. Its function was to accelerate the ions to a higher velocity, so as to increase the ion transmission efficiency through the magnetic field. There were also other electrodes present to assist the ions to reach the analyzer cell. XDFL and YDFL were two pairs of deflecting plates used to correct the path of the ion beam in x- and y-direction respectively. They were floated at the potential of HVO. EV1 was the entrance electrode of the analyzer cell. It was set at a slightly negative potential (for positive ion mode) to pull the decelerated ions into the analyzer cell. EV2 and DEV2 was a pair of split electrodes that located behind EV1. They were used to provide a "kicker voltage" to deflect the ion beam along the xy plane. It could increase the trapping efficiency of the cell.

2.1.2.4 Infinity^{TM} Cell

The analyzer cell used in this FTICR-MS was an Infinity^{TM} Cell [74] (Bruker-spectrospin, Fällanden, Switzerland). The Infinity^{TM} Cell was a cylindrical cell with dimensions of 60 mm in diameter and 60 mm in length. The electrodes in the Infinity^{TM} Cell were all gold-coated. PV1 and PV2 were two trapping electrodes at the front and rear ends of the Infinity^{TM} Cell. There was a circular aperture (6 mm in diameter) in the centre of each trapping plate, which allowed the entry and exit of ions and/ or electrons. Four curved electrodes were installed orthogonal to the trapping plates. The shorter pair of electrodes was the excitation plates, which *rf*-excitation pulses would be applied to these two plates. During the excitation event, the waveform generated by a high frequency unit (HFU) located inside the APEX III console (Bruker Daltonics Inc., Billerica, US) was amplified by a *rf*-power amplifier. The excitation waveform used for broadband mode was the chip excitation. The

other pair of electrodes acted as the detection plates. They detected the image current generated by the cyclotron motion of the trapped ions.

The Infinity™ Cell has some advantages over standard analyzer cells. The trapping plates of the Infinity™ Cell were segmented to avoid undesirable z-axial ejection of the trapped ions during ion excitation event. In addition, the trapping condition of the Infinity™ Cell is also different from other standard analyzer cells. The potential of the front trapping plate (PV1) is kept constant throughout the whole event. During ion accumulation, the potential of EV1, EV2 and DEV2 were set at some preset values for the admission of ions into the cell, which would be restored to same potential as PV1 to close the cell after ion accumulation.

2.1.2.5 Electron emission source

The Infinity™ Cell was equipped with an electrically heated filament for electron emission. A schematic diagram of the heated filament electron source is shown in Figure 2.6. The filament was made of a ~0.5 mm wide rhenium ribbon. It was spot-welded onto two metal pins (pin 1 and pin2), which separated from each other at ~6 mm. Under ambient conditions, the resistance of the filament was 0.5 Ω. A metal plate that directly connected to pin2 was placed at the back of the filament. It was used to repel the electrons when a negative potential was applied to pin2 for electron injection into the analyzer cell. Under typical conditions which there was no filament heating current and electron irradiation, equal potential of +13.2 V was applied to both pin1 and pin2. When current flew through the filament, different potentials were loaded onto pin1 and pin2. The resulting potential of pin1 would be higher than that of pin2. During electron irradiation in ECD, the potentials of pin1 and pin2 were ramped down to a negative value. Since pin2 would have a more negative value than pin1, electrons emitted from the filament would be repelled by

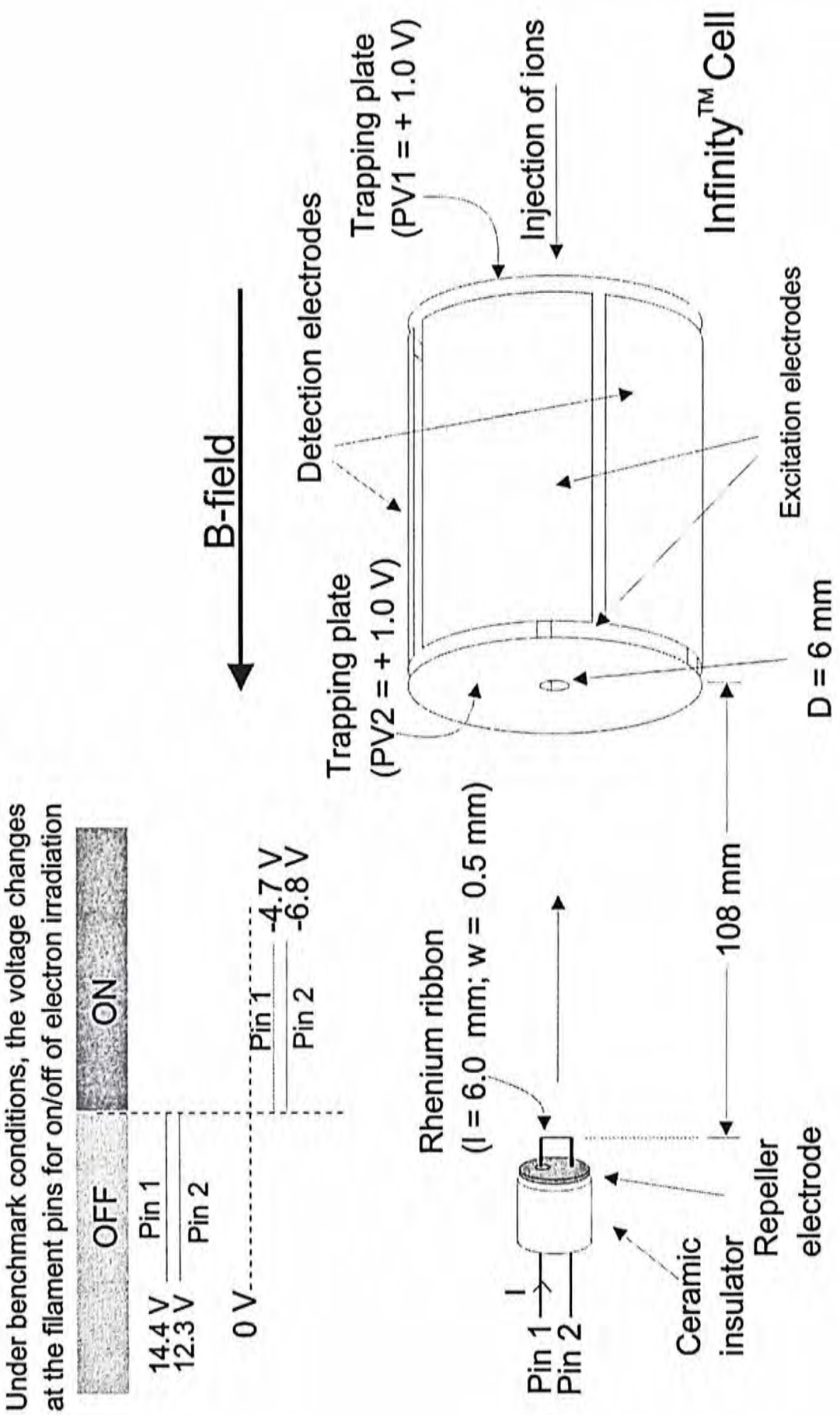

Figure 2.6 A schematic diagram of the heated filament electron source and the Infinity™ Cell.

the metal plate and entered the analyzer cell.

2.1.2.6 Data acquisition system

The console of the FTICR-MS was connected to a Dell window-based workstation PWS530 (Dell computer Corporation, Texas, US). It was equipped with an Intel (R) XEO microprocessor and 32 megabytes (Mb) of base memory and operated under the Microsoft Windows 2000 operation system. A user-interface program XMASS version 6.1.0 (Bruker Daltonics, Billerica, US) running on the workstation was used for tuning of experimental parameters, data acquisition and data manipulation.

The free induction decay (FID) signal was received and amplified by either FADC 12-bit digitizer (for broadband mode) or SADC 16-bit digitizer (for narrow-band mode). The maximum size of the time domain signal was 1 Mbytes. The FID signal was transferred to the Dell workstation after data acquisition had been completed. It was then zero-filled once and converted to the frequency domain signal (mass spectrum) by Fast Fourier transform (FFT) algorithm and magnitude calculation method.

2.2 Experimental

2.2.1 Acquisition pulse program

A pulse program described the data acquisition procedure for the experiments performed in the FTICR-MS. During acquisition, a sequence of pulses was sent to different units of the FTICR-MS to control the corresponding events according to the pulse program. The source code of the pulse programs used is stated in Appendix II.

2.2.1.1 Simple ESI acquisition pulse program (MS experiment)

Figure 2.7 shows the pulse program for obtaining a simple ESI mass spectrum in a FTICR-MS experiment. In general, there were four steps in each acquisition cycle, which were ion quench, ion accumulation, ion excitation and ion detection. The acquisition cycle started with the removal of all ions in the Infinity™ cell and ESI source. For the Infinity™ cell, a quench control pulse was sent to the voltage control board to pulse the potential of the rear trapping plate (PV2) to negative potential (-10 V) for the positive ion mode or positive potential (+10 V) for the negative ion mode. It was then followed by sending the quench control pulse to the voltage control board to change the potential of the gate electrode inside the ESI source. The gate electrode was pulsed to negative potential for positive ion mode and positive potential for negative ion mode to remove any residue positive ions in the hexapole ion guide. After the quench pulses, a short delay was applied to restore the potential of the rear trapping electrode and gate electrode back to the preset values.

Ion accumulation event was carried out by storing the ions generated from the nanospray source in the hexapole ion guide for a predefined delay period. An ion ejection pulse was then executed by changing the gate potential to the preset extraction potential in order to extract the ions to the electrostatic ion focusing region. After the extraction process, the deflector voltages (DPL2 and DPL4) and the entrance electrodes of the Infinity™ Cell (EV1, EV2 and DEV2) were adjusted to the preset values so as to guide the ions towards the Cell. The ions were then accumulated inside the Cell for a predefined period of time. This was followed by restoring the deflector voltages to ground voltages and the voltages of the entrance electrode to the same potential as PV1.

After ion injection event, an injection pulse was executed. A chip of *rf*-waveform was transmitted through the excitation electrodes of the Infinity™ Cell. The *rf*-waveform scanned from the cyclotron frequency of the lowest detection mass

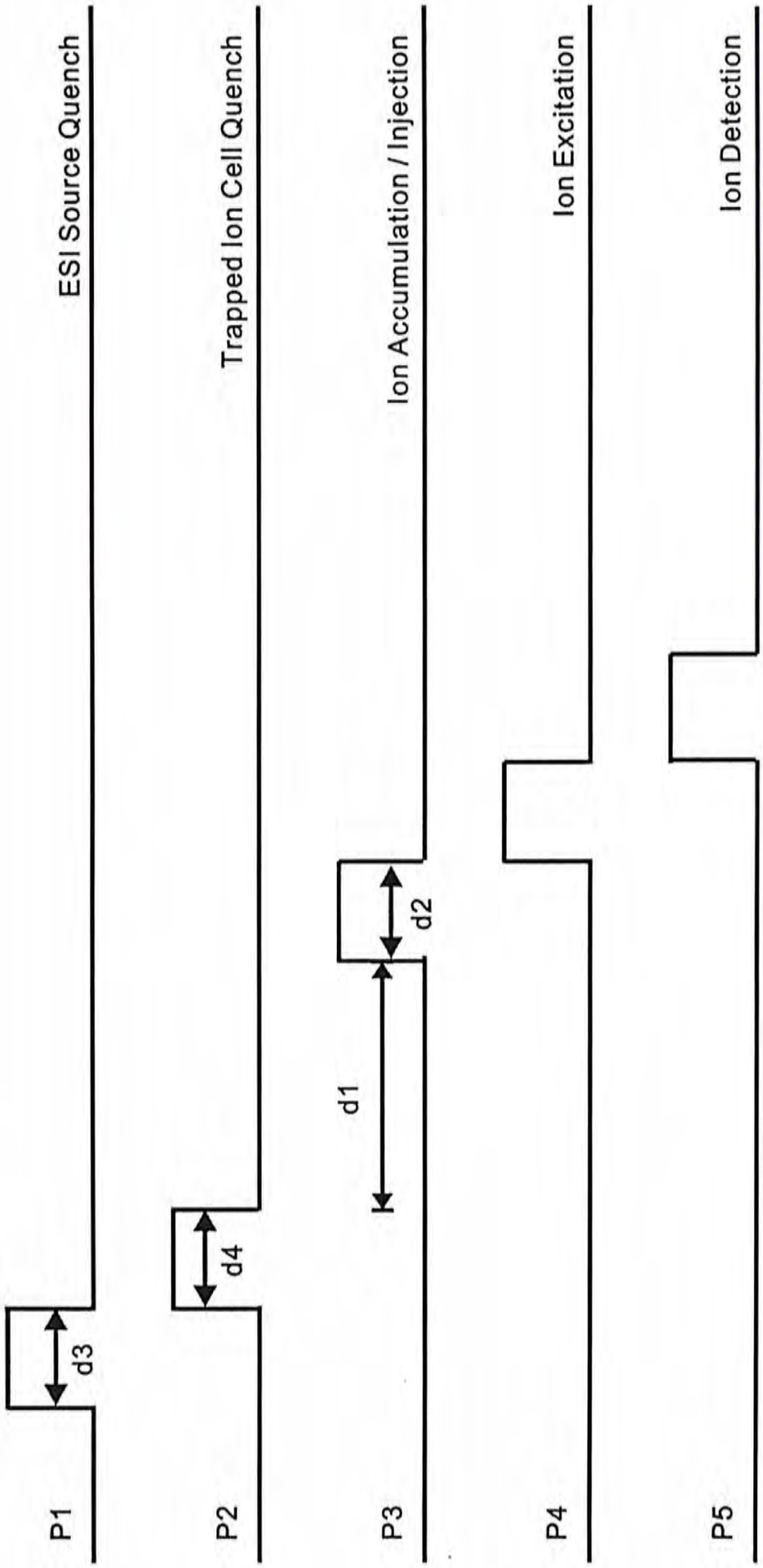

d1 : Ion accumulation delay d2 : Ion flight time d3 : Ion guide quench time d4 : Cell quench time

Figure 2.7 A pulse sequence program for simple ESI FTICR-MS experiments.

(highest frequency) to the highest detection mass (lowest frequency), in which the amplitude and duration of the *rf*-waveform could be optimized to give an intense signal.

The last step of the pulse program was ion detection. The *rf*-detector plates of the Infinity™ Cell detected the image current generated from the cyclotron motions of the excited ions and FID signal was obtained. The above acquisition cycle were repeated for a pre-defined number of times and the signal for each scan were summed up to improve the signal to noise ratio.

2.2.1.2 ESI-ECD acquisition pulse program (MS^2 experiment)

To perform the tandem mass spectrometry experiments, the ions of interest are isolated out for activation process. For ECD experiments, the precursor ions were irradiated with low energy (< 5 eV) electrons. The pulse program of electron capture dissociation is shown in Figure 2.8. It was similar to that of the simple ESI acquisition experiment. Two additional steps were added in between the ion accumulation and ion excitation processes, which were ion selection and electron irradiation. After the ion accumulation process, an ion selection pulse was executed. The ions of interest were isolated by applying a correlation sweep (a modified chirp of *rf*-waveform). All the unwanted ions were over-excited. To minimize the excitation of the ions of interest and maximize the ion ejection efficiency, the amplitude and duration of *rf*-waveform were carefully adjusted and the "ejection safety belt" was optimized. An electron irradiation pulse was executed after the ion selection process. The potential of the two pins on the electron source (pin1 and pin2) were pulsed and changed from positive to negative. An electron beam was then emitted and directed into the Cell to interact with the selected ions for a preset period of time. The electron flux and electron energy were adjusted by varying the filament

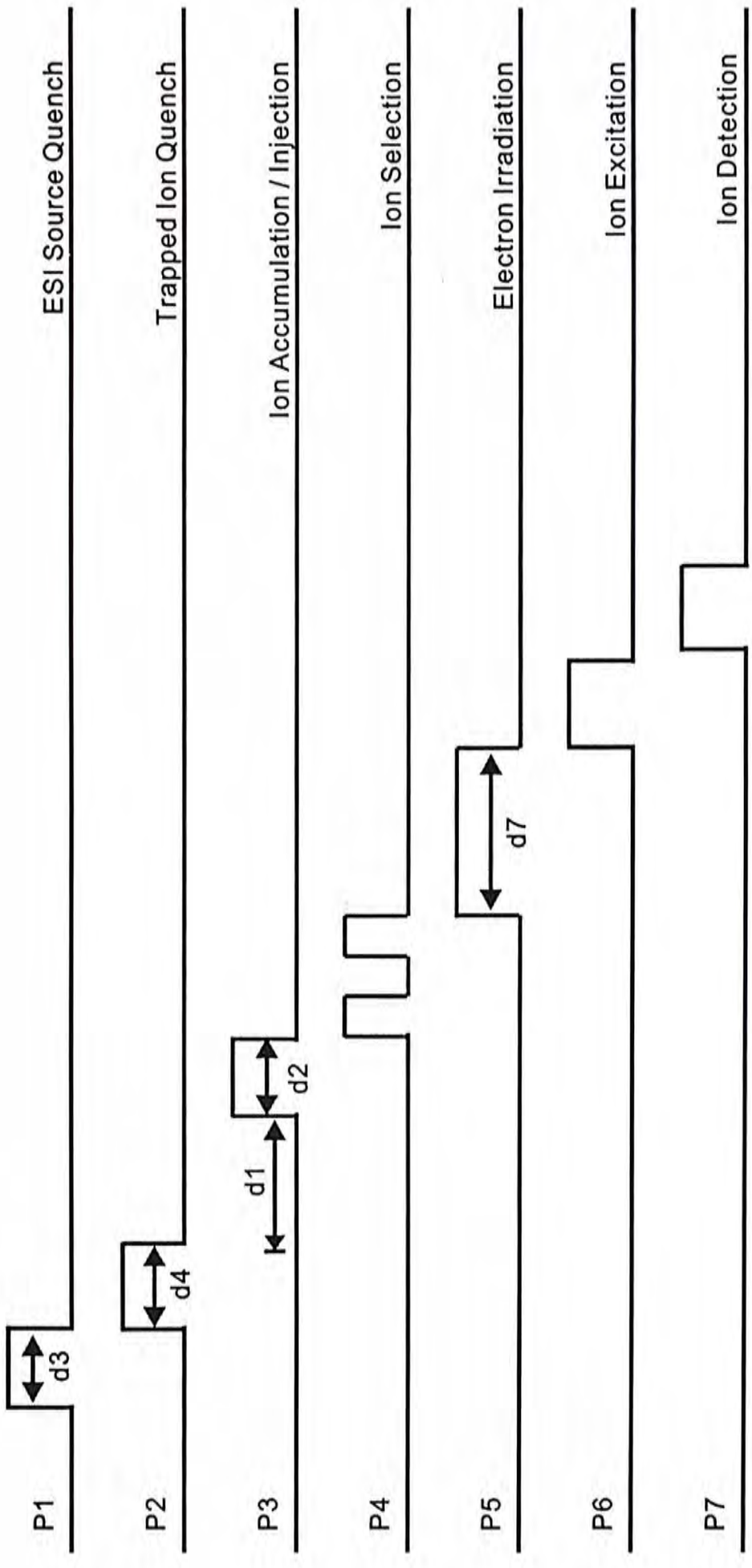

d1: Ion accumulation delay d2: Ion flight time d3: Ion guide quench time
d4 : Cell quench time d7: Electron irradiation time

Figure 2.8 A pulse sequence program for ESI-ECD FTICR-MS experiments.

heat current and the average filament voltage respectively to maximize the ECD fragment intensities.

2.2.2 Molecular mechanics calculation

Low energy conformers of target model peptides were found and obtained by performing molecular mechanics using MacroModel Program (ver. 5; Schrödinger Inc., Portland, OR, USA). Merck molecular force fields (MMFFs) and conformational searching were used, in which the mixed Monte Carlo Multiple Minimum (MCMM) [75] and Low Mode Conformational Search (LMCS) method were chosen. All the bonds were allowed for random rotation [76]. The minimization method used was Truncated Newton Conjugate Gradient (TNCG). Initial search was first done by doing 5000 steps of conformational search to find the low energy conformers. The structures being stored would have the energy not greater than 50 $kJmol^{-1}$ compared to that of the lowest energy conformer. At most 10 structurally different structures from the initial search were chosen to perform another 5000 steps conformational search. Energies of all the structures were then aligned and the relative abundance of the low energy conformers was calculated using Boltzmann distribution. Only those low energy conformers with abundance > 1 % were chosen to study the hydrogen bonding pattern.

Chapter 3

Structural Parameters Affecting Suppression of N-C_α Cleavages of Peptides Ions after Electron Capture

3.1 Introduction

The non-selective nature of the backbone cleavages of polypeptide ions and the preservation of post-translational modifications (PTMs) [39-41] in fragment ions are important features in ECD, making it an indispensible tool for peptides/ proteins sequencing. In a typical ECD experiment, the multiply charged precursor ion captures a low energy electron to form the charge-reduced precursor ion, $[M+nH]^{(n-1)+\bullet}$. With the liberation of recombination energy and the instability of the radical ions formed, typical fragmentation of $[M+nH]^{(n-1)+\bullet}$ which involves the major dissociation of backbone N-C_α bond to give *c*-/*z*$^\bullet$- ions, a minor dissociation pathway to give *a*$^\bullet$-/*y*- ions and loss of hydrogen atom ($H^\bullet$), small neutral molecules and side chain of amino acid residues from $[M+nH]^{(n-1)+\bullet}$ were resulted.

Despite the popularity of ECD method for peptides/ proteins sequencing, the mechanistic aspects of the dissociation process remain controversial. The "hot hydrogen atom" model and the "amide-superbase" model are two prevailing mechanisms that were proposed to explain the cleavage of N-C_α bond. However, there are still some characteristic ECD fragmentation patterns that required much more mechanistic details to fully explain those fragmentation behaviors. The little influence of the primary sequence of the polypeptide ions on the ECD dissociation has hindered the fundamental studies of the dissociation process(es).

ECD is a radical driven dissociation process. Some groups have used the

method of chemical tagging, such as the radical trap [77], spin trap [78], fixed charge tag [79-81] and electron affinity tag [82], to show the importance of the formation of radical and its role in initiating the backbone cleavage to give fragment ions. It was an interesting approach to study the ECD process, but the effect of the chemical tagging is multitude. ECD related dissociation pathways might be masked by the dissociation of the chemical tags.

Selective dissociation was observed in the ECD analysis of Substance P at low temperature (86 K) [83]. Limited conformational structures of peptide ions at such low temperature was believed to be the reason leading to fewer cleavage sites. Suppression of backbone cleavages was found in ECD analysis of triantennary complex-type N-glycosylated peptides [84]. This suppression effect might be caused by the presence of carbamoylmethylated cysteine that acts as a "radical trap". Recently, peptide with nitrated tyrosine, which is one of the PTMs in peptides/ proteins, was found to have suppression in backbone fragmentation after electron capture [85]. The nitrotyrosine is suggested to act as an "electron predator" that capture an electron and form the anion radical. It then further abstracted a proton from the peptide ions and hindered the normal ECD events. In our previous study, we discovered that there are natural peptides that could suppress ion fragmentation after electron capture. Diarginated peptides of 15 amino acid residues with variable number of glutamic acid (E) or asparagines (N) residues were analyzed under typical ECD conditions [86]. Doubly protonated peptide ions with (E+N) $\geq$ 4 were found to give predominantly the charge-reduced precursor ions $[M+2H]^{+\bullet}$ with little or no $H^\bullet$ loss and N-C_α bond cleavages. Subjected to collision activation, the suppressed dissociation pathway could be re-activated and led to the generation of *c*-/*z*$^\bullet$- ions and $[M+H]^+$. In a preliminary proposal, the neutralized proton might be resonantly

stabilized between the backbone amide nitrogen and the carboxylic oxygen of E side chain through hydrogen bonding and thus preventing the usual N-C_α bond cleavages.

Based on our recent findings, further study on the factors affecting the suppression of dissociation in natural peptides was conducted to get more insight on the dissociation process of ECD. Several structural parameters, including the number and nature of proton carriers and peptide chain length were investigated. In the previous studies, peptides with two arginine (R) residues and different number of glutamic acid residues were used to demonstrate the suppression effect in the ECD experiment of doubly protonated peptides. In order to examine whether the triply protonated peptide ions would have suppression of backbone fragmentation, 15-mer model peptides with different number of E residues and three R residues were used. To further investigate the role of proton carrier in suppression of backbone fragmentation in ECD process, the basic amino acid residues in the model peptides were replaced by either histidine (H) or lysine (K) residues. Peptide ions with different number of amino acid residues and same number of E residues were then used to study the chain length effect on inhibition of dissociation of peptide ions after electron capture.

3.2 Experimental section

Model peptides of sequences RGGGGEGGGGRGGGR, RGGEGGRGGEGGEGR, RGEGEGEREGEGEGR, HGEGEGEGEGEGEGH, HGEGEGEHEGEGEGH, KGEGEGEGEGEGEGK, KGEGEGEKEGEGEGK, REEEEEER, RGEGEGEGEGEGEGR, RGGEGGEGGEGGGEGGEGGEGGR, RGGGGGGEGGGGGGR and RGGGGGGGGGGEGGGGGGGGGR were custom-synthesized by Peptron Inc., (Daejeon, South Korea) and used without further purification. All samples were prepared in 30-50% methanol (Labscan Ltd.,

Bangkok, Thailand) at concentration of $2.5\text{-}5.0\times10^{-4}$ M with 2-5 % acetic acid (Riedel-de Haen, Seelze, Germany).

All ECD experiments were performed using the 4.7 Tesla Fourier-transform ion cyclotron resonance mass spectrometer (FTICR-MS) (APEX I; Bruker Instrument Inc., Boston, MA, USA). The computer system and associated electronics were upgraded to APEX III. The details for the instrumental arrangements and sample preparation procedures were stated in Chapter 2.

Typical ECD experimental conditions were 3.2 A filament heating current, 4.0 V average filament bias voltage and 300 ms electron irradiation time. For the ion activation experiments, argon gas was pulsed from a pressure-regulated cylinder (3 bar) into the analyzer region using a solenoid pulse-valve for 1200 μs. The cell pressure was raised from 1.0×10^{-8} Torr up to 5×10^{-7} Torr. The analyzer cell pressure was pumped down to the base level during a reaction delay of 3.5 s prior to the detection event. All mass spectra were acquired in broadband mode using 128 kbyte data points. 50 scans were summed to improve the signal-to-noise ratio. All time domain signals were zero-filled once before Fourier transformation.

Low energy conformers of RGGGGGGEGGGGGGR and RGGGGGGGGGGEGGGGGGGGGGR were obtained by performing molecular mechanics using MacroModel Program (ver. 5; Schrödinger Inc., Portland, OR, USA) (See Chapter 2 for details).

3.3 Results and Discussion

3.3.1 Peptides with three arginine residues

3.3.1.1 General ECD mass spectra features

Three 15-mer triarginated model peptides with 1 E, 3 E and 6 E residues were

used to study the effect on suppression of backbone fragmentation with three arginine (R) residues. Figure 3.1(a-c) shows the ECD mass spectra of doubly protonated model peptides RGGGGEGGGGRGGGR, RGGEGGRGGEGGEGR and RGEGEGEREGEGEGR.

In general, all three doubly protonated precursor ions gave *c-/z•-* ions as the major backbone fragment ions after electron capture. Hydrogen atom transfer from c^+ to $z^{+\bullet}$ was also commonly observed forming series of $c^{+\bullet}$ and z^+ respectively. There were also $H^\bullet$, NH_3, CO and amino acid side chain loss (either E or R residues) from the charge-reduced precursor ions, $[M+2H]^{+\bullet}$. However, as the number of E residue increased from 1 to 6, there was a significant decrease in both the intensity of *c-/z•-* ions and number of backbone cleavage sites (see Figure 3.1(c)). $[M+2H]^{+\bullet}$ remained intense for RGEGEGEREGEGEGR and was the major product ions. It indicated that electron capture by the precursor ions were successful. The charge-reduced precursor ions remained intact after electron capture event.

Figure 3.2(a-c) shows the ECD mass spectra of triply protonated RGGGGEGGGGRGGGR, RGGEGGRGGEGGEGR and RGEGEGEREGEGEGR ions. Series of *c-/z•-* ions were observed as the major backbone fragments. There were also small amount of *a-*, *b-* and *y-* ions formed. No intermolecular hydrogen atom transfer was observed between the fragment ions. Secondary dissociation of *z•-* ions were commonly observed, in which the side chain of E residue (the odd electron or even electron species) was lost from *z•-* ions. No charge-reduced precursor ions, $[M+3H]^{2+\bullet}$, could be observed in the mass spectra for all three model peptides. All $[M+3H]^{2+\bullet}$ lost $H^\bullet$ atom to give $[M+2H]^{2+}$. The effect of the number of E residues on the suppression of dissociation was not observed in the ECD of the triply-protonated species.

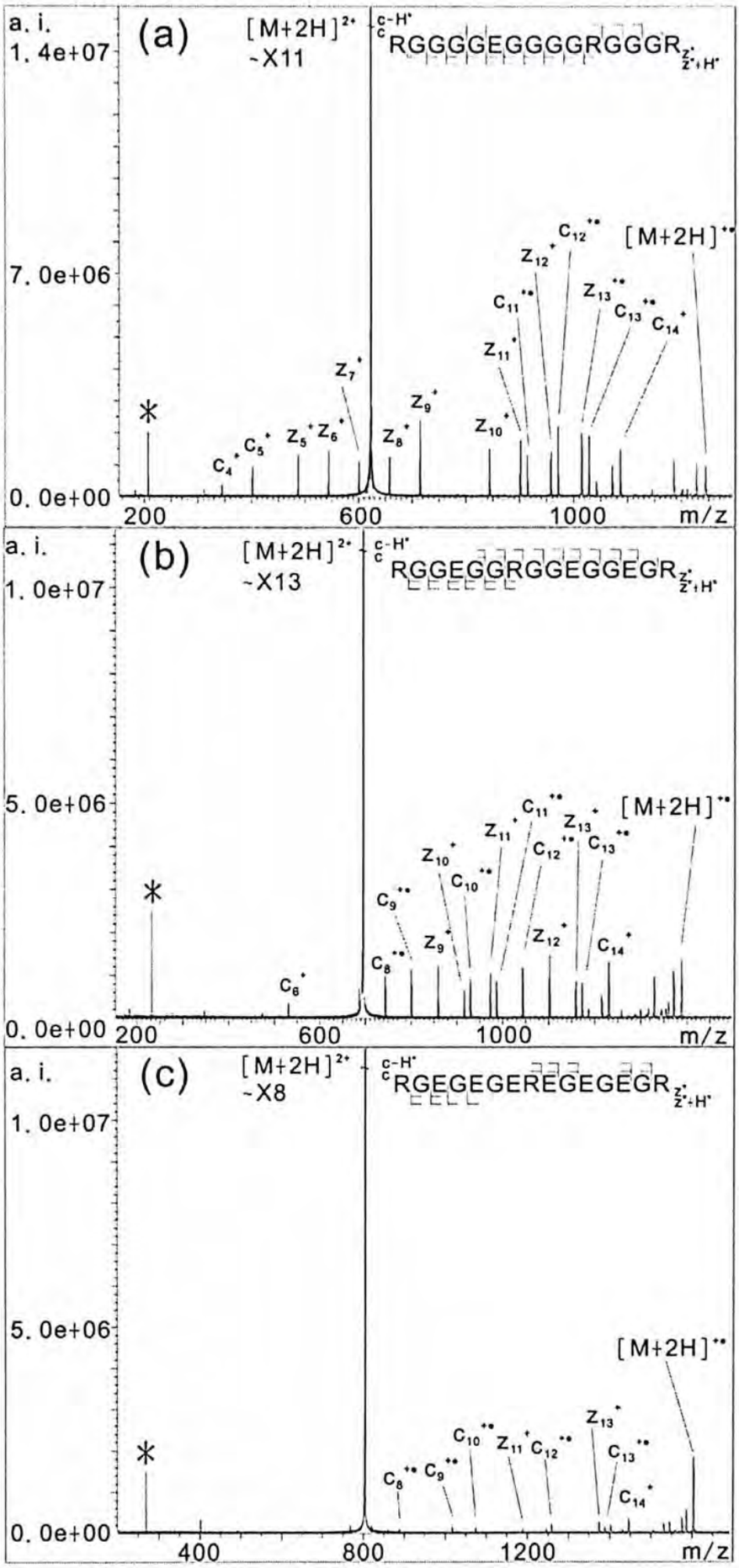

Figure 3.1 ECD mass spectra of doubly protonated precursor ions of (a) RGGGGEGGGGRGGGR (b) RGGEGGRGGEGGEGR and (c) RGEGEGEREGEGEGR

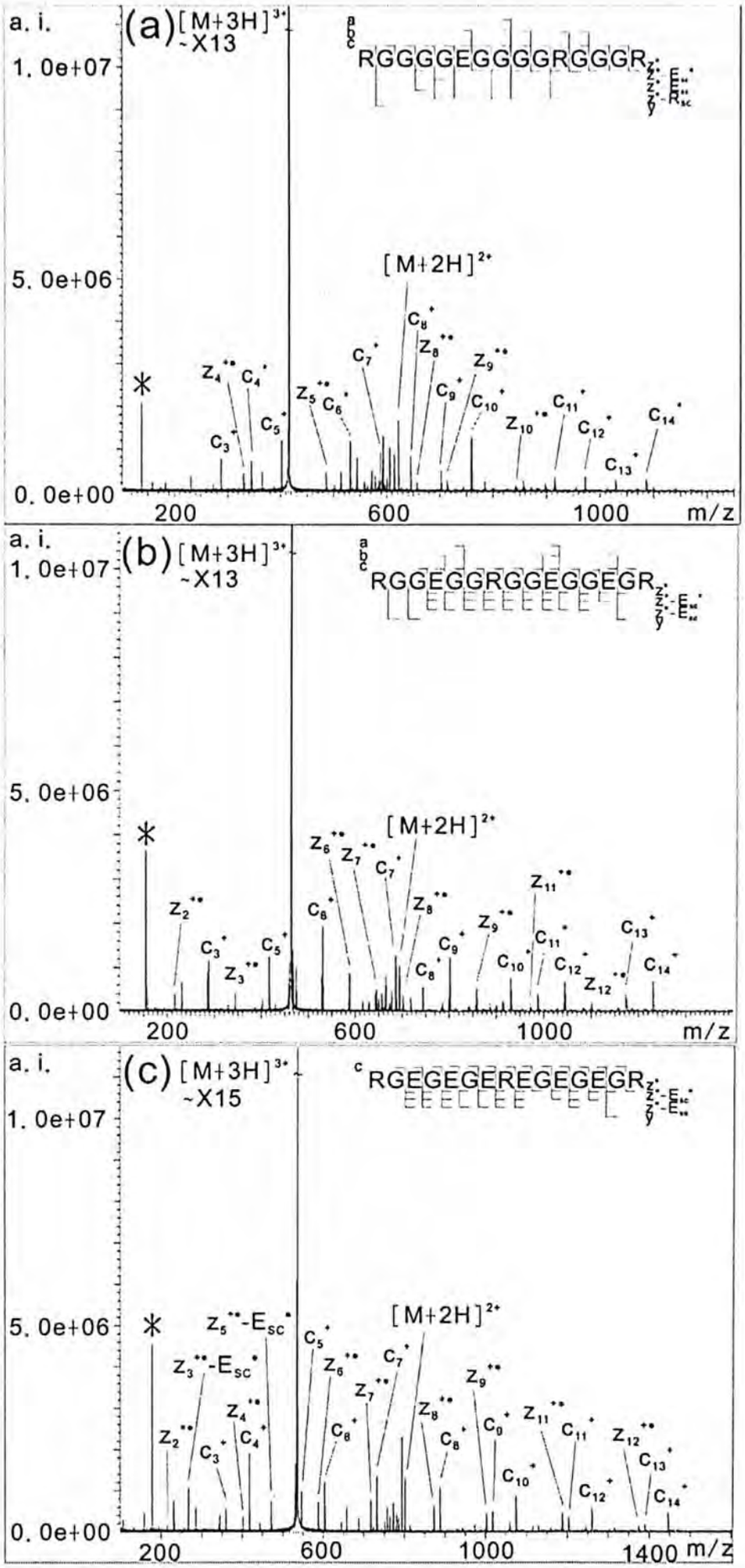

Figure 3.2 ECD mass spectra of triply protonated precursor ions of (a) RGGGGEGGGGRGGGR (b) RGGEGGRGGEGGEGR and (c) RGEGEGEREGEGEGR

Based on the above observation, the amount of backbone fragment ions and the $H^\bullet$ loss from the charge-reduced precursor ions, $[M+nH]^{(n-1)+\bullet}$, could be used as the indications for the suppression of backbone fragmentation in peptide after electron capture. In order to quantify the extent of the suppression effect, probability for dissociation (P(D)) after electron capture by the precursor ions and percentage of $H^\bullet$ loss from $[M+nH]^{(n-1)+\bullet}$ (%$H^\bullet$ loss) were calculated using equations 3.1 and 3.2 respectively:

$$P(D)=\frac{\Sigma I_{BF}}{\Sigma I_{BF}+I_{CRPI\text{-}SC}+I_{CRPI-H^\bullet}+I_{CRPI}}\times 100\% \qquad [3.1]$$

$$\%H^\bullet loss=\frac{I_{CRPI-H^\bullet}}{I_{CRPI-H^\bullet}+I_{CRPI}}\times 100\% \qquad [3.2]$$

where BF stands for typical ECD backbone fragments, including all *c-/z•* -ions, their related ions (*c•-/z-* ions and *[z•-SC]* ions) and *a•-/y-* ions; CRPI represents the charge-reduced precursor ions and SC represents side chain. The isotopic contribution of $[M+(n-1)H]^{(n-1)+}$ on the intensity of $[M+nH]^{(n-1)+\bullet}$ was also corrected in the calculation.

Figure 3.3(a) and (b) show P(D) and %$H^\bullet$ loss for $[M+2H]^{+\bullet}$ and $[M+3H]^{2+\bullet}$ of the tri-arginated model peptides, respectively. In Figure 3.3 (a), the percentage of dissociation of $[M+2H]^{+\bullet}$ to form backbone fragments decreased from 87 % for model peptide with 1 E residue to 43 % for the model peptide with 6 E residues. For the dissociation of $[M+3H]^{2+\bullet}$, P(D) of model peptides with different number of E residues remained relatively the same. Almost half of $[M+2H]^{+\bullet}$ lost $H^\bullet$ to give $[M+H]^+$ for model peptide with a single glutamic acid residue (See Figure 3.3 (b)). The formation of $[M+H]^+$ decreases gradually as the number of E increases and reaches 0 % when there are 6 E residues in the peptide. While in the case of $[M+3H]^{2+\bullet}$, all three model peptides were found to have 100 % loss of $H^\bullet$ to give $[M+2H]^{2+}$.

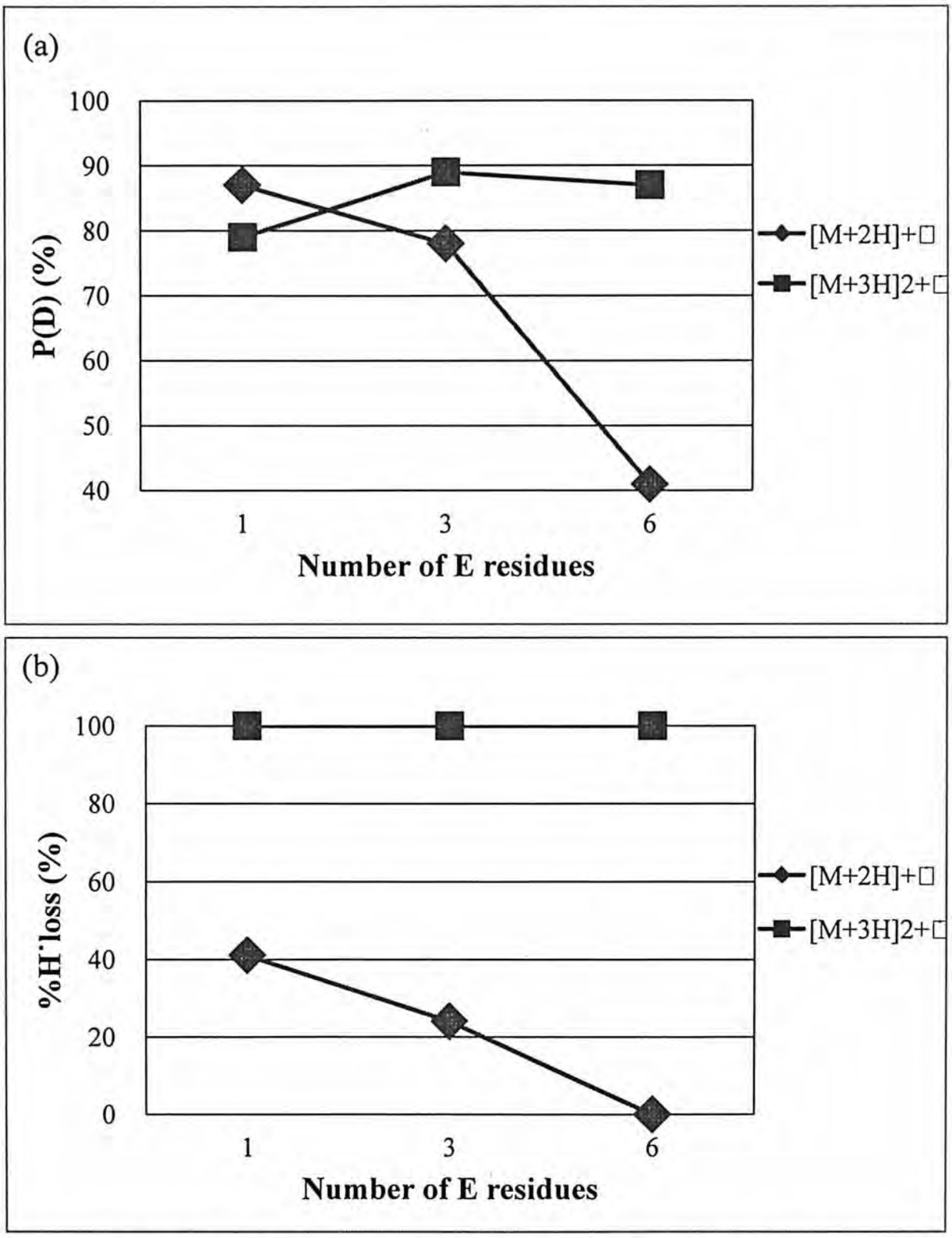

Figure 3.3 (a) Probability for dissociation P(D) of $[M+nH]^{(n-1)+\bullet}$ and (b) Percentage of H˙ loss from $[M+nH]^{(n-1)+\bullet}$ for the tri-arginated peptide ions

3.3.1.2 Comparison of the extent of suppression of triariginated and diarginated model peptides

As from our previous studies, the diarginated model peptides with the sequences RGGGGEGGGEGGGGR, RGEGGEGGGEGGEGR and RGEGEGEGEGEGEGR showed suppression of backbone fragmentation when E: R ratio increased from 1:1 to 3:1. This observation was only true for the doubly protonated precursor ions, but not the triply protonated one. For the addition of another R residue to the diarginated model peptides, similar results were obtained. Only the doubly protonated precursor ions showed suppression of dissociation when the number of E increases to 6 (E to R ratio equals to 2:1). The extent of backbone fragmentation of triply protonated peptides was also not affected by the number of E residues as in the diarginated peptide ions.

Even though the role of arginine residues in the suppression of backbone fragmentation is unknown, our experimental results showed that addition of another R did not result in any suppression effect for the triply protonated peptide ions. This may be explained by the two charges that present on the charge-reduced precursor ions, $[M+3H]^{2+\bullet}$. Due presumably to the Columbic repulsion between the two charges, the peptide ions might adopt a more extended conformation. The probability of forming an extended chain of hydrogen bonding between the backbone amide hydrogen and carboxylic group of E side chain might be greatly reduced. A series of c^+ and $z^{+\bullet}$ were then formed after electron capture. Hydrogen atom transfer between *c-/z˙*-ions, which is proposed to be due to the intra-molecular hydrogen bonding present between the fragment ions, was not observed in the triply charged peptide ions. It further supported that the Columbic repulsion between the charges might result an extended conformation of ions.

3.3.2 Peptides with histidine and lysine as proton carriers

3.3.2.1 General features of ECD mass spectra

15-mer model peptide with 6 E residues was chosen to study the effect of the nature of proton carrier on the suppression of backbone fragmentation of peptide ions after electron capture. Histidine (H) or lysine (K) residues were used to replace R residues for ECD experiments. Six peptides used in this study were XGEGEGEGEGEGEGX and XGEGEGEXEGEGEGX, where X = H, K or R.

ECD of doubly and triply protonated peptide ions were performed. Figure 3.4 (a-d) shows the ECD mass spectra for the doubly protonated peptide ions with H and K residues as the proton carriers. The fragment ions for the dihistidinated and trihistidinated peptide ions were similar as shown in Figure 3.4(a) and (b). A series of c_8^+ to c_{14}^+ and $z_9^{+\bullet}$ to $z_{14}^{+\bullet}$ ions were observed. Series of $c^{+\bullet}$ and z^+ ions formed from the hydrogen atom transfer between the *c*-ions and $z^\bullet$-ions were also observed. A number of $a^\bullet$- and *y*-ions were formed as the minor product ions. The intensity of the charge-reduced precursor ions, $[M+2H]^{+\bullet}$, was relatively high when compared to that of the fragment ions. Some fragment ions peaks corresponding to the loss of NH_3, CO and E side chain from $[M+2H]^{+\bullet}$ were observed, however, there was limited $H^\bullet$ loss from $[M+2H]^{+\bullet}$. ECD spectra of doubly protonated peptide ions containing lysine residues were shown in Figure 3.4(c) and (d). From the mass spectra, typical $c/z^\bullet$- ions were formed after ECD for both the dilysinated and trilysinated peptide ions. There were hydrogen atom transfer between the $c/z^\bullet$-fragment ions; and some $a^\bullet$-/*y*- ions were formed as minor products. Though the amount of $H^\bullet$ loss from $[M+2H]^{+\bullet}$ was not high in both peptides, the intensity of $[M+2H]^{+\bullet}$ was much lower than the fragment ions formed in the spectra.

Generally, the ECD mass spectra of the triply protonated peptide ions shown in

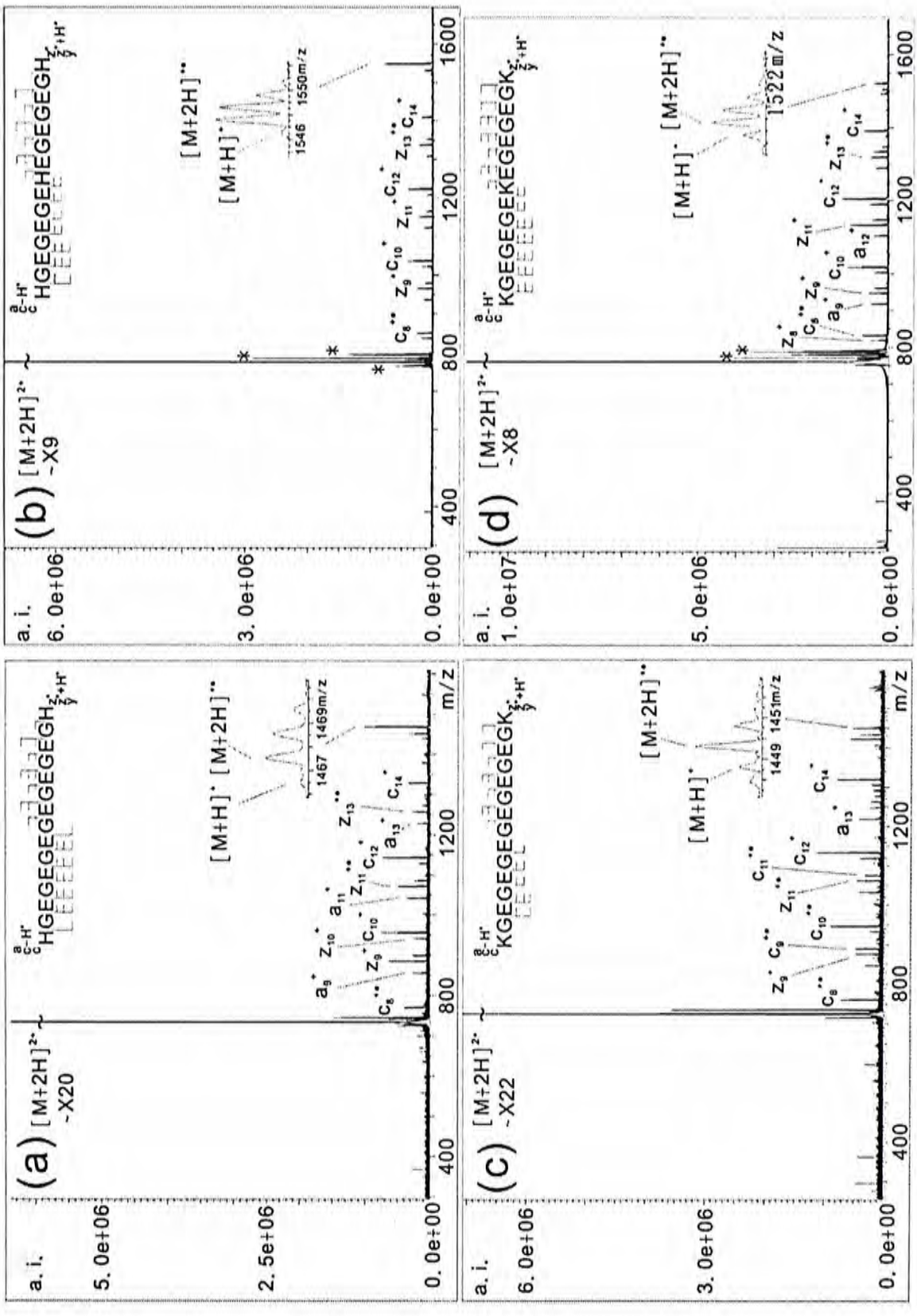

Figure 3.4 ECD mass spectra of doubly protonated (a) HGEGEGEGEGEGEGH (b) HGEGEGEHEGEGEGH (c)KGEGEGEGEGEGEGK and (d) KGEGEGEKEGEGEGK

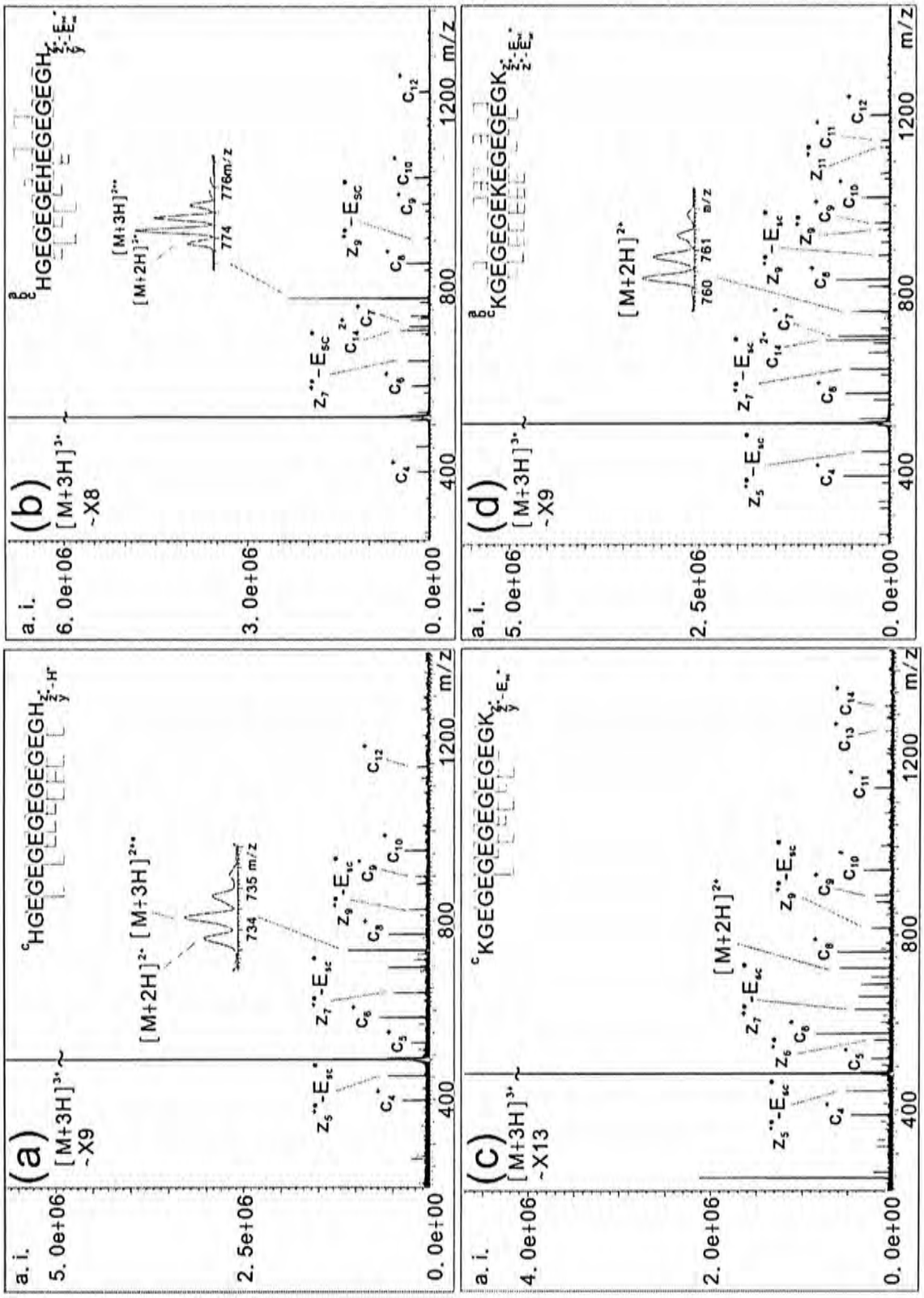

Figure 3.5 ECD mass spectra of triply protonated (a) HGEGEGEGEGEGEGH (b) HGEGEGEHEGEGEGH (c) KGEGEGEGEGEGEGK and (d) KGEGEGEKEGEGEGK

Figure 3.5 (a-d) were similar to that of doubly protonated peptide ions, in which typical ECD fragment ions were generated. One noticeably difference is that the charge-reduced precursor ions, $[M+3H]^{2+\bullet}$, of HGEGEGEGEGEGEGH was relatively intense. For both R and K containing peptide ions, complete loss of $H^{\bullet}$ from $[M+3H]^{2+\bullet}$ to give $[M+2H]^{2+}$ were found.

3.3.2.2 Comparison of ECD behaviour of peptide ions with different proton carriers

Table 3.1 shows the summary of the fragment ions that obtained from the ECD of (a) doubly and (b) triply protonated precursor ions of XGEGEGEGEGEGEGX and XGEGEGEXEGEGEGX, where X = H, K or R.

Regarding to the intensity and number of backbone fragments, doubly protonated histidine and lysine peptides did not show any signs of suppression of backbone cleavages. The P(D) of peptides with R was 63.6 % and 42.5 % for diarginated and triarginated peptides respectively, whereas the P(D) for the peptides with H (or K) were consistently over 80 %. The percentage of $H^{\bullet}$ loss from $[M+2H]^{+\bullet}$ of the peptides was highest in lysine containing peptides and lowest in arginine containing peptides. However, for the triply protonated peptide ions, only the trihistidinated peptide ions had P(D) lower than 80 %, with a relatively low percentage of $H^{\bullet}$ loss (31.5 %).

The difference in the ECD behaviour of histidine, lysine and arginine as proton carriers could be justified by the stability of the radical cation after electron capture. Histidine, lysine and arginine are basic amino acids with different side chain functionalities. Their side chains are imidazole ring, primary amine and guanidinium group respectively. The proton affinity and the hydrogen atom affinity for these

Table 3.1 (a) Normalized abundance of the fragment ions of ECD of $[M+2H]^{2+}$ (%)

	X	c_n^+	$c_n^{-\bullet}$	$z_n^{-\bullet}$	z_n^+	a_n^-	y_n^-	$[M+2H-X_{\alpha}/E_{\alpha}/NL^*]^{-\bullet}$	$[M+H]^-$	$[M+2H]^{-\bullet}$
XGEGEGEGEGEGEGX	H	22.4	15.2	14.9	11.9	8.0	10.0	5.5	2.2	10.0
	K	28.4	25.5	10.9	11.9	9.2	0.7	9.4	1.7	3.9
	R	17.7	36.7	1.2	6.1	1.8	--	20.1	2.2	14.2
XGEGEGEXEGEGEGX	H	22.2	16.2	14.1	14.1	8.5	6.0	3.4	1.9	13.6
	K	26.6	15.3	17.4	14.7	8.0	10.6	4.2	1.3	1.9
	R	13.2	17.1	3.4	8.9	--	--	25.2	0.0	32.3

Table 3.1 (b) Normalized abundance of the fragment ions of ECD of $[M+3H]^{3-}$ (%)

	X	c_n^-	$z_n^{-\bullet}$	$z_n^{-\bullet}$-E_{α}	a_n^+	b_n^-	y_n^-	$[M+2H-X_{\alpha}/E_{\alpha}/NL^*]^{-\bullet}$	$[M+H]^-$	$[M+2H]^{-\bullet}$
XGEGEGEGEGEGEGX	H	42.7	10.7	21.9	--	--	10.2	5.7	4.7	4.1
	K	44.1	17.3	20.5	1.5	--	5.0	6.8	4.8	0.0
	R	40.6	24.9	19.5	5.7	--	1.7	5.2	2.4	0.0
XGEGEGEXEGEGEGX	H	41.9	11.8	12.8	1.5	--	3.3	7.4	6.7	14.6
	K	52.4	15.7	21.7	4.2	1.8	--	2.3	2.6	0.1
	R	42.9	26.8	15.6	--	--	1.4	10.6	2.7	0.0

*NL represent neutral molecules loss

amino acid side chains were quite different. The tendency of hydrogen transfer from these sites to the amide after electron capture would be different. Based on theoretical calculation [87], Tureček et al. claimed that hydrogen transfer from a protonated amine site is a facile process, whereas the guanidyl radical site is a poor hydrogen atom donor [88]. Their findings were consistent with the high percentage of backbone cleavages and $H^{\bullet}$ loss from $[M+nH]^{(n-1)+\bullet}$ in lysinated peptide ions. The high percentage of the amino acid side chain loss from $[M+nH]^{(n-1)+\bullet}$ in arginated peptide ions also implied that the radical might spend a considerable period of time in the guanidinium group of R residue. For histidinated peptide ions, the unexpected low percentage of $H^{\bullet}$ loss might be due to the stable imidazolium radical formed after electron capture [89]. The radical might be delocalized in the imidazole ring and thus preventing it's elimination from the charge-reduced species, $[M+nH]^{(n-1)+\bullet}$. The transfer of the hydrogen radical to backbone amide could still occur through presumably the "amide superbase" model. It has been reported that there was at high abundance of the charge-reduced precursor ions for trihistidinated peptides ion after ETD [90].

For the difference between the extents of backbone fragmentation in peptides with different proton carriers, the possible reason might be the different conformations of these peptide ions. The major feature of the proposed model for inhibition of diariginated E-rich peptide ions was the hydrogen bond forming between the backbone amide hydrogen and carboxylic group of E side chain. The probability of the formation of such structural feature was believed to be conformation dependent. Lesser extent of intra-molecular hydrogen bonding might be formed in the structures of peptides with H and K residues. This could be deduced from the lower percentage of the formation of $c^{+\bullet}$ and z^{+} ions than the ariginated

peptide ions. With a lower probability of the formation of hydrogen bond between backbone amide hydrogen and E side chain, the inhibition of backbone fragmentation might not be significant.

3.3.3 Peptides with various chain lengths

3.3.3.1 General ECD mass spectra features

Based on the previous study, the suppression of backbone fragmentation after electron capture was most obvious and loss of $H^{\bullet}$ from $[M+2H]^{+\bullet}$ was minimal when the E: R ratio equals to 3: 1 for the model peptide, RGEGEGEGEGEGEGR. In order to study whether the chain length would affect the suppression effect observed, the number of amino acids of model peptides was varied by adding or removing glycine residues (G). The E: R ratio was kept at a constant value, 3: 1. The model peptides used were REEEEEER, RGEGEGEGEGEGEGR and RGGEGGEGGEGGGEGGEGGEGGR, consisting 8, 15 and 23 amino acid residues respectively. Figure 3.6 (a-f) shows the typical ECD mass spectra of doubly protonated and triply protonated model peptides.

For doubly protonated precursor ions, the three model peptides showed a great difference in their behavior under ECD. Major ECD fragments of $[REEEEEER+2H]^{2+}$ were typical *c-/z•-* ions. Odd electron and even electron E side chain loss from *z•*-ions were common to be observed. Hydrogen atom rearrangement between c^{+} and $z^{+\bullet}$ to give $c^{+\bullet}$ and z^{+} respectively were also observed. Some *b-/y-* ions formed by the non-ECD channel were formed as minor fragments. Besides of backbone fragments, small neutral molecules such as NH_3 and CO, side chain of E and R, and $H^{\bullet}$ loss from the charge-reduced precursor ions were also observed in the ECD mass spectrum.

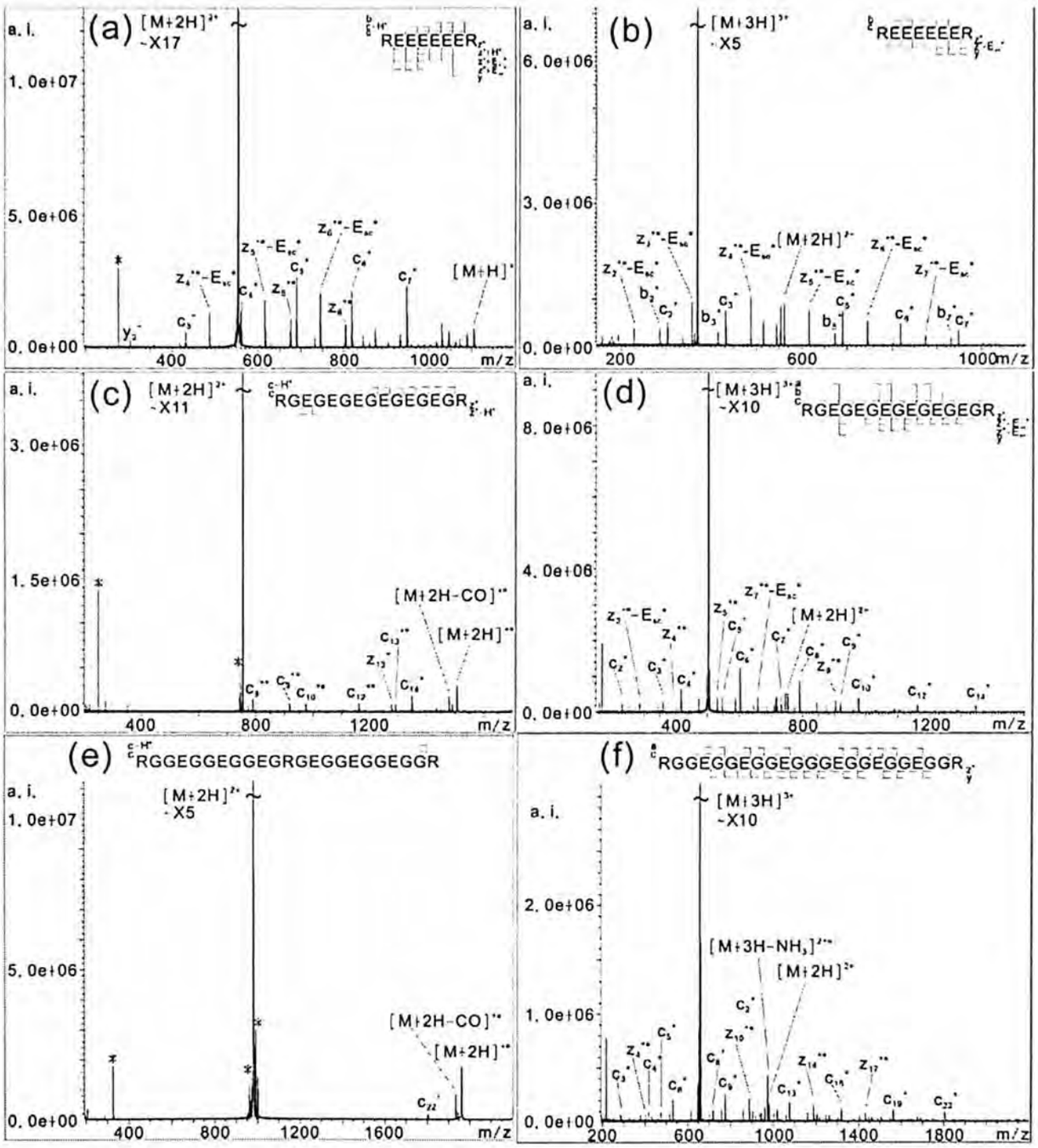

Figure 3.6 ECD mass spectra of doubly and triply protonated (a-b) REEEEEER (c-d) RGEGEGEGEGEGEGR (e-f) RGGEGGEGGEGGGEGGEGGEGGR

When the number of amino acid residues was increased to 15-mer using G as spacers, the suppression phenomenon was begun to be observed, which was even more significant in 23-mer polypeptides. For doubly protonated 15-mer diarginated peptides, large mass *c-/z˙*-ions, i.e. c_8^+-c_{14}^+ and $z_{13}^{+\bullet}$ and their corresponding hydrogen atom rearrangement ions were observed. H˙ loss from $[M+2H]^{+\bullet}$ was greatly reduced when compared to REEEEEER. Only $c_{22}^{+\bullet}$ could be observed from the ECD mass spectrum for 23-mer polypeptide. The intensity of $[M+2H]^{+\bullet}$ was high. Some small neutral molecules and side chain of E and R loss could still observe, while no H˙ loss from $[M+2H]^{+\bullet}$ was observed.

For triply protonated precursor ions, the suppression effect observed in longer polypeptides of doubly protonated precursor ions was not observed. In general, the sequence coverage was very high. Typical c_2^+ to c_{n-1}^+ and $z_2^{+\bullet}$ to $z_{n-1}^{+\bullet}$ fragments were observed. There were some E side chain losses from z˙ ions. Hydrogen atom rearrangement were absence between *c-/z˙*- ions of $[M+3H]^{2+\bullet}$. $[M+3H]^{2+\bullet}$ was not observed, instead the loss of small neutral molecules, side chain of E and R and H˙ from $[M+3H]^{2+\bullet}$ were observed. Besides the major *c-/z˙*-ions, some minor *a˙-/y*-ions were also formed. There were some *b-/y*-ions formed, especially for the peptides with fewer amino acid residues.

There was a significant decrease in the formation of the backbone fragments when increasing the total number of residues for doubly protonated peptide ions. Figure 3.7 shows the calculated P(D) and %H˙ loss of the peptide ions. The P(D) decreased from 86 % to 13 % for 8-mer and 23-mer polypeptides respectively. H˙ loss from $[M+2H]^{+\bullet}$ also showed a large decrease. %H˙ loss even reached 0 % for 23-mer polypeptide. As observed from the above experimental results, it appeared that the number of amino acid residues also had a significant effect on the

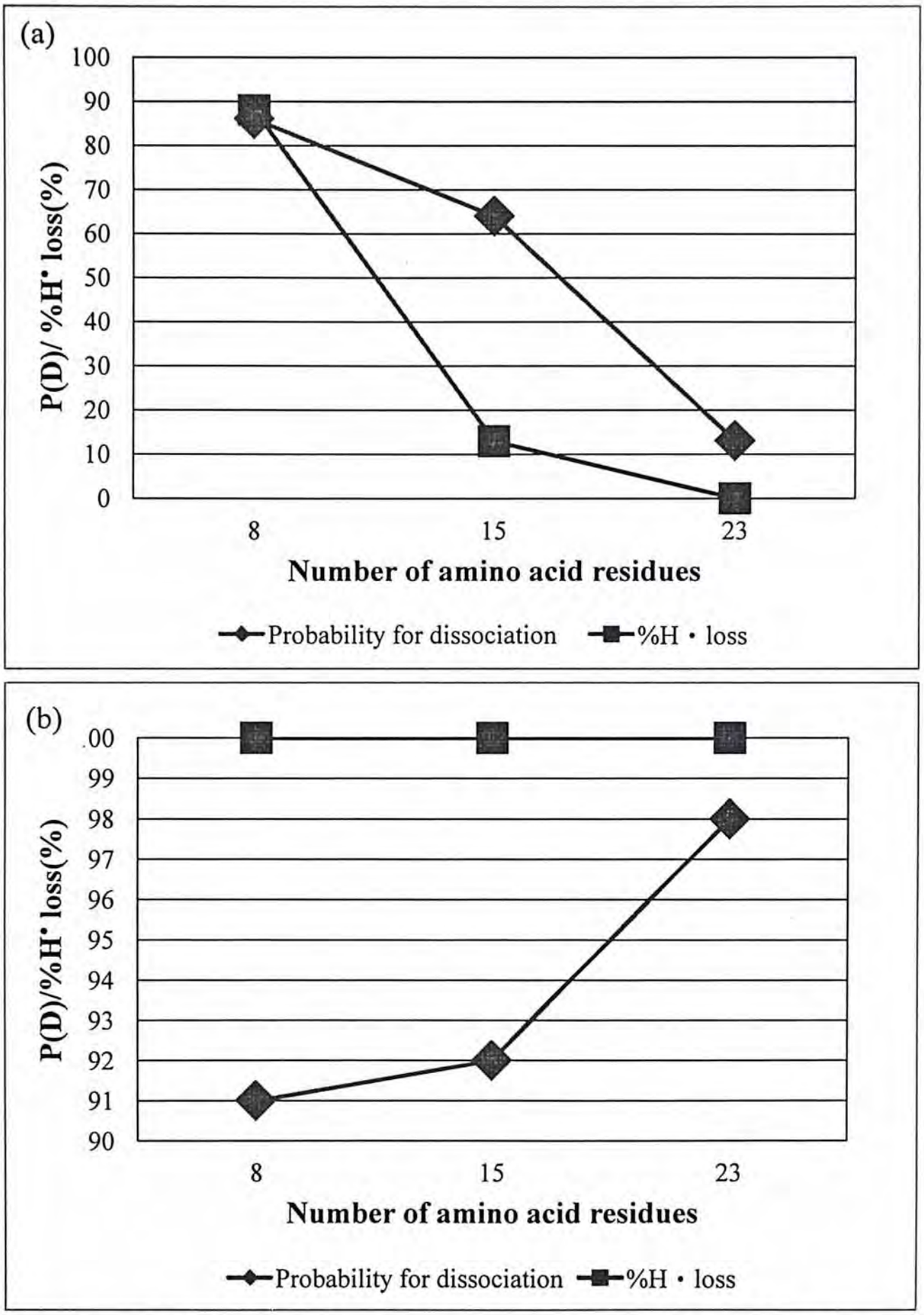

Figure 3.7 P(D) and %H• loss for (a) doubly protonated and (b) triply protonated REEEEEER, RGEGEGEGEGEGEGR and RGGEGGEGGEGGGEGGEGGEGGR

suppression effect of ECD. For the same E: R ratio (3:1), the doubly protonated shortest model peptide (REEEEEER) could be fragmented and every backbone cleavage could be obtained. The suppression effect started to be observed when increasing the number of amino acid residues to 15-mer and was most significant in 23-mer. E: R ratio might not be the only factor to determine the degree of suppression effect. Further experiments were required to verify this observation.

3.3.3.2 Re-activation of $[M+2H]^{+\bullet}$ by collision activation

To ensure that the high intensity of $[M+2H]^{+\bullet}$ was solely due to the inhibition of backbone cleavage after electron capture but not the holding of fragment ions by the non-covalent interactions, argon gas was pulsed into the cell after ECD to re-activate $[M+2H]^{+\bullet}$, where M is the 23-mer polypeptide. More *c-/z•*-ions and *c•-/z*-ions were formed after introduction of argon gas. *b-/y*-ions observed were believed to be come from the non-ECD dissociation channel of the doubly protonated precursor ions. Preferential cleavage of C-termini of E residues resulted in higher intensity of *b/y*-ions [27, 28]. More importantly, $H^\bullet$ loss from $[M+2H]^{+\bullet}$ was observed and gave $[M+H]^+$. This suggested that $[M+2H]^{+\bullet}$ was an intact molecule as it would be energetically unfavourable for the fragment ions to lose a hydrogen radical. Figure 3.8 shows the mass spectrum obtained.

3.3.3.3 Significance of glutamic acid residues

In order to gain more insight on the E: R ratio effect on the long peptides, the model peptides, with E: R ratio of 1: 2, were used to perform ECD. The sequences used were RGGGGGGEGGGGGGR and RGGGGGGGGGGGEGGGGGGGGGGR (RG_6EG_6R and $RG_{10}EG_{10}R$), which they consist of 15 and 23 amino acid residues respectively. Figure 3.9 shows the ECD mass spectra of doubly protonated peptide

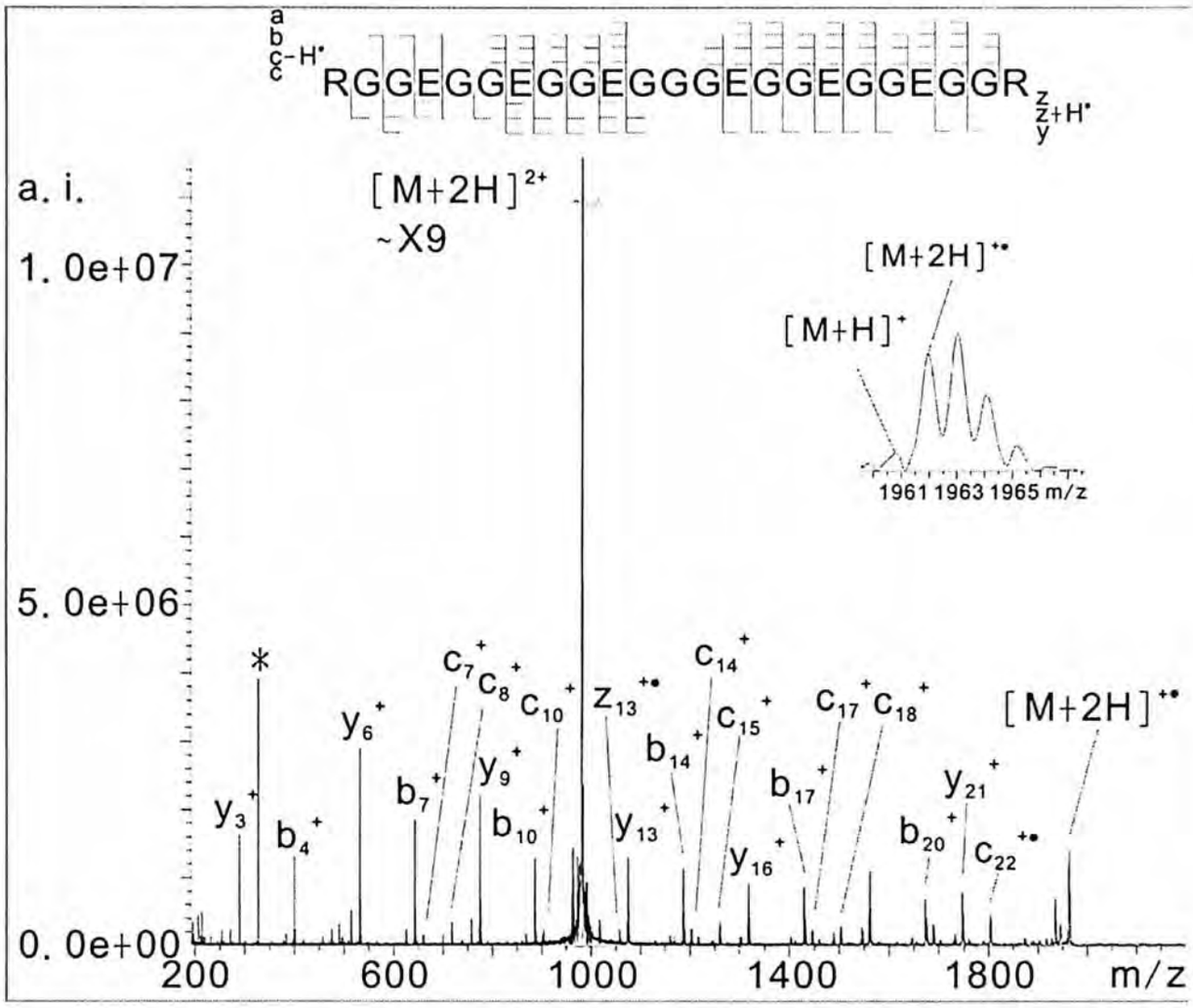

Figure 3.8 Mass spectrum of $[RGGEGGEGGEGGGEGGEGGEGGR+2H]^{2+}$ obtained with ECD followed by collision activation of ions

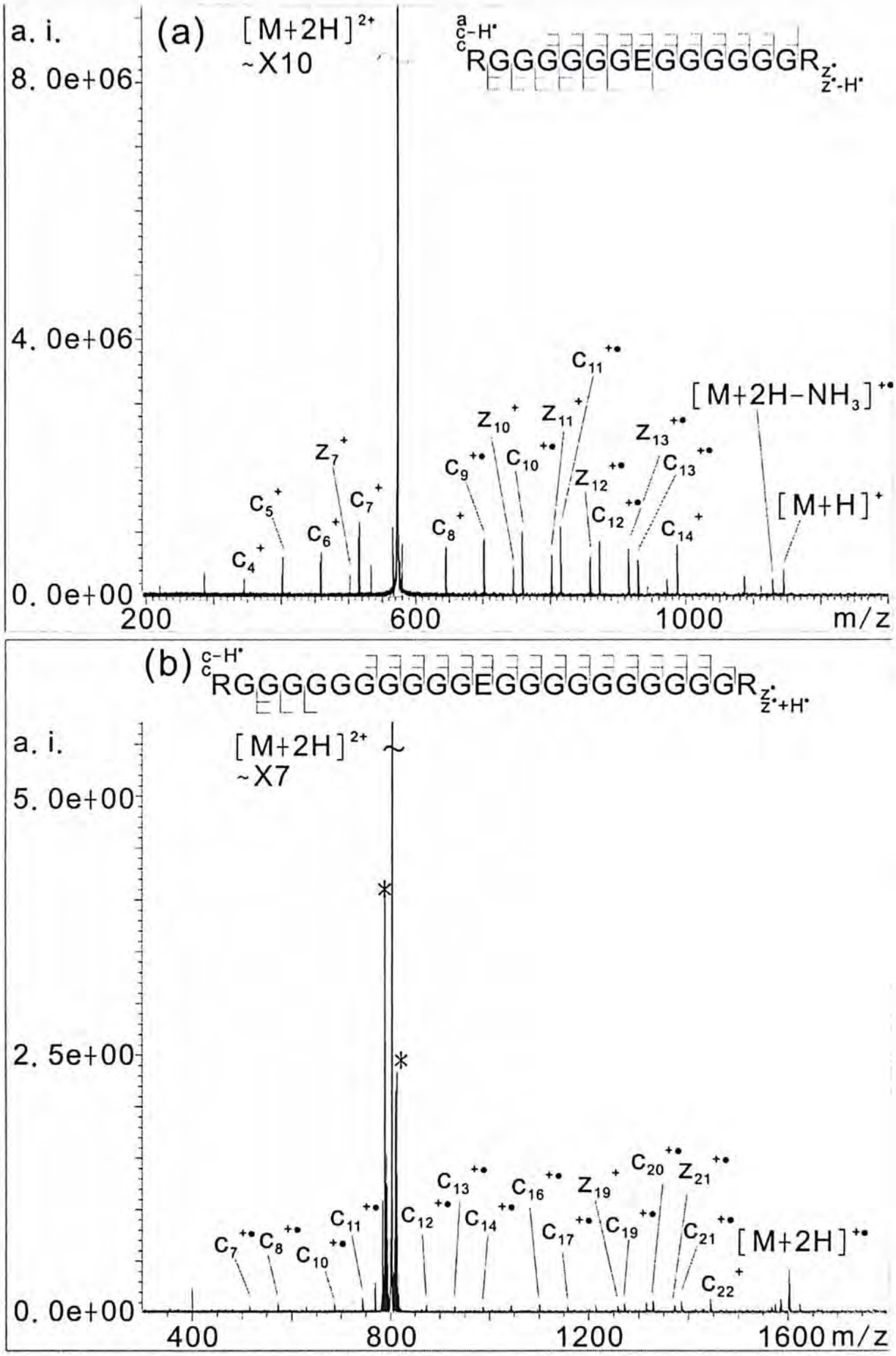

Figure 3.9 ECD mass spectra of doubly protonated (a) RGGGGGGEGGGGGGR (b) RGGGGGGGGGGGEGGGGGGGGGGR

ions.

ECD of $[RG_6EG_6R +2H]^{2+}$ gave a typical mass spectrum, in which most c^+ and $z^{+\bullet}$ could be observed. There was also $H^\bullet$ transfer between *c-/z·*-ions. P(D) reached 93% and %$H^\bullet$ loss from $[M+2H]^{+\bullet}$ was 100%. No suppression was observed when the doubly protonated peptide ion was 15-mer and E: R ratio was 1: 2. This result was resembled to that in previous study that suppression effect was observed only when E: R ratio greater or equal to 2:1.

ECD of $[RG_{10}EG_{10}R+2H]^{2+}$ gave c_7^+- c_{22}^+ and z_{19}^+- z_{21}^+. Even though most of the backbone cleavages observed, the intensity of the fragment ions were relatively low when compared to that of RG_6EG_6R. Furthermore, the charge-reduced precursor ion was of high intensity. P(D) of $[M+2H]^{+\bullet}$ was 77%. There was no $H^\bullet$ loss from $[M+2H]^{+\bullet}$, but small neutral molecules losses from $[M+2H]^{+\bullet}$ were still present.

Here the results showed that E: R ratio still played a role in the suppression effect observed in 23-mer polypeptides as the suppression effect was much more significant when 6 E residues present. The number of E residues was still important in determining the extent of suppression of backbone cleavages. However, the phenomenon that observed in longer peptide should not be neglected. There was a decrease of the backbone fragmentation in both 23-mer polypeptides when compared to the 15-mer polypeptides, especially when there was only 1 E residue. To study the reason that causing inhibition of backbone fragmentation in long polypeptide, conformational searches using $[RG_6EG_6R+2H]^{2+}$ and $[RG_{10}EG_{10}R+2H]^{2+}$ were performed.

3.3.3.4 Result of conformational searches

Model peptides with 1 E residue were chosen so as to reduce the complexity of the model under conformational search. The initial structure for performing

conformational search was the zwitterionic form between the N-terminal and C-terminal with two protons on two R side chains. Previous study showed that the zwitterionic form [91] would be presumably more favourable in doubly protonated Bradykinin [92, 93]. In addition, the E carboxylic acid side chain would have a lower pKa when compared to the carboxylic acid group of the amino acid [94]. Thus, it would be more favourable for the carboxylic end of peptide ions to lose proton to form zwitterions.

Only those low energy conformers with the relative abundance greater than 1% were taken into consideration. Hydrogen bonding pattern of the low energy conformers were being focused. Figure 3.10 and 3.11 showed the conformation of the lowest energy conformers of $[RG_6EG_6R+2H]^{2+}$ and $[RG_{10}EG_{10}R+2H]^{2+}$ respectively. In general, a lot more hydrogen bonding could be observed in the 23-mer polypeptides when compared to 15-mer polypeptides. This was within expectation as there were more backbone amide hydrogen atoms that can form the hydrogen bond with backbone carbonyl oxygen. Under detailed examination, it was to be discovered that there were some special features for the hydrogen bonding pattern of 23-mer polypeptides, which was not existed in 15-mer polypeptides. Extensive hydrogen bonding could be found in the long chain polypeptide. The hydrogen bonding "ladder" was first traced from the protonated sites. If the protonated site forms hydrogen bond with backbone carbonyl oxygen, then its neighbouring amide hydrogen is checked to see of it has formed hydrogen bond with other backbone carboxylic oxygen atoms or any other functional groups. The hydrogen bonding "ladder" found in these two conformers was summarized in the figures. The one being bold was the longest hydrogen bonding chain that found in the conformer and was highlighted in the structure.

Figure 3.10 The lowest energy conformation of $[RG_6EG_4R+2H]^{2+}$ and its hydrogen bonding pattern

Figure 3.11 The lowest energy conformation of $[RG_{10}EG_{10}R+2H]^{2+}$ and its hydrogen bonding pattern

For $[RG_{10}EG_{10}R+2H]^{2+}$, there were some hydrogen bonding chains observed, which appeared in the $[RG_6EG_6R+2H]^{2+}$ less often. These chains were also comparatively longer than that in the $[RG_{10}EG_{10}R+2H]^{2+}$. This may account for the decrease of the backbone fragments and no $H^{\bullet}$ loss that observed in the doubly protonated 23-mer polypeptides ions. Instead of cleaving the N-C_α bond after the hydrogen radical attacked the C=O bond, the hydrogen atom may be resonant along the chains of hydrogen bonding and resulted the trapping of the hydrogen radical. The proposed model is shown in Scheme 3.1. The "ladder" prevented the hydrogen atom from causing the N-C_α bond cleavage. It was similar to that of E-rich peptide ions, instead the one forming hydrogen bonding with the amide hydrogen bonding was the backbone carbonyl group rather than the E side chain. Since the model only consists of 1 E residue, E side chain effect may not be observed from the structure. It was postulated that the effect would be more significant in the E-rich 23-mer peptide ions.

3.4 Conclusions

Further study on the suppression effect of natural motifs in polypeptide was done. For triarginated peptide ions, the suppression of backbone fragmentation after electron capture was similar to that of the diarginated peptide ions. Only doubly protonated E-rich peptide ions showed suppression, but not in the triply protonated one. This may due to the more extended structure of triply protonated peptide ions resulted by the Columbic repulsion between the positive charges, which the formation of the conjugate structure was not allowed.

With different proton carriers, their behaviours under ECD were different. Histidine and lysine containing peptide ions gave more backbone fragments when compared to arginated peptide ions. This might because the different conformation

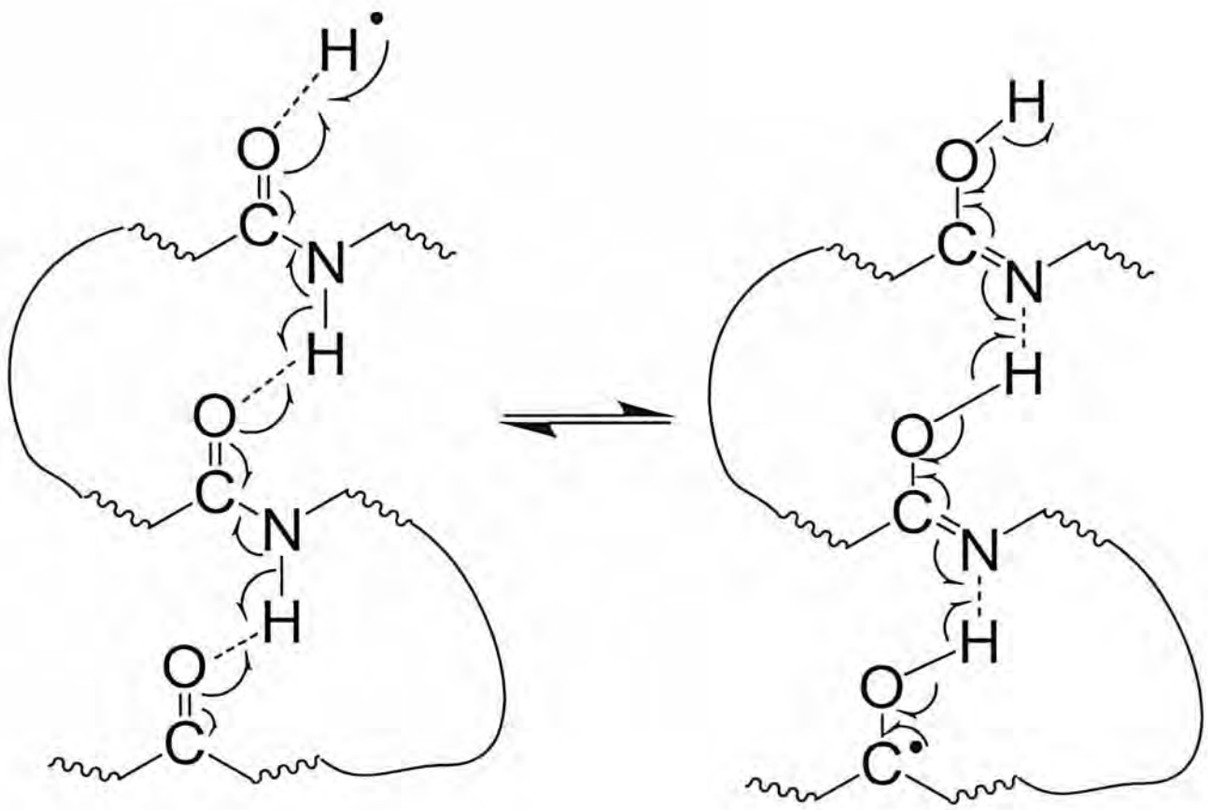

Scheme 3.1 Proposed model for the stabilization of H˙ in $[M+2H]^{+\bullet}$, where M is 23-mer polypeptide

that formed for different proton carriers, which did not favour the formation of the hydrogen bonding between the backbone amide hydrogen and E side chain in histidinated and lysinated peptide ions.

By using the peptides with various chain length, suppression of backbone cleavage and $H^{\bullet}$ loss from $[M+2H]^{+\bullet}$ appears only when number of amino acid residues greater or equal to 15. The effect was even more significant in 23-mer polypeptide ions. It appears that number of E residues might not be the only determining factor for the suppression effect that observed. Furthermore, suppression effect occurred even when the number of E residues reduced to one. By performing conformational searches of $[RG_6EG_6R+2H]^{2+}$ and $[RG_{10}EG_{10}R+2H]^{2+}$, it was found that backbone amide hydrogen might play an important role in resulting the inhibition of backbone cleavage and $H^{\bullet}$ loss from $[M+2H]^{+\bullet}$. A hypothesis based on the result of conformational searches was proposed for the experimental observation in 23-mer polypeptide ions. The backbone amide hydrogen formed hydrogen bond with the backbone carbonyl oxygen to give an extensive resonance structure. This could stabilize the hydrogen radical and reduce backbone fragmentation. In shorter polypeptides (15-mer), the hydrogen bond "ladder" had a lower probability to form, so more E residues had to be present in order to have suppression of backbone fragmentation. Both the number of E residues and peptide chain length contribute to the suppression of backbone fragmentation, but it is difficult to differentiate these two effects are additive or synergistic in nature.

Chapter 4

Investigation of the Role of Conformation of Peptide Ions in Suppression of Backbone Fragmentation

4.1 Introduction

ECD has been widely used for peptides/ proteins sequencing because of its ability to induce non-selective backbone cleavage. Together with "slow heating" ion activation methods, de Novo peptide sequencing and characterization of PTMs can be achieved by using MS methods. However, some studies showed that the probability of the cleavage of N-C_α bond might be governed by the conformation of peptides/ proteins [95-97]. Tsybin et al. has studied the product ions abundance (PIA) of ECD using the amphipathic peptides with α-helical structures [98]. Periodic PIA behavior was observed with the preferential cleavage sites along the hydrogen-bonding network that connect the charge sites and the most hydrophilic residues in each turn. This observation was in-line with the "neutral hydrogen bonding" mechanism proposed by Zubarev and colleagues [99]. Electron is first attached to the nitrogen atom that involved in hydrogen bonding. The backbone carbonyl then abstracts the $H^\bullet$ and initiates the N-C_α bond cleavage. Furthermore, the formation of $z^\bullet$-ions with the radical stabilization for certain amino acids (such as phenylalanine and tyrosine) showed a higher abundance compared to other product ions [100]. Conformation of peptide ions might result in preferential cleavages of particular backbone sites.

The use of metal ions as charge carrier might result in different conformation of the peptide ions when compared to that of the protonated peptide ions. ECD of

various metal ions adducted peptide ions yield different products of the same peptide. The difference might be due to the metal ion itself or the conformational difference between these species [60]. Behaviors of divalent transition metal ions adducted peptide under ECD are quite different [57-61]. In general, Mn(II), Zn(II) and Cd(II) adducted peptides generate fragment ions that are similar to those of the alkali metal ions and alkaline earth metal ions adducted peptide ions. Typical *c-/z*$^{\bullet}$-ions and their metalated species were observed. Co(II) and Ni(II) adducted peptide ions generally gives metalated *a-/y*-ions as major product ions. Cu(II) adducted peptide generates *b-/y-* ions and the metalated fragment ions. Hg(II) adducted peptide gives $M^{+\bullet}$ and forms mainly *a-* ions.

In the previous chapter, we proposed that the conformation of E-rich peptide ions and 23-mer polypeptide ions might play an important role in forming the resonance structure that is in-turn responsible for the suppression of backbone fragmentation and loss of $H^{\bullet}$ from $[M+2H]^{+\bullet}$ under ECD condition. The non-covalent interaction and hydrogen bonds formed between backbone amide hydrogen and carboxylic group of E side chain (or backbone carbonyl oxygen) were believed to be the main structural feature to cause this cleavage suppression effect. To verify our hypothesis, further experiments using three different approaches to alter the conformations (or the formation of hydrogen bonding by the backbone amide hydrogen) were performed. The first approach involved the use of N-methylated amino acid residues to study the effect of removing the backbone amide hydrogen on the suppression of the backbone fragmentation. ETD of the peptides with N-methylated amino acid residues have previously been performed. Typical *c-/z*$^{\bullet}$-ions were observed [104]. The second approach used proline residues (P) to replace some of the glycine residues (G) in the model peptides. With the ring

structure in the backbone of the polypeptide ions, the inclusion of multiple proline residues should reduce the flexibility of the peptide chain and thus limiting the extent of the formation of the hydrogen bonding network. The third approach was the use of transition metal ions instead of protons as charge carrier for the model peptides. Effect of the first row transition metal ions and the Group IIB metal ions were studied.

4.2 Experimental section

Model peptides of sequences $RSar_mESar_mESar_mESar_mESar_mESar_mESarR$ (Sar is Sarcosine/ or N-methylglycine residues and $_mE$ represents N-methylglutamic acid residues), RGPGPGPEGPGPGGGPGPGPR, RPEPEPEREPEPEPR, RGPGPGPGRGPGPGPGR, $RG_mAG_mAG_mAGRG_mAG_mAG_mAGR$ ($_mA$ represents N-methylalanine residue), RGGGGGGEGGGGGGR and RGGGEGGGR were custom-synthesized by Peptron Inc., (Daejeon, South Korea) and used without further purification. All samples were prepared in 50 % methanol (Labscan Ltd., Bangkok, Thailand) at concentration of $2.5\text{-}5.0\times10^{-4}$ M with 2-5 % acetic acid (Riedel-de Haen, Seelze, Germany) for obtaining protonated precursor ions. Metal salts were obtained commercially without further purification. Magnesium (II) acetate and copper (II) acetate were obtained from Beijing HuaGongChang (Beijing, China); cobalt (II) acetate, nickel (II) acetate, zinc (II) acetate and cadmium (II) acetate were obtained from Riedel-de Haen (Seelze, Germany); Mercury (II) nitrate was obtained from Sigma and Aldrich (St. Louis, MO, USA). The concentration of metal salts was 2.5×10^{-4} M in peptide solutions.

All ECD experiments were performed using a 4.7 Tesla Fourier-transform ion cyclotron resonance mass spectrometer (FTICR-MS) (APEX I; Bruker Instrument Inc., Boston, MA, USA). The computer system and associated electronics were

upgraded to APEX III. The details for the instrumental arrangements and sample preparation procedures were described in Chapter 2.

Typical ECD experimental conditions were 3.2 A filament heating current, 4.0 V average filament bias voltage and 300 ms electron irradiation time. For the ion activation experiments, argon gas was pulsed from a pressure-regulated cylinder (3 bar) into the analyzer region using a solenoid pulse-valve for 1200 μs. The cell pressure was raised from 1.0×10^{-8} Torr up to 5×10^{-7} Torr. The analyzer cell pressure was pumped down to the base level using a reaction delay of 3.5 s prior to excitation and detection events. All mass spectra were acquired in broadband mode using 128 kbyte data points. 50 -100 scans were summed to improve the signal-to-noise ratio. All time domain signals were zero-filled once before Fourier transformation.

4.3 Results and Discussion

4.3.1 Peptide with N-methylated amino acid residues

To validate the proposed suppression model, the role of amide hydrogen on the electron capture dissociation of peptide ions was investigated. Since the E-rich 15-mer is the smallest polypeptides that displayed a significant degree of suppression effect, RGEGEGEGEGEGEGR was chosen for the present study. All glycine and glutamic acid residues were changed to their corresponding N-methylated residues. The resulting sequence is $RSar_mESar_mESar_mESar_mESar_mESar_mESarR$.

4.3.1.1 General features of ECD mass spectra

Figure 4.1 shows the ECD mass spectrum of the doubly protonated N-methylated peptide ions. Series of c_5^+ to c_{14}^+ (except c_7^+ which its m/z is closed to that of the precursor ion) and $z_9^{+\bullet}$ to $z_{14}^{+\bullet}$ fragments were formed. There were also

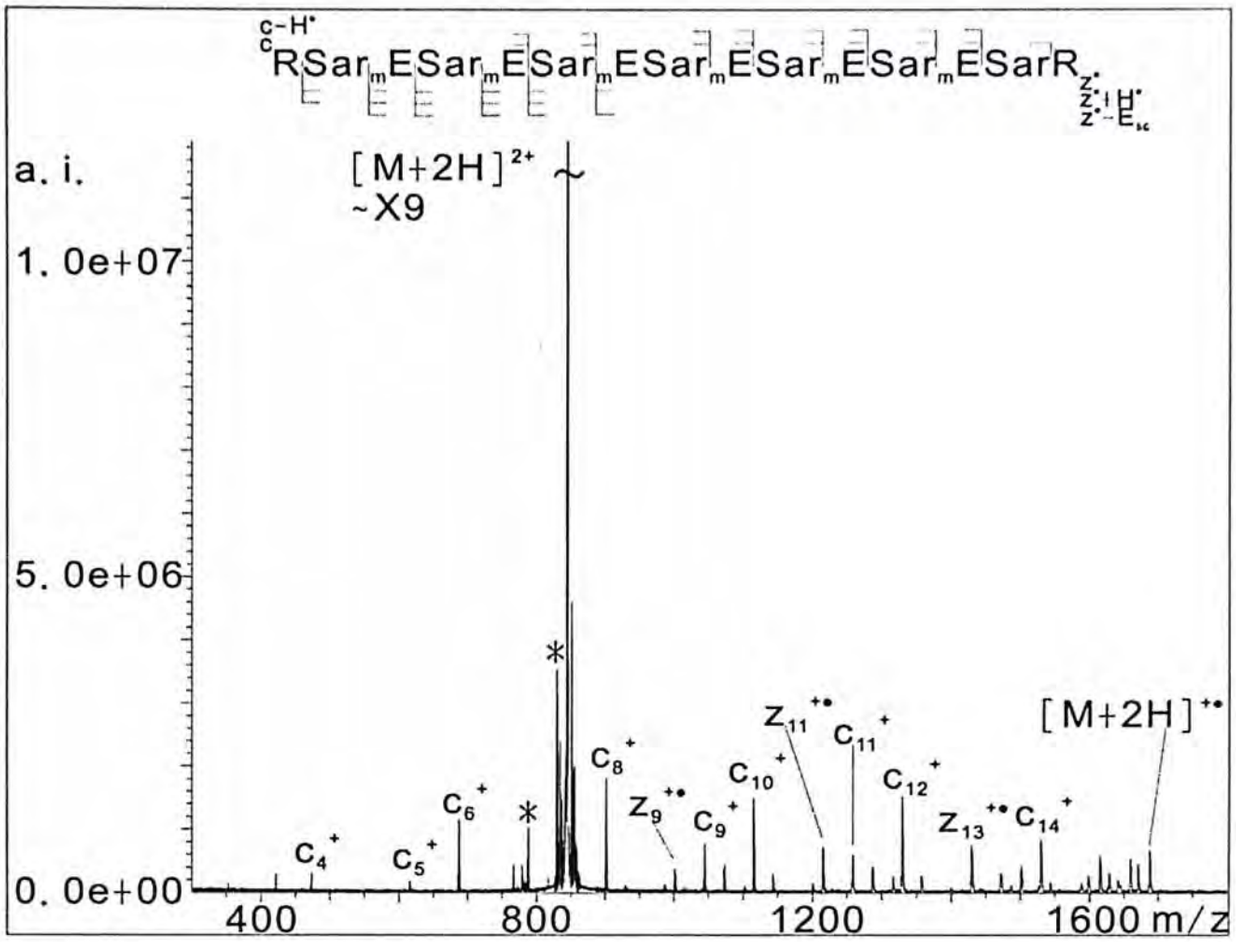

Figure 4.1 ECD mass spectrum of doubly protonated RSar$_m$ESar$_m$ESar$_m$ESar$_m$ESar$_m$ESar$_m$ESarR

some hydrogen atom rearrangement between *c*-/*z*•- ions, but the extent was small as compared to that of the unmodified peptide. Most of the observed *z*•- ions lost E side chain to form *w*-ions. Loss of small neutral molecules such as NH_3 and CO, side chain of E and R residues from the charge-reduced precursor ions $[M+2H]^{+\bullet}$ were also found. However, no H• loss from $[M+2H]^{+\bullet}$ was observed.

4.3.1.2 Comparison between normal and N-methylated peptide ions under ECD

The replacement of normal amino acid residues by the N-methylated residues has induced more fragment ions and their intensities were more intense. Besides of the high mass fragment ions as in the case of ECD of RGEGEGEGEGEGEGR, some low mass *c*-ions were formed in the ECD of N-methylated peptide. The P(D) had also increased from 64 % to 85 %. The suppression of the backbone cleavages that observed in the E-rich 15-mer peptide ions had been alleviated a large extent after changing most of the amide hydrogen to methyl group. This observation is consistent with our expectation based on the proposed suppression model. Removal of the amide hydrogen atom should limit the formation of hydrogen bonding network. The possibility of forming an extended hydrogen bonding chain to stabilize and trap the hydrogen radical after electron capture event should thus be reduced. The percentage of the hydrogen atom rearrangement between the *c*-/*z*•-ions was greatly reduced from 69 % in RGEGEGEGEGEGEGR to 21 %. This is consistent with the expected reduction of the number of intra-molecular hydrogen bonds.

As shown in Figure 4.1, the usual H• loss from $[M+2H]^{+\bullet}$ was not observed. Since the major difference between the N-methylated peptide ions and the other unmodified model peptide ions is the fewer number of the amide hydrogen that present in the former ions, we proposed that the origin of the H• loss that observed

from $[M+2H]^{+\bullet}$ was from the amide hydrogen, rather than the neutralized proton. Upon capturing of an electron by a proton, the neutral hydrogen radical should migrate to the backbone carbonyl oxygen leading to the formation of the aminoketyl radical intermediate. The radical could take two dissociation pathways, including cleaving the N-C_α bond to give the usual *c*-/*z*$^\bullet$-ions or cleaving the N-H bond to give $[M+(n-1)H]^{(n-1)+}$. With the hydrogen atom being substituted by the methyl group, the formation of the methyl radical would not be energetically feasible [105]. Neither H$^\bullet$ nor $^\bullet CH_3$ loss from the charge-reduced species ($[M+2H]^{+\bullet}$) was observed. Scheme 5.1 summarizes the proposed dissociation pathways.

4.3.2 Peptides with proline residues

To gain further insight into the origin of the suppression effect, the dissociation behavior of proline-rich peptides were investigated. Proline residue has a pyridinyl-ring and has fewer degrees of freedom. Peptides having multiple proline residues are known to adopt a more extended conformation and fewer intra-molecular hydrogen bonds [101-103]. A comparative study of the dissociation behavior of a model peptide with the corresponding proline-rich peptides should give complementary information regarding the origin of the suppression effect. Peptides with sequences RPEPEPEREPEPEPR and RGPGPGPEGPGPGPGGGPGPGPR were used.

4.3.2.1 General ECD mass spectra features

Figure 4.2 (a-d) shows the ECD mass spectra of doubly protonated and triply protonated mass spectra of RPEPEPEREPEPEPR and RGPGPGPEGPGPGPGGGPGPGPR. For both peptides, ECD of the doubly

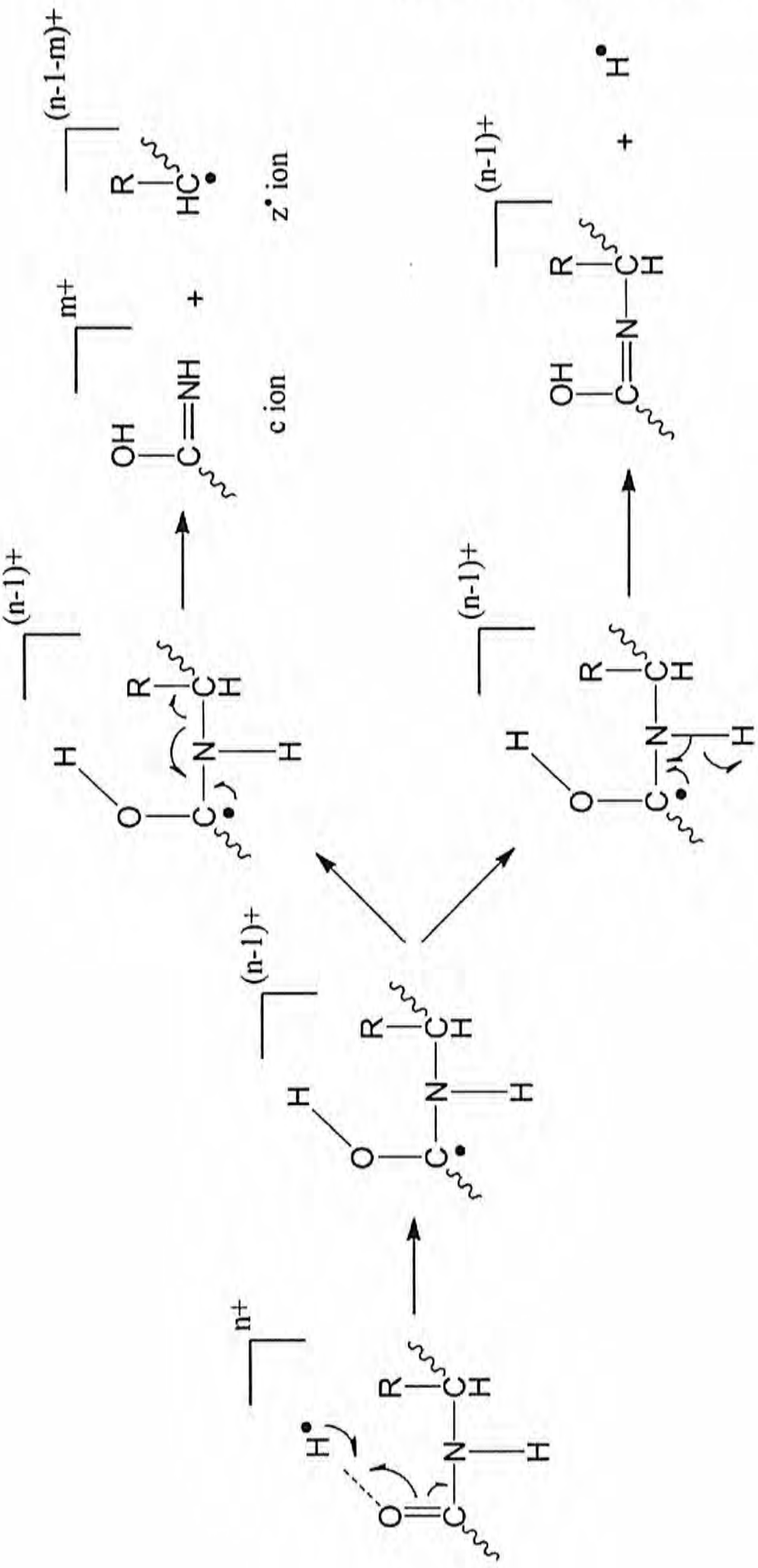

Scheme 4.1 Proposed H• loss from $[M+2H]^{+\bullet}$ and N-C_α bond cleavage from the aminoketyl radical imtermediate

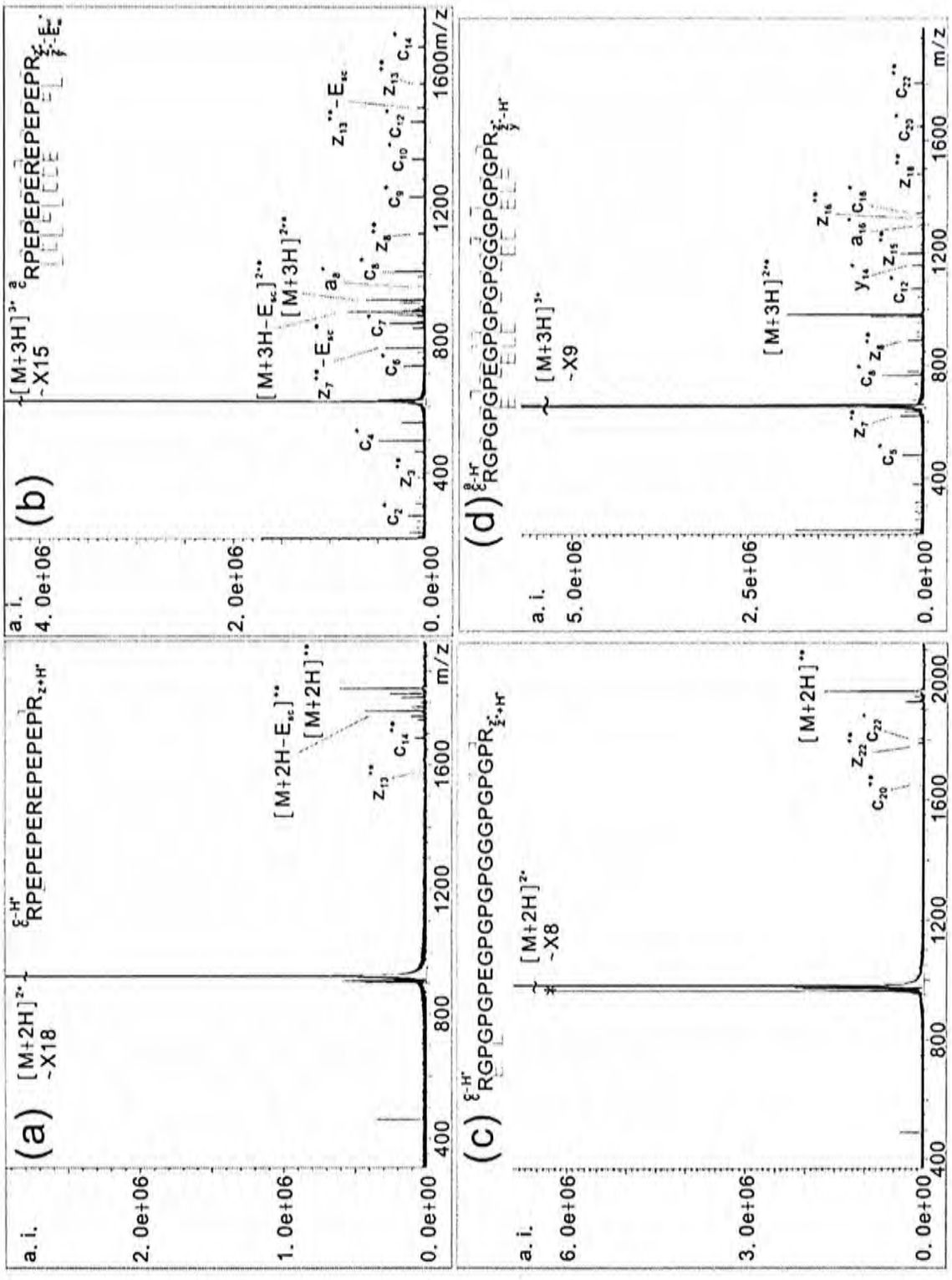

Figure 4.2 ECD mass spectra of doubly and triply protonated (a-b) RPEPEPEREPEPEPR and (c-d) RGPGPGPRGPGPGPGGGPGPGPR.

protonated precursor ions yielded relatively few backbone fragments. Only high mass fragment ions were observed. The major product ions for both peptides were the charge-reduced precursor ions, $[M+2H]^{+\bullet}$. For the E-rich 15-mer peptide ions, loss of NH_3, CO, E and R side chain from $[M+2H]^{+\bullet}$ were abundant. For 23-mer polypeptide, fewer loss of small neutral molecules from $[M+2H]^{+\bullet}$ was observed. P(D) for the 15-mer and 23-mer peptide ions were 8 % and 14 % respectively. Both peptides exhibited no $H^{\bullet}$ loss from the $[M+2H]^{+\bullet}$ observed.

For the triply protonated peptide ions, series of c_n^{+} and $z_n^{+\bullet}$ were formed for both peptides. Secondary loss of E side chain (odd or even electron species) from $z_n^{+\bullet}$ was also observed. Some *a-/y-* ions were formed as minor product ions. One of the special features in the spectra was that there was a relatively high abundance of $[M+3H]^{2+\bullet}$. P(D) for the 15-mer and 23-mer peptide ions were 77 % and 70 % respectively. No loss of $H^{\bullet}$ from $[M+3H]^{2+\bullet}$ was observed.

4.3.2.2 Comparison of ECD of peptide ions with and without proline residues

It was expected that the incorporation of multiple P residues would reduce the degree of freedom of the peptide chain and thus limiting the formation of hydrogen bond within the polypeptide ions. In addition, proline residue does not contain any amide hydrogen. Similar to the N-methylated glycine residues, proline residues should therefore reduce the extent of formation of the hydrogen bonding chain. The suppression effect observed in the model peptides should therefore be eliminated by the proline-substituded analogues. As expected, the ECD spectra of the triply protonated peptide ions show no obvious suppression effect as deduced from the number and intensity of the fragment ions and the calculated P(D) value. However, the ECD spectra of doubly protonated peptide ions with proline residues show very

limited backbone fragmentation. This is in consistent with our hypothesis.

A feasible explanation to account for the observed phenomenon is that there was preferential cleavage of the N-C_α bond of P residues. However, the cleavage of a single N-C_α bond in the pyrrolidine ring of P residues would not form the fragments. Thus, the product ions would still appear as the mass of $[M+2H]^{+\bullet}$ in the spectrum. To evaluate this hypothesis, further experiments were performed using two model peptides, RGPGPGPGRGPGPGPGR and $RG_mAG_mAG_mAGRG_mAG_mAG_mAGR$ ($_mA$ represents N-methylated alanine residue). One of the characteristics of P residue is that both the N atom and the C_α atom were bonded to the aliphatic chain. To mimic a P residue, N-methylated alanine residue ($_mA$) was used. Alanine is one of the natural amino acids that the side chain on the C_α atom is a methyl group. With N-modified residue, the hydrogen atom on N was substituted by a methyl group. Thus, both N and C_α atom were bonded to an aliphatic chain. Figure 4.3 shows the ECD mass spectra of both doubly protonated peptide ions. In general, only large mass fragment ions were generated for both peptides ions after ECD. Fragment ions next to the N-terminal P residues for RGPGPGPGRGPGPGPGR, i.e. c_{10}^+, c_{12}^+, c_{14}^+, $z_{11}^{+\bullet}$, $z_{13}^{+\bullet}$ and $z_{15}^{+\bullet}$ were not observed as expected. There were some hydrogen atom rearrangements between *c-/z*$^\bullet$- ions. Charge-reduced precursor ions and loss of NH_3 and R side chain from $[M+2H]^{+\bullet}$ were also observed.

From the mass spectrum of peptide ions with P being replaced by $_mA$, the number and the intensity of fragment ions observed were almost the same. N-C_α linkages next to the N-termini of $_mA$ residue were also cleaved giving rise to series of c_n^+ (n = 9-15) and z_n^+ (n = 10-16). Figure 4.4 (a) and (b) show the normalized fragment ions intensity for each backbone cleavage site of both peptides. The fragment ions generated by cleavage at the N-termini of $_mA$ residues were of similar

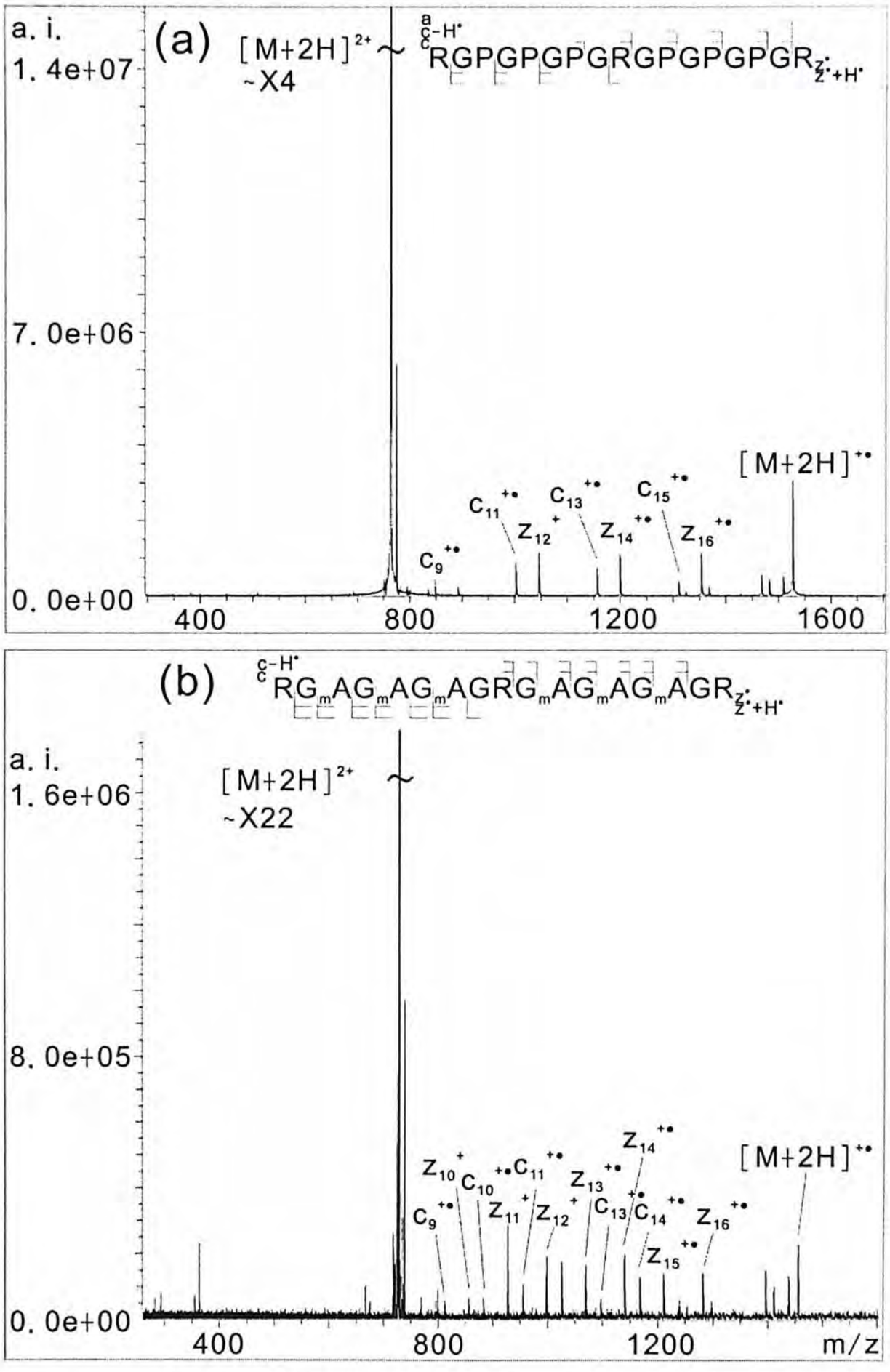

Figure 4.3 ECD mass spectra of doubly protonated
(a) RGPGPGPGRGPGPGPGR and (b) $RG_mAG_mAG_mAGRG_mAG_mAG_mAGR$

(a) $^{a}_{c}$–H$^{\bullet}$
^{c}RGPGPGPGRGPGPGPGR$_{z}^{\bullet}$
$\bar{z}^{\bullet}$+H$^{\bullet}$

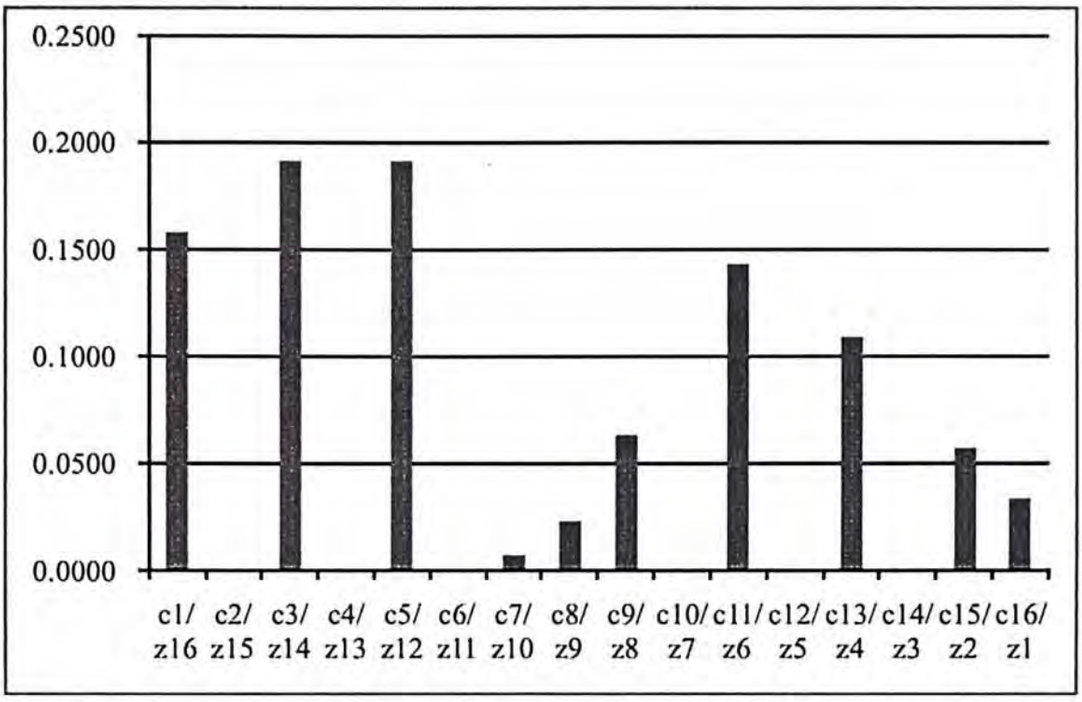

(b) $^{c}_{c}$–H$^{\bullet}$
^{c}RG$_m$AG$_m$AG$_m$AGRG$_m$AG$_m$AG$_m$AGR$_{z}^{\bullet}$
$\bar{z}^{\bullet}$+H$^{\bullet}$

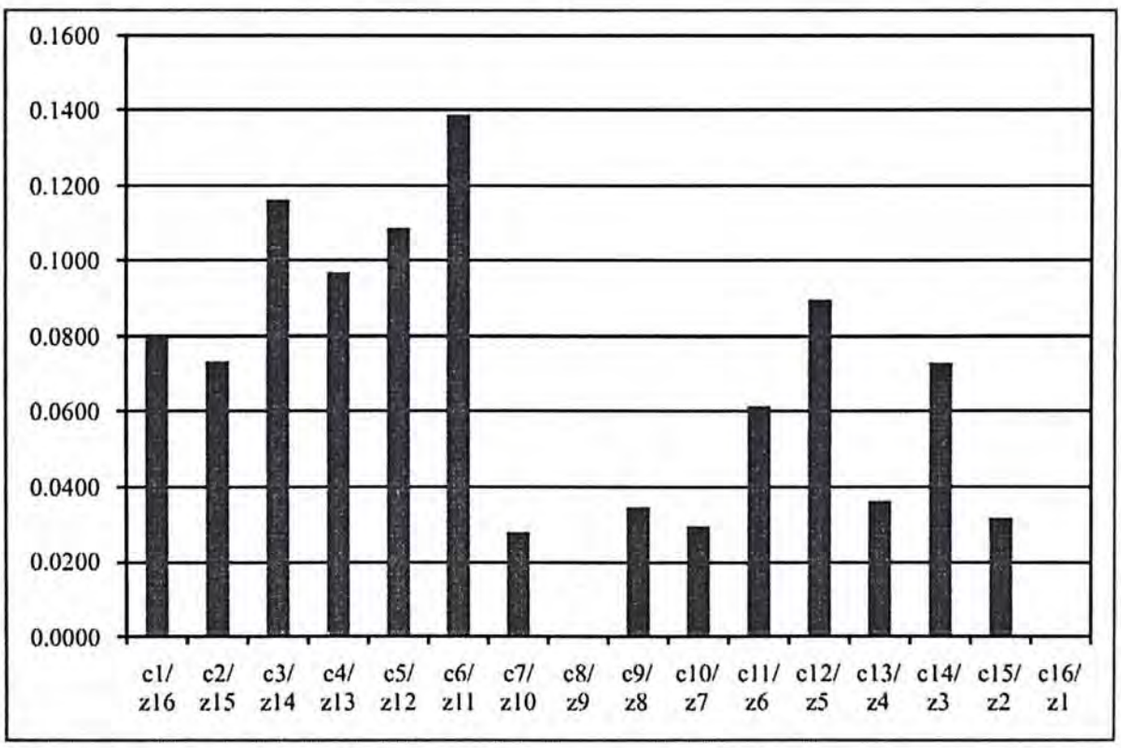

Figure 4.4 The normalized abundance of each backbone cleavage sites for doubly protonated (a) RGPGPGPGRGPGPGPGR and (b) RG$_m$AG$_m$AG$_m$AGRG$_m$AG$_m$AG$_m$AGR.

abundance compared to the fragment ions generated by cleavage at the N-termini of glycine residues. The total c_n^+/ $c_n^{+\bullet}$ and $z_n^{+\bullet}$/ z_n^+ intensity at $_m$A's N-terminal and other backbone sites were calculated, which they were almost in 1: 1 ratio. From these results, we concluded that there was no preferential cleavage at $_m$A residue and so as P residue.

Since there was no preferential cleavage at the P residues, the limited backbone fragment ions might be attributed to the suppression of the backbone cleavages. Figure 4.5 shows the mass spectra of ECD followed by collision activation of RPEPEPEREPEPEPR. Many *c-/z•*- ions were formed, and H$^\bullet$ loss from $[M+2H]^{+\bullet}$ was observed. This showed that the $[M+2H]^{+\bullet}$ might be re-activated to cleave N-C_α bond. The reasons causing suppression in the proline containing peptide ions were still unknown. More experiments should be carried out to ascertain the origin of the suppression effects.

4.3.3 Transition metal ions as charge carriers

In this section, the use of metal ions as charge carriers was explored. Due presumably to the multi-dentate nature of metal ions, peptide adducted with metal ions are known to adopt a rather different conformation as compared to the corresponding protonated species. First row divalent transition metal ions (Mn(II), Co(II), Ni(II), Cu(II), Zn(II)) and group IIB metal ions (Cd(II) and Hg(II)) adducted peptides were investigated. The model peptide adopted for this study was RGEGEGEGEGEGEGR. Another model peptide with the same number of amino acids but with 1 E residue, RGGGGGGEGGGGGGR, was used as control.

4.3.3.1 General ECD mass spectra features

Figure 4.6 (a-h) and 4.7 (a-h) show the ECD mass spectra of protonated and

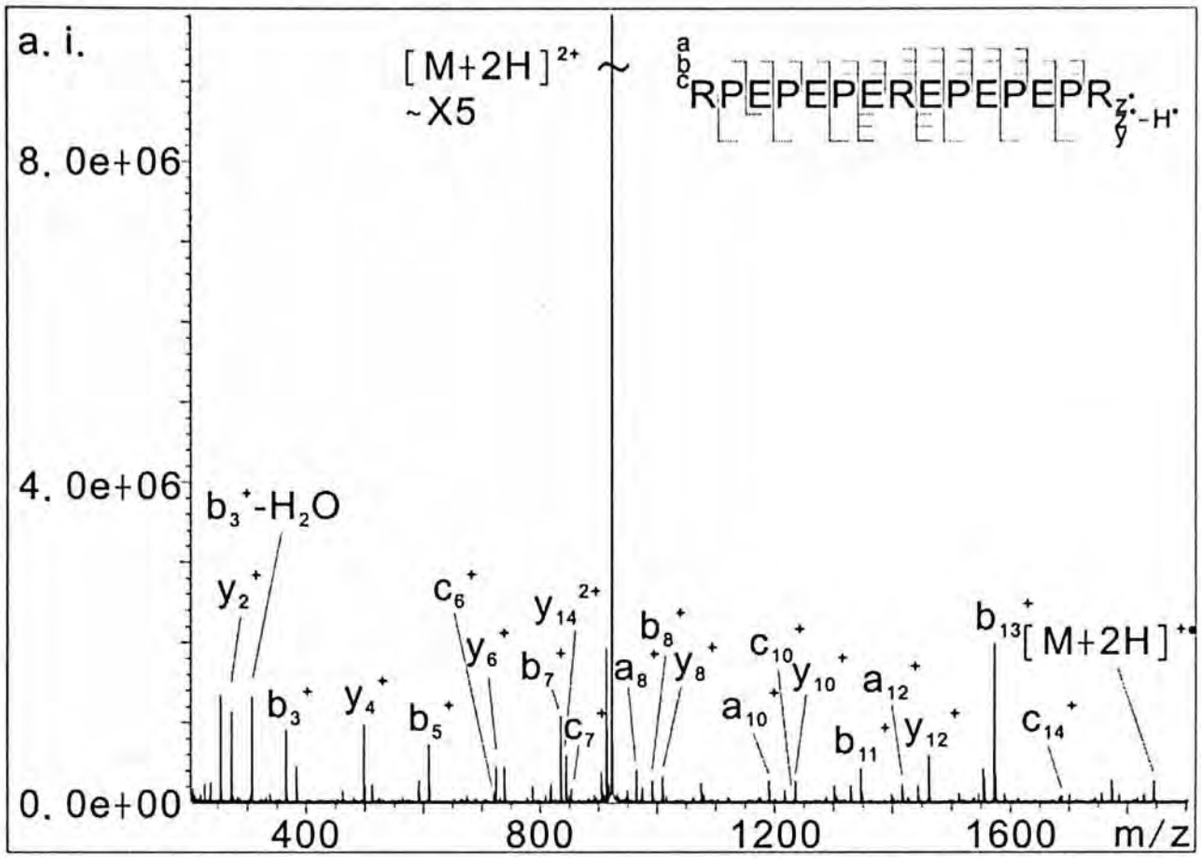

Figure 4.5 Mass spectrum of ECD followed by pulsing argon gas of doubly protonated RPEPEPEREPEPEPR.

metal ions-adducted RGEGEGEGEGEGEGR and RGGGGGGEGGGGGGR respectively. As from the type of fragment ions formed, the ECD behaviour of peptides adducted with different metal ions could be divided into following groups: (i) Mn^{2+}-, Zn^{2+}- and Cd^{2+}-, (ii) Co^{2+}- and Ni^{2+}-, (iii) Cu^{2+}- and (iv) Hg^{2+}- adducted peptides.

From the mass spectra of RGEGEGEGEGEGEGR, only a few high mass metalated backbone fragment ions were observed. Their intensities were relatively low as compared to the metalated charge-reduced precursor ions ($[M+Cat]^+$) and the neutral loss of NH_3, H_2O, CO, E or R side chain loss from $[M+Cat]^+$. For Hg(II) adducted peptide ions, $M^{+\bullet}$ ions were formed after the electron capture. Neutral loss of CO_2 and H_2O and E or R side chain loss from $M^{+\bullet}$ were also observed. ECD of $[M+Hg]^{2+}$ gave only two backbone fragments, i.e. a_8^+ and a_{12}^+. No metalated fragment ion was observed. In general, the suppression effect that observed in the protonated species was even more significant when the metal ions were used as charge carriers.

For RGGGGGGEGGGGGGR, much more backbone fragment ions were observed. For Mn^{2+}-, Zn^{2+}- and Cd^{2+}-adducted peptide ions, small non-metalated *c-/z•*- ions and large metalated *c-/z•*- ions were observed. The charge-reduced precursor ions were present in almost all ECD spectra, together with some fragment ions generated by loss of neutral molecules (NH_3 and H_2O), E and R side chain loss from $[M+Cat]^+$. For Co^{2+}- and Ni^{2+}-adducted peptides, metalated *a-/y-* ion were observed apart from the expected metalated and non-metalated *c-/z•*- ions. For Ni^{2+}-adducted peptides, the intensity of $[M+Ni]^+$ and and $[M+Ni-CO]^+$ were comparatively higher than that of Co^{2+}. However, for Cu^{2+}- and Hg^{2+}-adducted peptides, the number and intensity of fragment ions were greatly reduced. In the case

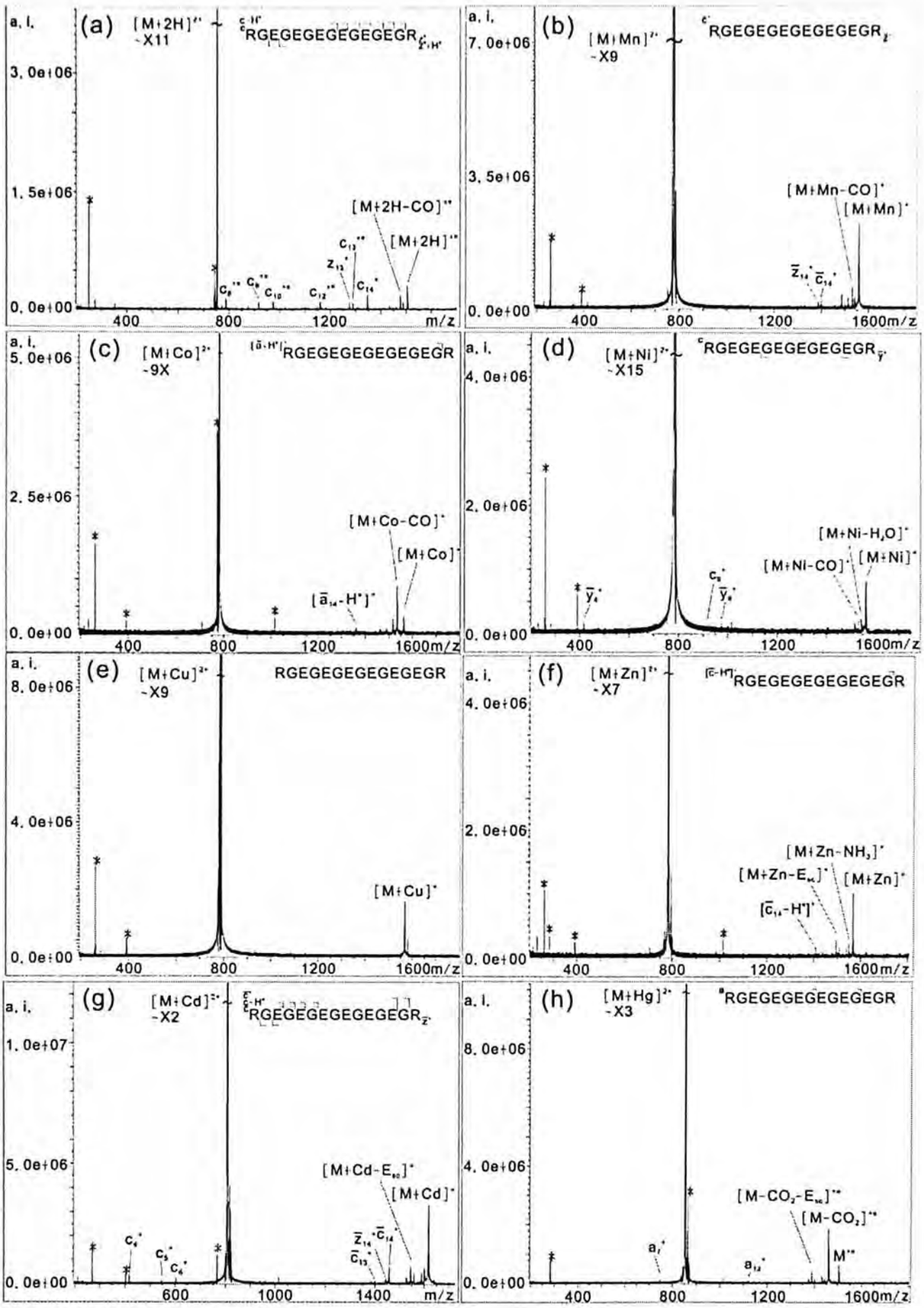

*represent electronic noises
metalated-a/y/c/z ions were denoted as $\bar{a}$, $\bar{y}$, $\bar{c}$ and $\bar{z}$.

Figure 4.6 ECD mass spectra of RGEGEGEGEGEGEGR with (a) H^+ (b) Mn^{2+} (c) Co^{2+} (d) Ni^{2+} (e) Cu^{2+} (f) Zn^{2+} (g) Cd^{2+} (h) Hg^{2+} as charge carrier.

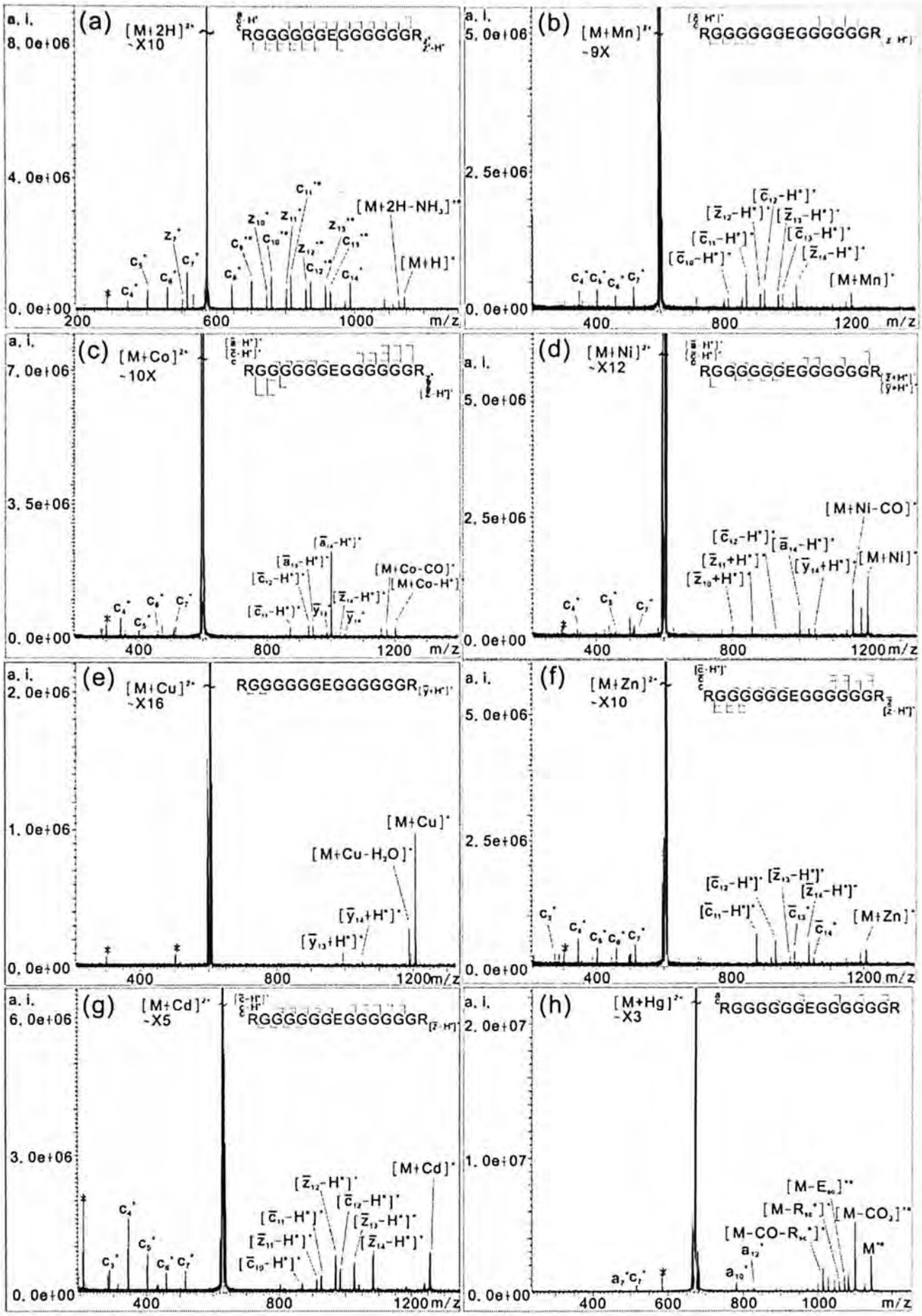

*represent electronic noises
metalated-a/y/c/z ions were denoted as $\bar{a}$, $\bar{y}$, $\bar{c}$ and $\bar{z}$ respectively.

Figure 4.7 ECD mass spectra of RGGGGGGEGGGGGGR with (a) H^+ (b) Mn^{2+} (c) Co^{2+} (d) Ni^{2+} (e) Cu^{2+} (f) Zn^{2+} (g) Cd^{2+} (h) Hg^{2+} as charge carrier.

high mass metalated *y*-ions were formed. $[M+Cu]^+$ remained very intense. For of Cu^{2+}-adducted peptides, only two Hg^{2+}-adducted peptides, a few *a*- ions and *c*- ions were formed. Same as ECD of $[RGEGEGEGEGEGEGR+Hg]^{2+}$, $M^{+\bullet}$ was formed instead of $[M+Hg]^+$. There were abundant ion with loss of CO_2, E and R side chains from $M^{+\bullet}$.

4.3.3.2 Comparison of ECD behaviour using proton and metal ions as charge carrier

Figure 4.8 summarizes the P(D) of the proton and metal ions adducted peptides. For RGEGEGEGEGEGEGR, all metal ions adducted peptides gave fewer backbone fragments under typical ECD conditions. The number of E residues might be an important factor leading to this suppression of backbone cleavage. For RGGGGGGEGGGGGGR, almost all metal ion adducted peptide (except Cu^{2+}- and Hg^{2+}-adducted peptides) gave extensive backbone fragmentation. Their results were consistent with those observed for the protonated system.

Table 4.1 shows the normalized abundance of the all product ions for ECD of $[M+Hg]^{2+}$. For Hg^{2+}-adducted peptide, $M^{+\bullet}$ was formed instead of $[M+Hg]^+$ after the electron capture event. It was proposed previously that metal ion reduction of the $[M+Hg]^{2+}$ would spontaneously induce an electron transfer from the peptide moiety to the charge-reduced metal ions. Peptide radical cations, $M^{+\bullet}$, were then formed. The reduced in backbone fragmentation might be due to the preferential loss of neutral molecules and E or R side chains from $M^{+\bullet}$.

For Cu^{2+}-adducted peptides, it was unexpected that there was not much backbone fragments formed even for RGGGGGGEGGGGGGR. To investigate the cause of this observation, the ECD behaviour of a shorter model peptide,

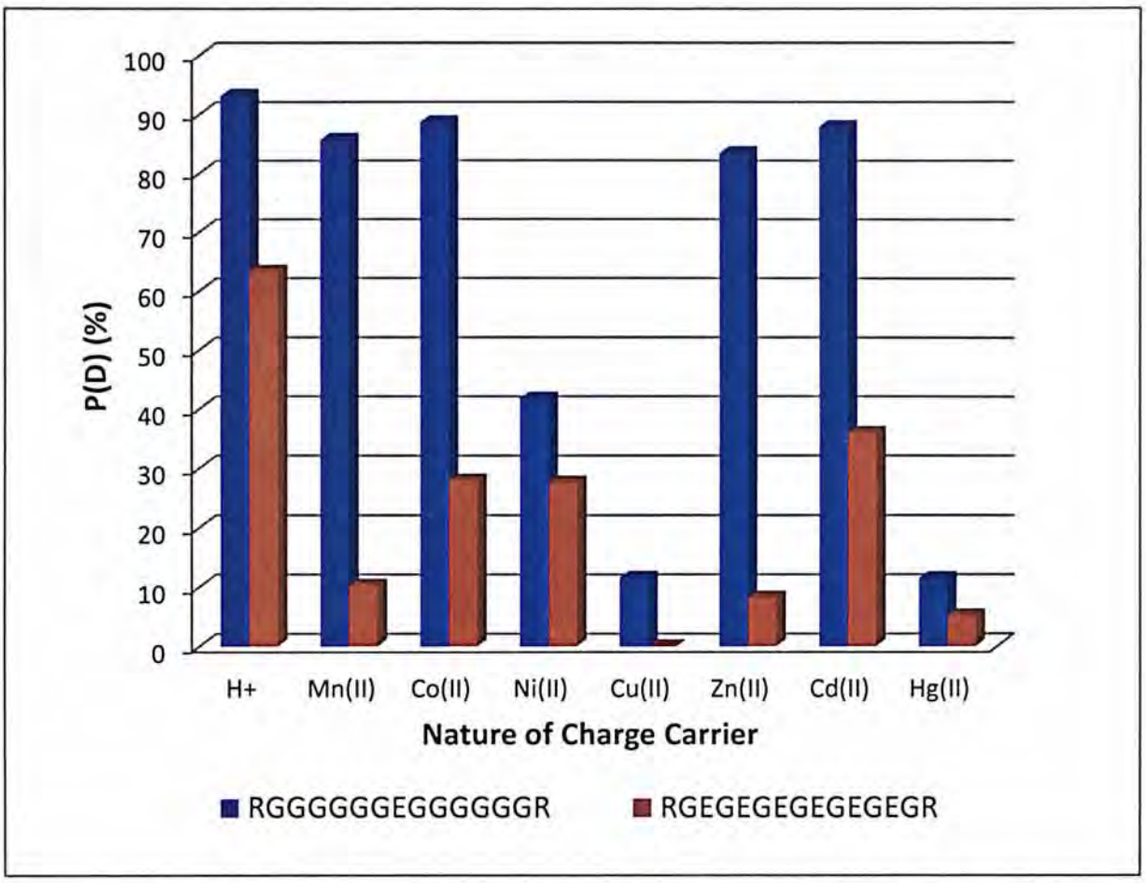

Figure 4.8 P(D) of ECD of model peptides, RGGGGGGEGGGGGGR and RGEGEGEGEGEGEGR, with different charge carriers.

Table 4.1 Percentage of product ions from ECD of $[M+Hg]^{2+}$(%)

Ion	RGGGGGGEGGGGGGR	RGEGEGEGEGEGEGR
c_n^+	4.6	--
a_n^+	4.7	5.4
$[M-C_4H_9N_3-CO_2]^{+\bullet}$	3.0	--
$[M-C_3H_8N_3^{\bullet}-CO_2]^+$	9.7	2.1
$[M-E_{sc}-CO_2]^{+\bullet}$	6.0	11.5
$[M-C_4H_9N_3]^{+\bullet}$	4.7	--
$[M-C_3H_8N_3^{\bullet}]^+$	4.1	--
$[M-E_{sc}]^{+\bullet}$	6.8	7.6
$[M-CO_2-H_2O]^{+\bullet}$	7.4	4.9
$[M-CO_2]^{+\bullet}$	30.0	51.5
$[M-H_2O]^{+\bullet}$	3.5	--
$M^{+\bullet}$	15.4	17.0

RGGGEGGGR (9-mer), was evaluated. Figure 4.9 shows the ECD mass spectrum of $[RGGGEGGGR+Cu]^{2+}$. Many metalated *b*-ions (i.e. $[b\text{-H}]^+$) and *y*-ions (i.e. $[y\text{-H}]^+$) were formed. The charge-reduced precursor ion with $H^\bullet$ loss was also present, but the intensity was relatively lower when compared to backbone fragment ions. The suppression effect that observed in 15-mer 1 E model peptide was not observed in this 9-mer peptide. It is obvious that the chain length was responsible for inhibiting the backbone fragmentation. The binding of Cu^{2+} to RGGGGGGEGGGGGGR might enhance the extent of the formation of the hydrogen bonding resonance structure and thus inhibiting the backbone cleavages.

The conformation of the metal ions-adducted peptide ions might not be very different from that of doubly protonated 15-mer E-rich peptide ions. The proposed model for the suppression of backbone cleavage was still valid and resulted in the limited backbone fragment ions. The expected alternation of the conformation by metal ions might not occur. Perhaps the metal ions were coordinated at the C-terminal rather than disrupting the gross conformation of the peptide ions. Further investigation has to be done to validate this argument.

4.4 Conclusions

Experiments on the study of the importance of amide hydrogen in forming the proposed hydrogen bonding resonance structure had been performed using N-methylated amino acid residues, proline residues instead of glycine residues and metal ions as charge carriers.

Substitution of the amide hydrogen atoms by methyl groups in the 15-mer E-rich peptide lifted the suppression effect and generated lots of backbone fragments. This finding was in agreement with our proposed model in explaining the effect of

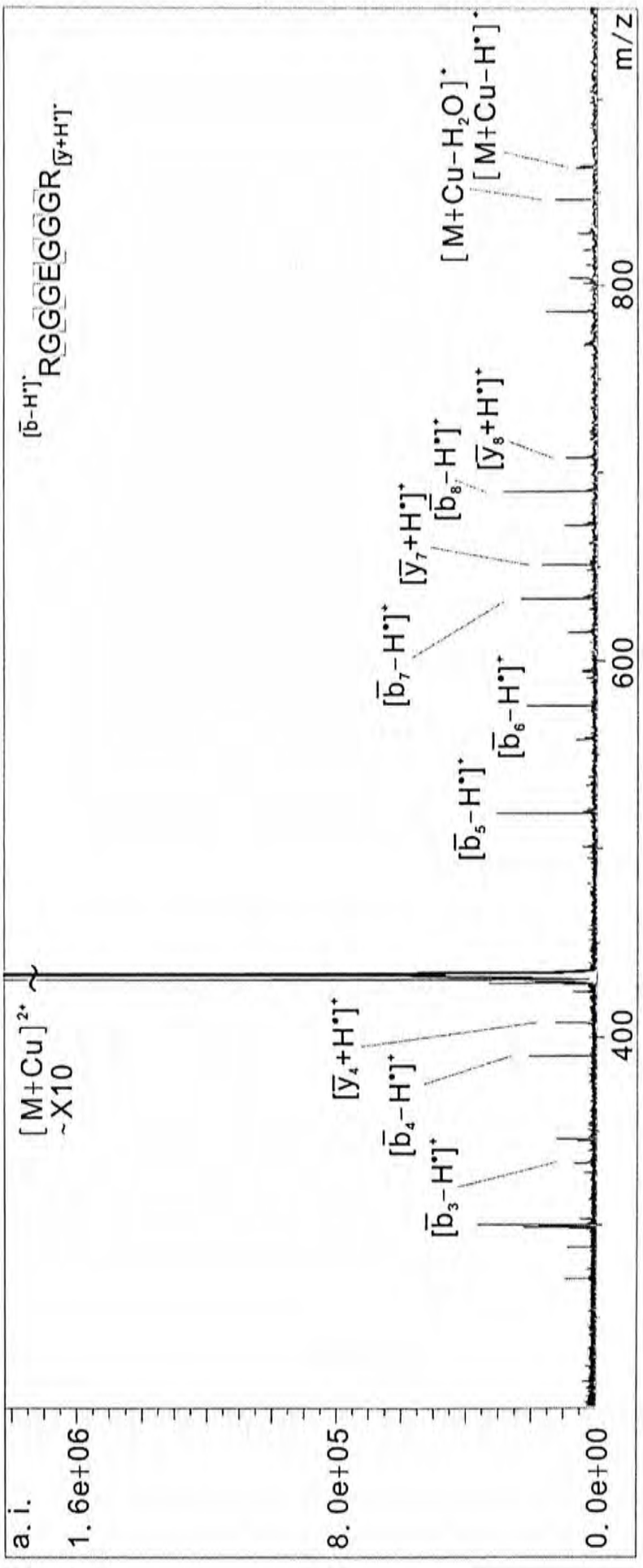

metalated-b/y ions were denoted as $\bar{b}$ and $\bar{y}$ respectively.

Figure 4.9 ECD mass spectrum of $[RGGGEGGGR+Cu]^{2+}$.

suppression of backbone dissociation under ECD condition. Without any amide hydrogen, a lower extent of hydrogen bonding network could be formed and the hydrogen radical formed would not be effectively trapped. Extensive backbone cleavage would be resulted. Furthermore, it was proposed that $H^{\bullet}$ loss from $[M+nH]^{(n-1)+\bullet}$ was originated from the amide hydrogen, but not the ejection of the neutralized proton.

With the incorporation of proline residues in 15-mer E-rich peptide or 23-mer polypeptide ions, suppression effect was still observed. Using model peptide with $_{m}A$ residues (mimic P residue), the possibility of preferential cleavage at N-C_{α} bond of P residue was eliminated. Furthermore, the post ECD activation experiment showed that the N-C_{α} bond cleavage could be re-activated. More experiments should be carried out to ascertain the origin of the proline-induced suppression effects.

The use of the metal ions as charge carrier was intended to alter the conformation of the peptide ions so as to disrupt the hydrogen bonding resonance structure and to reduce the suppression effect. However, ECD of metalated E-rich peptide did not show more backbone fragments. It seemed that the effect of E residues which formed hydrogen bond with amide hydrogen was still present. Further experiments had to be performed to verify the importance of such structure in the suppression of backbone cleavages.

Chapter 5

Conclusions

A systematic investigation was conducted to study the structural parameters of peptide ions that could lead to suppression of backbone fragmentation under ECD conditions. Three structural parameters were studied, including the number and nature of proton carrier and peptide chain length. Among these parameters, the most pronounced suppression effect was observed in increasing the peptide chain length. By increasing the number of amino acids from 8 to 23 for a glutamic acid containing peptide, ECD of the doubly protonated peptide ions showed a significant decrease in backbone fragmentation and $H^{\bullet}$ loss from $[M+2H]^{+\bullet}$. Based on the results of conformational searches, a hydrogen bonding "ladder" model was proposed. The $H^{\bullet}$ was being trapped along the hydrogen bonding framework formed between the backbone amide hydrogen atoms and carbonyl oxygen atoms. Regarding the number of proton carrier, increasing R residues from 2 to 3 had no observable difference on the observed suppression effect. Altering the proton carrier from R to other basic amino acid residues, such as K or H, in 15-mer E-rich peptide showed a lesser extent of suppression effect. We tentatively attributed this effect to a change of peptide ions conformation, in which the formation of the hydrogen bonding between the backbone amide hydrogen and E side chain was not favoured.

To evaluate the validity of this model, experiments were performed to study the importance of forming the proposed hydrogen bonding resonance structure in suppression effect. ECD of E-rich 15-mer peptide ions with N-methyl amino acid residues lead to abundant backbone fragments. This is consistent with our postulation that amide hydrogen atoms are essential in forming the resonant structure.

Furthermore, H$^{\bullet}$ loss from $[M+nH]^{(n-1)+\bullet}$ was proposed to be originated from the amide hydrogen, but not the ejection of the neutralized proton as no $[M+2H-H]^{+}$ observed. P residue lacks of amide hydrogen and with the rigid ring. Peptides with P residues were expected to have fewer chances to form intra-molecular hydrogen bonding and thus could alleviate the suppression effect, while even more significant suppression was observed. Furthermore, ECD of metalated E-rich peptide did not result more backbone fragments. It seemed that the effect of E residues which form hydrogen bond with amide hydrogen was still present, disregard the multi-dentate property of transition metal ions. More experiments, such as the reactivation of metalated charge-reduced species by pulsing argon gas after ECD experiments, should be carried out to ascertain the origin of the suppression effects.

References

1. Stryer, L. Biochemistry, 3rd edition, W. H. Freeman and Company, New Work, 1988, pp15-16.
2. Edman, P. *Acta Chemica Scandinavica* 1950; **4**: 283.
3. Edman, P. *Acta Chemica Scandinavica* 1956; **10**: 761.
4. Thomson, J. J. *Phil. Mag.* 1899; **48**: 575.
5. Bleakney, W. *Phys. Rev.* 1929; **34**: 157.
6. Munson, M. S. B.; Field, F. H. *J. Am. Chem. Soc.* 1966; **88**: 2621.
7. Winkler, H. U.; Beckey, H. D. *Biochem. Biophys Res. Commun.* 1972; **46**: 391.
8. Torgerson, D. F.; Skowronski, R. P.; Macfarlane, R. D. *Biochem. Biophys Res. Commun.* 1974; **60**: 616.
9. Barder, M.; Bordoli, R. S.; Sedgewick, R. D.; Tyler, A. N. J. Chem. Soc. Chem. Commun. 1981; **7**: 325.
10. Dole, M.; Mack, L. L.; Hines, R. L.; Mobley, R. C.; Ferguson, L. D.; Alice, M. B. *J. Chem. Phys.* 1968; **49**: 2240.
11. Karas, M.; Bachmann, D.; Bahr, U.; Hillenkamp, F. *Int. J. Mass Spectrom. Ion Proc.* 1987; **78**: 53.
12. Yamashita, M.; Fenn, J. B. *J. Phys. Chem.* 1984; **88**; 4451.
13. Fenn, J. B.; Mann, M.; Meng, C. K.; Wong, S. F.; Whitehouse, C. M. *Science* 1989; **246**: 64.
14. Brill, L. M.; Motamedchaboki, K.; Wu, S.; Wolf, D. A. *Methods* 2009; **48**: 311.
15. Kelleher, N L.; Lin, H. Y.; Valaskovic, G. A.; Aaserad., D. J.; Fridriksson, E. K.; McLafferty, F. W. *J. Am. Chem. Soc.* 1999; **121**: 806.
16. Kelleher, N L. *Anal. Chem.* 2004; **76**: 196A.
17. Mortz, E.; O'Connor, P. B.; Roepstroff, P.; Kelleher, N. L.; Wodd, T. D.; McLafferty, F. W.; Mann, M. *Proc. Natl. Acad. Sci. USA* 1996; **93**: 8264.
18. Sze, S. K.; Ge, Y.; Oh, H.; McLafferty, F. W. *Proc. Natl. Acad. Sci. USA* 2002; **99**: 1774.
19. Han, J.; Borchers, C. H. *Proteomics* 2010; **10**: 3621.
20. Roepstroff, R.; Fohlmen, *J. Biomed. Mass Spectrom.* 1984; **11**: 601.
21. Johnson, R. S.; Martin, S. A.; Biemann, K.; Stults, J. T.; Watson, J. T. *Anal. Chem.* 1987; **59**: 2621.
22. Haddon, W. F.; McLafferty, F. W. *J. Am. Chem. Soc.* 1968; **90**: 4745.
23. Grant, E. R.; Coggiola, M. J.; Leem, Y. T.; Schulz, P. A.; Sudbo, A. S.; Shen, Y. R. *Chem. Phys. Lett.* 1977; **52**: 595.
24. Little, D. P.; Speir, J. P.; Senka, M. W.; O'Connor, P. B.; McLafferty, F. W. *Anal.*

Chem. 1994; **66**: 2809.

25. Price, W. D.; Schnier, P. D.; Williams, E. R. *Anal. Chem.* 1996; **68**: 859.
26. McLuckey, S. A.; Goeringer, D. B. *J. Mass Spectrom.* 1997; **32**: 461.
27. Loo, J. A.; Edmonds, C. G.; Smith, R. D. *Anal. Chem.* 1993; **65**: 425.
28. Yu, W.; Vath, J. E.; Huberty, M. C.; Martin, S. A. *Anal. Chem.* 1993; **65**: 3015.
29. Cody, R. B.; Burnier, R. C.; Freiser, B. S. *Anal. Chem.* 1982; **54**: 96.
30. Carlin, T. J.; Freiser, B. S. *Anal. Chem.* 1983; **55**: 571.
31. Lee, S. A.; Jiao, C. Q.; Huang, Y.; Freiser, B. S. *Rapid Commun. Mass Spectrom.* 1993; **7**: 819.
32. Heck, A. J. R.; de Koning, L. J.; Pinkse, F. A.; Nibbering, N. M. M. *Rapid Commun. Mass Spectrom.* 1991; **5**: 406.
33. Gauthier, J. W.; Trautman, T. R.; Jacobson, D. B. *Anal. Chim. Acta.* 1991; **246**: 211.
34. Boering, K. A.; Rolfe, J.; Brauman, J. I. *Rapid Commun. Mass Spectrom.* 1992; **6**: 303.
35. Boering, K. A.; Rolfe, J.; Brauman, J. I. *Int. J. Mass Spectrom. Ion Processes* 1992; **117**: 357.
36. Senko, M. W.; Speir, J. P.; McLafferty, F. W. *Anal. Chem.* 1994; **66**: 2801.
37. Zubarev, R. A.; Kelleher, N. L.; McLafferty, F. W. *J. Am. Chem. Soc.* 1998; **120**: 3265.
38. Syka, J. E.; Coon, J. J.; Schroeder, M. J.; Shabanowitz, J.; Hunt, D. F. *Proc. Natl. Acad. Sci. USA* 2004; **101**: 9528.
39. Kelleher, N. L.; Zubarev, R. A.; Bush, K.; Furie, B.; Furie, B. C.; McLafferty, F. W.; Walsh, C. T. *Anal. Chem.* 1999; **71**: 4250.
40. Shi, S. D.-H.; Hemling, M. E.; Carr, S. A.; Horn, D. M.; Lindh, I.; McLafferty, F. W. *Anal. Chem.* 2001; **73**: 19.
41. Mirgorodskaya, E.; Roepstorff, P.; Zubarev, R. *Anal. Chem.* 1999; **71**: 4431.
42. Håkansson, K.; Cooper, H. J.; Emmett, M. R., Costello, C. E.; Marshall, A. G.; Nilsson, C. L. *Anal. Chem.* 2001; **73**: 4530.
43. Tsybin, Y. O.; Quinn, J. P.; Tsybin, O. Y.; Hendrickson, C. L.; Marshall, A. L. *J. Am. Soc. Mass Spectrom.* 2008; **19**: 762.
44. Zubarev, R. A.; Kruger, N. A.; Fridriksson, E. K.; Lewis, M. A.; Horn, D. M.; Carpenter, B. K.; McLafferty, F. W. *J. Am. Chem. Soc.* 1999; **121**: 2857.
45. Syrstad, E. A.; Tureček, F. *J. Am. Soc. Mass Spectrom.* 2005; **16**: 208.
46. Leymarie, N.; Costello, C. E.; O'Connor, P. B. *J. Am. Chem. Soc.* 2003; **125**: 8949.
47. Tsybin, Y. O.; Håkansson, P.; Budnik, B. A.; Haselmann, K. F.; Kjeldsen, F.; Gorshkov, M.; Zubarev, R. A. *Rapid Commun. Mass Spectrom.* 2001; **15**: 1849.
48. Oh, H.; McLafferty, F. W. *Bull. Korean Chem. Soc.* 2006; **27**: 389.

49. Kjeldsen, F.; Haselmann, K. F.; Budnik, B. A.; Hensen, F.; Zubarev, R. A. *Chem. Phys. Lett.* 2002; **356**: 201.
50. Haselmann, K. F.; Budnik, B. A.; Olsen, J. V.; Nielsen, M. L.; Reis, C. A.; Clausen, H.; Johnsen, A. H.; Zubarev, R. A. *Anal. Chem.* 2001; **73**: 2998.
51. Gorshkov, M. V.; Masselon, C. D.; Nikolaev, E. N.; Udseth, H. R.; Pasa-Tolic, L.; Smith, R. D. *Int. J. Mass Spectrom.* 2004; **234**: 131.
52. Håkansson, K.; Chalmers, M. J.; Quinn, J. P.; McFarland, M. A.; Hendrikson, C. L.; Marshall, A. G. *Anal. Chem.* 2003; **75**: 3256.
53. Breuker, K.; Oh, H.; Horn, D. M.; Cerda, B. A.; McLafferty, F. W. *J. Am. Chem. Soc.* 2002; **124**: 6407.
54. Horn, D. M.; Ge, Y.; McLafferty, F. W. *Anal. Chem.* 2000; **72**: 4778.
55. Zubarev, R. A.; Horn, D. M.; Fridriksson, E. K.; Kelleher, N. L.; Kruger, N. A.; Lewis, M. A.; Carpenter, B. K.; McLafferty, F. W. *Anal. Chem.* 2000; **72**: 563.
56. Sze, S. K.; Ge, Y.; Oh, H.; McLafferty, F. W. *Anal. Chem.* 2003; **75**: 1599.
57. Iavarone, A. T.; Paech, K.; Williams, E. R. *Anal. Chem.* 2004; **76**: 2231.
58. Fung, Y. M. E.; Liu, H.; Chan, T. W. D. *J. Am. Soc. Mass Spectrom.* 2006; **17**: 757.
59. Håkansson, K.; Liu, H. *J. Am. Soc. Mass Spectrom.* 2006; **17**: 1731.
60. Van der Burgt, Y. E. M.; Palmblad, M.; Dalebout, H.; Heeren, R. M. A.; Deelder, A. M. *Rapid Commum. Mass Spectrom.* 2009; **23**: 31.
61. Chen, X.; Chan, W. Y. K.; Wong, P. S.; Yeung, H. S.; Chan, T. W. D. *J. Am. Soc. Mass Spectrom.* 2011; **22**: 233.
62. Lawrence, E. O.; Edlefsen, N. E. *Science* 1930; **72**: 376.
63. Sommer, H.; Thomas, H. A.; Hipple, J. A. *Phys. Rev.* 1949; **76**: 1877.
64. Comisarow, M.B.; Marshall, A. G. *Chem. Phys. Lett.* 1974; **25**:282.
65. Marshall, A. G.; Comisarow, M.B.; Parisod, G. *J. Chem. Phys.* 1979; **71**: 4434.
66. Grosshans, P. B.; Shields, P. J.; Marshall, A. G. *Chem. Phys.* 1991; **94**:5341.
67. Marshall, A. G.; Grosshans, P. B. *Anal. Chem.* 1991; **63**: A215.
68. Dunbar, R.C. *Int. J. Mass Spectrom. Ion Processes* 1984; **56:** 1.
69. Dunbar, R.C.; Chen, J. H.; Hays, J. D. *Int. J. Mass Spectrom. Ion Processes* 1984; **57**: 39.
70. Mitchel, D. W. *Int. J. Mass Spectrom. Ion Processes* 1991; **107**: 417.
71. Schweikhard, L; Ziegler, J.; Bopp, H.; Lutzenkirchen, K. *Int. J. Mass Spectrom. Ion Processes* 1995; **141**: 77,
72. Marshall, A. G.; Hendrickson, C. L.; Jackson, G. S. *Mass Spectrom. Rev.* 1998; **17**: 1.
73. Fong, W. Y. K.; Chan, T. W. D. *J. Am. Soc. Mass Spectrom.* 1999; **10**: 72.
74. Caravatti, P.; Allemann, M. *Org. Mass Spectrom.* 1991; **26**: 514.
75. Ozkan, S. B.; Meirovitch, H. *J. Phys. Chem. B* 2003; **107**: 9128.

76. Kolossvary, I.; Guida, W. C. *J. Comp. Chem.* 1999; **20**: 1671.
77. Balyayev, M. A.; Cournoyer, J. J.; Lin, C.; O'Connor, P. B. *J. Am. Soc. Mass Spectrom.* 2006; **17**: 1428.
78. Jones, J. W.; Sasaki, T.; Goodlett, D. R.; Tureček, F. *J. Am. Soc. Mass Spectrom.* 2007; **18**: 432.
79. Karnezis, A.; Barlow, C. K.; O'Hair, R. A. J.; McFadyen, W. D. *Rapid Commun. Mass Spectrom.* 2006; **20:** 2865.
80. Chamot-Rooke, J.; Malosse, C.; Frison, G.; Tureček, F. *J. Am. Soc. Mass Spectrom.* 2007; **18:** 2146.
81. Li, X.; Cournoyer, J. J.; Lin, C.; O'connor, P. B. *J. Am. Soc. Mass Spectrom.* 2008; **19:** 1514.
82. Sohn, C. H.; Chung, C. K.; Yin, S.; Ramachandran, P.; Loo, J. A.; Beauchamp, J. L. *J. Am. Chem. Soc.* 2009; **131**: 5444.
83. Mihalca, R.; Kleinnijenhuis, A. J.; McDonnell, L. A.; Heck A. J. R.; Heeren, R. M. A. *J. Am. Soc. Mass Spectrom.* 2004; **15**: 1869.
84. Hongo, Y.; Nakamura, T.; Sato, A. *J. Mass Spectrom. Soc. Jpn.* 2007; **55**: 77.
85. Jones, A. W.; Mikhailov, V. A.; Iniesta, J.; Cooper, H. J. *J. Am. Soc. Mass Spectrom.* 2010; **21**: 268.
86. Chan, W. Y. K.; Chan, T. W. D. *J. Am. Soc. Mass Spectrom.* 2010; **21**: 1235.
87. Tureček, F. *J. Am. Chem. Soc.* 2003; **125**: 5954.
88. Chen, X. H.; Tureček, F. *J. Am. Chem. Soc.* 2006; **128:** 12520.
89. Jones, J. W.; Sasaki, T.; Goodlett, D. R.; Tureček, F. *J. Am. Soc. Mass Spectrom.* 2007; **18**: 432.
90. Xia, Y.; Gunawardena, H. P.; Erickson, D. E.; McLuckey, S. A. *J. Am. Chem. Soc.* 2007; **129**: 12232.
91. Julian, R. R.; Beauchamp, J. L.; Goddard III, W. A. *J. Phys. Chem. A* 2002; **106:** 32.
92. Strittmatter, E. F.; Williams, E. R. *J. Phy. Chem. A* 2000; **104**: 6069.
93. Rodriquez, C. F.; Orlova, G., Guo, Y.; Li, X.; Siu, C.-K.; Hopkinson, A. C.; Siu, K. W. M. *J. Phys. Chem. B* 2006; **110**: 7528.
94. Li, Z.; Matus, M. H.; Velazquez, H. A.; Dixon, D. A.; Cassady, C. J. *Int. J. Mass Spectrom.* 2007; **265:** 213.
95. Oh, H.; Breuker, K.; Sze, S. K.; Ge, Y.; Carpenter, B. K.; McLafferty, F. W. *Proc. Natl. Acad. Sci. USA* 2002; **99**: 15863.
96. Budnik, B. A.; Nielsen, M. L.; Olsen, J. V.; Haselmann, K. F.; Hörth, P.; Haehnel, W.; Zubarev, R. A. *Int. J. Mass Spectrom.* 2002; **219**: 283.
97. Breuker, K.; Oh, H.; Lin, C.; Carpenter, B. K.; McLafferty, F. W. *Proc. Natl. Acad. Sci. USA* 2004; **101**: 14011.
98. Hamidane, H. B.; He, H.; Tsybin, O. Y.; Emmett, M. R.; Hendrickson, C. L.;

Marshall, A. G.; Tsybin, Y. O. *J. Am. Soc. Mass Spectrom.* 2009; **20**: 1182.

99. Patriksson, A.; Adams, C.; Kjeldsen, F.; Raber, J.; van der Spoel, D.; Zubarev, R. A. *Int. J. Mass Spectrom.* 2006; **248**: 124.
100. Vorobyev, A.; Hamidane, H. B.; Tsybin, O. Y. *J. Am. Soc. Mass Spectrom.* 2009; **20**: 2273.
101. Vitagliano, L.; Berisio, R.; Mastrangelo, A.; Mazzarella, L.; Zagari, A. *Protein Science* 2001; **10**: 2627.
102. Schwartz, T. W. *FEBS Letters* 1986; **200**: 1.
103. Powers, J. S.; Hancock, R. E.W. *Peptides* 2003; **24**: 1681.
104. Crizer, D. M.; McLuckey, S. *J. Am. Soc. Mass Spectrom.* 2009; **20:** 1349.
105. Syrstad, E. A.; Stephens, D. D.; Tureček, F. *J. Phys. Chem. A* 2003; **107**: 115.

Appendix I

Twenty common amino acids

	Common side chain loss from $z_n^{+\bullet}$ fragments	
Amino Acid	**Odd-electron species**	**Even-Electron speices**
Alanine (A)	-	-
Arginine (R)	-	$H_2C{=}CHCH_2\text{-}NHC(NH)NH_2$
Asparagine (N)	$^{\bullet}C(O)NH_2$	-
Aspartic acid (D)	-	O=C=O
Cysteine (C)	$^{\bullet}SH$	$S{=}CH_2$
Glutamic acid (E)	$^{\bullet}CH_2COOH$	$CH_2{=}CHCOOH$
Glutamine (Q)	$^{\bullet}CH_2C(O)NH_2$	$CH_2{=}CHSCH_3$
Glycine (G)	-	-
Histidine (H)	-	-
Isoleucine (I)	$^{\bullet}CH_2CH_3$	$CH_3CH{=}CHCH_3$
Leucine (L)	$^{\bullet}CH(CH_3)_2$	$CH_2{=}(CH_3)_2$
Lysine (K)	$^{\bullet}CH_2CH_2CH_2NH_2$	$H_2C{=}CHCH_2CH_2NH_2$
Methionine (M)	$^{\bullet}CH_2CH_3$	$H_2C{=}CHSHCH_3$
Phenylalanine (F)	-	-
Proline (P)	-	-
Serine (S)	-	-
Threonine (T)	-	-
Tryptophan (W)	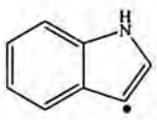	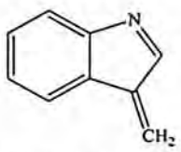
Tyrosine (Y)	-	$CH_2(C_6H_4O)$
Valine (V)	$^{\bullet}CH_3$	-

Appendix II

Pulse Programs for MS and MS^n experiments

The source codes for experiments in FTICR-MS are as follows:

(a) Simple ESI experiments (MS experiments)

```
;-----------------------------------------------------------------
; APEX III Simple ESI Experiment
;-----------------------------------------------------------------
;Experiment description
;#XS_label "Static Trapping ESI - APEX III"

;Initialization Block
;#ES_block "Initialization"
;#ES_bitmap "init3.bmp"
;#ES_conditional_pp DM bb      1u setnmr3|30   ; bit 30 hi = unmixed signal to
ADC
;#ES_conditional_pp DM hires     1u setnmr3^30     ; bit 30 low = mixed signal to
ADC
;#ES_conditional_pp RGAIN high     1u setnmr3^28 ; bit 28 low = Receiver gain
high
;#ES_conditional_pp RGAIN low      1u setnmr3|28   ; bit 28 hi = Receiver gain low

;Start Scan Accum Block (NS loop)
;#ES_block "Start Experiment"
;#ES_bitmap "start2.bmp"
;#ES_eventtype user_delay
;#ES_parameter d0
1   ze                ; clear memory buffers in RCU
10 d0 setnmr4|7           ; turn on Ultra RF amp (AGPP_OUT[0])
                ; NOTE: d0 must be 100ms or greater!
    10u reset:f1          ; reset phase of DDS in FCU 1

;Source Quench Block
;#ES_block "ESI Source Quench" optional
;#ES_bitmap "ESIquench1.bmp"
```

```
;#ES_eventtype quench
;#ES_parameter d3
    d3 setnmr3|24   ; quench the ion guide (DEFLECTION)
    1u setnmr3^24

;Cell Quench Block
;#ES_block "Cell Quench" optional
;#ES_bitmap "quench.bmp"
;#ES_eventtype quench
;#ES_parameter d4
    d4 setnmr3|27   ; cell quench (QUENCH)
    1u setnmr3^27

;Hexapole Accumulation Block
;#ES_block "Hexapole Accumulation"
;#ES_bitmap "hex_fill.bmp"
;#ES_eventtype user_delay
;#ES_parameter d1
    d1              ; post quench delay

;Ionization Block
;#ES_block "Ion Generation"
;#ES_bitmap "ion_gen2.bmp"
;#ES_eventtype user_pulse
;#ES_parameter d2 d5
    d2 setnmr3|24   ; external ionization pulse (DEFLECTION)
    1u setnmr3^24
    d5              ; post ionization delay

;================================================================
;           EXCITATION AND DETECTION
;================================================================
;Excitation Block
;#ES_block "Excitation"
;#ES_bitmap "excite.bmp"
;#ES_eventtype excitation_sweep
;#ES_parameter p3 pl3
    10u pl3:f1      ; set attenuation for excitation (FCU-1)
```

```
;#ES_conditional_pp EM shot      (p3 ph1 fq1):f1      ; detection excitation shot
;#ES_conditional_pp EM shot                           ;#FC_ fq1:f1 excitation_shot

;#ES_conditional_pp EM sweep 40 (p3 ph1 fq1):f1      ; detection excitation sweep
;#ES_conditional_pp EM sweep      lo to 40 times l31; L[31] steps in sweep
;#ES_conditional_pp EM sweep                          ;#FC_ fq1:f1 excitation_sweep

;Detection Block
;#ES_block "Detection"
;#ES_bitmap "detect.bmp"
;#ES_eventtype detection
;#ES_parameter d30
    1u setnmr4^7          ; turn off Ultra RF amp before detect (AGPP_OUT[0])
    d30                ; receiver dead time
    go = 10 ph1           ; scan accumulation (loop to 10 times NS)

;Stop Block
;#ES_block "Exit"
;#ES_bitmap "exit.bmp"
    wr #0       ; write data to disk
    exit                ; end acquisition/experiment

; Phase program definitions for FCUs
    ph1=0 0 2 2           ; phase program: 0 0 180 180 (exc/det RF)
```

(b) ESI-ECD experiments (MS^2 experiments)

```
;----------------------------------------------------------------------
; APEX III Dynamic Trapping ESI-ECD Experiment
;----------------------------------------------------------------------

;Experiment description
;#XS_label "Dynamic Trapping ECD - APEX III"

;Initialization Block
;#ES_block "Initialization"
;#ES_bitmap "init3.bmp"
;#ES_conditional_pp DM bb      1u setnmr3|30   ; bit 30 hi = unmixed signal to
ADC
;#ES_conditional_pp DM hires      1u setnmr3^30      ; bit 30 low = mixed signal to
ADC
;#ES_conditional_pp RGAIN high      1u setnmr3^28 ; bit 28 low = Receiver gain
high
;#ES_conditional_pp RGAIN low      1u setnmr3|28   ; bit 28 hi = Receiver gain low

;Start Scan Accum Block (NS loop)
;#ES_block "Start Experiment"
;#ES_bitmap "start2.bmp"
;#ES_eventtype user_delay
;#ES_parameter d0
1   ze                  ; clear memory buffers in RCU
10 d0 setnmr4|7             ; turn on Ultra RF amp (AGPP_OUT[0])
                ; NOTE: d0 must be 100ms or greater!
    10u reset:f1            ; reset phase of DDS in FCU 1

;Source Quench Block
;#ES_block "ESI Source Quench" optional on
;#ES_bitmap "ESIquench1.bmp"
;#ES_eventtype quench
;#ES_parameter d3
    d3 setnmr3|24   ; quench the ion guide (DEFLECTION)
    1u setnmr3^24

;Cell Quench Block
;#ES_block "Cell Quench" optional on
```

```
;#ES_bitmap "quench.bmp"
;#ES_eventtype quench
;#ES_parameter d4 d27
    d4 setnmr3|27   ; cell quench (QUENCH)
    1u setnmr3^27
    d27

;Trap Plate Block
;#ES_block "Raise trap potential" optional on
;#ES_bitmap "raise_trap.bmp"
    100u setnmr3|20      ; raise dynamic trap voltage (XGPP_OUT[10])
    1u    setnmr3^20

;Hexapole Accumulation Block
;#ES_block "Hexapole Accumulation"
;#ES_bitmap "hex_fill.bmp"
;#ES_eventtype user_delay
;#ES_parameter d1
20 d1                ; post quench delay

;Ionization Block
;#ES_block "Ion Generation"
;#ES_bitmap "ion_gen2.bmp"
;#ES_eventtype user_pulse
;#ES_parameter d2
    d2 setnmr3|24   ; external ionization pulse (DEFLECTION)
    1u setnmr3^24

;Pulsed Valve Block
;#ES_block "Cooling gas" optional off
;#ES_bitmap "p_valve.bmp"
;#ES_eventtype user_pulse
;#ES_parameter d26 d5
    d26 setnmr3|22 ; Pulsed Valve 1 (VALVE1)
    1u   setnmr3^22
    d5               ; Pulsed Valve pumpdown

;Ion Accumulation Block
;#ES_block "Ion Accumulation" optional on
```

```
;#ES_bitmap "ion_accum.bmp"
;#ES_eventtype user_pulse
;#ES_parameter d6 l30
    lo to 20 times l30      ; collect L[30] hexapole fillings
    d6

;=============================================================
;              STAGE 1 OF EXPERIMENT
;=============================================================
;MS/MS Selection Block
;#ES_block "Isolation (MS-2)" optional off
;#ES_bitmap "msms_sel_a.bmp"
;#ES_eventtype corr_sweep
;#ES_parameter p4 pl4
    10u pl4:f1          ; set attenuation for correlated sweep (FCU-1)
30 (p4 ph2 fq1):f1   ; correlated sweep
    lo to 30 times l0       ; L[0] steps in sweep
;#ES_flag_comment ;#FC_ fq1:f1 corr_sweep 0

;Cleanup Shots Block
;#ES_block "Isolation Shots (MS-2)" optional off
;#ES_bitmap "cl_shots.bmp"
;#ES_eventtype corr_shot
;#ES_parameter p7 pl7
    10u pl7:f1          ; set attenuation for shots (FCU-1)
40 (p7 ph2 fq1):f1   ; high resolution clean-up shots
    lo to 40 times l3       ; L[3] total shots
;#ES_flag_comment ;#FC_ fq1:f1 corr_shot 0

;Pulsed Valve Block
;#ES_block "Pulsed Valve (MS-2)" optional off
;#ES_bitmap "p_valve.bmp"
;#ES_eventtype user_pulse
;#ES_parameter d26
    d26 setnmr3|22 ; Pulsed Valve 1 (VALVE1)
    1u   setnmr3^22
```

```
;================================================================
;          STAGE 2 OF EXPERIMENT (ELECTRON CAPTURE)
;================================================================
;Ionization Block
;#ES_block "Electron injection" optional off
;#ES_bitmap "ion_gen2.bmp"
;#ES_eventtype user_pulse
;#ES_parameter p13
    p13 setnmr3|25 ; internal ionization pulse
    1u   setnmr3^25

;ECD Block
;#ES_block "ECD" optional off
;#ES_bitmap "ECD.bmp"
;#ES_eventtype user_pulse
;#ES_parameter d7
   d7   setnmr3|26  ; ECD pulse (INT_GATE)
   10u setnmr3^26

;Trap Plate Block
;#ES_block "Lower trap potential" optional on
;#ES_bitmap "lower_trap.bmp"
;#ES_eventtype user_pulse
;#ES_parameter d8 d9
50 d8 setnmr3|20    ; lower dynamic trap voltage with a voltage ramp
    1u setnmr3^20
    lo to 50 times l24     ; L[24] steps in voltage ramp
    d9                ; final pump down delay

;================================================================
;            EXCITATION AND DETECTION
;================================================================
;Excitation Block
;#ES_block "Excitation"
;#ES_bitmap "excite.bmp"
;#ES_eventtype excitation_sweep
;#ES_parameter p3 pl3
    10u pl3:f1        ; set attenuation for excitation (FCU-1)
```

```
;#ES_conditional_pp EM shot      (p3 ph1 fq1):f1      ; detection excitation shot
;#ES_conditional_pp EM shot                           ;#FC_ fq1:f1 excitation_shot

;#ES_conditional_pp EM sweep 60 (p3 ph1 fq1):f1      ; detection excitation sweep
;#ES_conditional_pp EM sweep      lo to 60 times l31; L[31] steps in sweep
;#ES_conditional_pp EM sweep                          ;#FC_ fq1:f1 excitation_sweep

;Detection Block
;#ES_block "Detection"
;#ES_bitmap "detect.bmp"
;#ES_eventtype detection
;#ES_parameter d30
    1u setnmr4^7          ; turn off Ultra RF amp before detect (AGPP_OUT[0])
    d30                ; receiver dead time
    go = 10 ph1           ; scan accumulation (loop to 10 times NS)

;Stop Block
;#ES_block "Exit"
;#ES_bitmap "exit.bmp"
    wr #0       ; write data to disk
    exit                ; end of acquisition/experiment

; Phase program definitions for FCUs
    ph1=0 0 2 2           ; phase program: 0 0 180 180 (exc/det RF)
    ph2=0 0 0 0           ; phase program: 0 0 0 0 (all other RF)
```